1998

Electron correlation

Kurt Raymond Glaesemann
Iowa State University

INFORMATION TO USERS

This manuscript has been reproduced from the microfilm master. UMI films the text directly from the original or copy submitted. Thus, some thesis and dissertation copies are in typewriter face, while others may be from any type of computer printer.

The quality of this reproduction is dependent upon the quality of the copy submitted. Broken or indistinct print, colored or poor quality illustrations and photographs, print bleedthrough, substandard margins, and improper alignment can adversely affect reproduction.

In the unlikely event that the author did not send UMI a complete manuscript and there are missing pages, these will be noted. Also, if unauthorized copyright material had to be removed, a note will indicate the deletion.

Oversize materials (e.g., maps, drawings, charts) are reproduced by sectioning the original, beginning at the upper left-hand corner and continuing from left to right in equal sections with small overlaps. Each original is also photographed in one exposure and is included in reduced form at the back of the book.

Photographs included in the original manuscript have been reproduced xerographically in this copy. Higher quality 6" x 9" black and white photographic prints are available for any photographs or illustrations appearing in this copy for an additional charge. Contact UMI directly to order.

UMI

A Bell & Howell Information Company
300 North Zeeb Road, Ann Arbor MI 48106-1346 USA
313/761-4700 800/521-0600

Electron correlation

by

Kurt Raymond Glaesemann

A dissertation submitted to the graduate faculty

in partial fulfillment of the requirements for the degree of

DOCTOR OF PHILOSOPHY

Major: Physical Chemistry

Major Professor: Mark S. Gordon

Iowa State University

Ames, Iowa

1998

Graduate College
Iowa State University

This is to certify that the Doctoral dissertation of

Kurt Raymond Glaesemann

has met the dissertation requirements of Iowa State University

Signature was redacted for privacy.

Committee Member

Signature was redacted for privacy.

Committee Member

Signature was redacted for privacy.

Committee Member

Signature was redacted for privacy.

Committee Member

Signature was redacted for privacy.

Major Professor

Signature was redacted for privacy.

For the Major Program

Signature was redacted for privacy.

For the Graduate College

Dedication

I would like to dedicate this thesis to my family who has supported me in my endeavors. My wife Karen, a fellow chemist, who provided emotional and intellectual support throughout my graduate school career. To my future children who drove me to finish sooner rather than later. To my mother who always cared enough to be interested, even when she did not understand what I was doing. To my sister who reminds me that there are more roads and paths to walk down in life than we will ever have to traverse, so we should choose our path well. To my father who inspired me to become a chemist with high school stories of wild laboratory experiments. To my extended family who loves me just the way I am. And finally to my God, who has blessed me all my days.

TABLE OF CONTENTS

ACKNOWLEDGEMENTS

There are many people to whom I owe gratitude, to for their help and assistance throughout not only my academic career, but my entire life. I must apologize for any names that I have misspelled, it has been a long time since I have seen or talked to many of these wonderful people.

As a small child, my own parents and the other parents in the neighborhood encouraged us children to have a wonder about the world. We learned that having fun and learning were not mutually exclusive. A little gardening and a little role playing as a child provide years of fond memories.

I had many wonderful teachers in elementary school. Mrs. McCurdy's math and science class was a delight. She made us all enjoy learning and knew how to push us to the higher ground. Learning was always an active endeavor. My fellow students were always a joy to work with. Mrs. Martinson's (elementary school principle) firm belief in intellectual and social development, forced the teachers at May Morley Elementary to do an exceptional job or be forced out.

In Junior High and High School, many teachers encouraged me to learn more than just enough to get an A. Dr. Durst in particular taught me in geology class the importance of having a wide breath of knowledge in addition to having a depth of knowledge in one particular subject. Miss. Penner taught us that hard work, determination, and naturally ability often paid off. She also taught us to deal with failure, when determination and ability were not enough.

At Northeast Missouri State University, my ability to think blossomed. The liberal arts education provide by NMSU forced me to work hard and think in all of my classes. I

owe a debt to my fellow chemistry students, and the student body in general, for being a vibrant and hard working group that always pushed the envelope of learning. Jamie Axthelm and Kim Foster in particular need my thanks for being good friends throughout my upper level chemistry classes. My freshman chemistry professor and advisor Dr. Pultz served as a mentor and as friend. He took a very practical approach to both life and chemistry. From him I learned my love of and respect for physical chemistry. Dr. Delaware encouraged me to ask the question "why" in organic class rather than just memorizing reactions.

I must thank my major professor for making me get the right answers for the right reasons. I greatly appreciate his strong desire to treat everyone fairly and with respect, because it fosters an environment in which scholarly learning flourishes. His drive for excellence in science is unstoppable.

Dr. Mike Schmidt has provided much insight into wavefunctions and their multi-reference character. I have spent many hours discussing spacial and spin symmetry with him. He always has time to answer question, whether it is about some obscure option in GAMESS or the theoretical basis of some method. His ability to bring all the Fortran code that Mark's group produces together is amazing.

The entire Gordon research group has helped me. They have answered my questions and thus speeded up my research. They also asked me questions, providing me an opportunity to share my knowledge and to build my confidence in teaching. They remind me day in and day out that there is no one right way to be a physical chemist.

Finally, I should thank my family. Without them I would not be who I am today. This thanks extends to my parents, my grandparents and all my aunts and uncles. I should

thank Karen in particular because she has put up with the ups and downs of graduate school. She even once stayed late and graded general chemistry tests for me. In addition to being my wife, she has served as chief comedian, head nurse, staff psychologist and chauffeur of our family. Without her love and support, I would not have survived.

ABSTRACT

Correlated treatment of chemical systems. $FeCO^+$ is an important chemical system because Fe^+ is a catalyst and CO has proven effective in modifying the reactivity of transition metals. $FeCO^+$, Fe^+ and CO were studied using several different *ab initio* methods: single-reference coupled-cluster techniques, multi-reference perturbation theory, and multi-reference configuration interaction. Although the ground state of Fe^+ is a sextet, upon interaction with the CO the ground state of $FeCO^+$ is found to be a quartet. This crossing of the quartet and sextet potential energy surfaces is used to explain the experimentally observed reactivity of Fe^+. Several complex problems are encountered in the analysis of the ground and excited state potential energy surfaces. They are discussed in detail including their causes and solutions.

Density Functional Theory(DFT). DFT is a method in which chemical properties are calculated directly from the electron density instead of the *ab initio* wavefunction. Integrating over the density usually is done using a numerical grid. A derivation of a grid-free (DFT) approach is described in detail with an emphasis on numerical rigor and the practical details of implementation without the use of grids. Since atomic basis sets normally used in molecular orbital calculations are usually found to be inadequate, extensive research devoted to developing auxiliary basis sets is presented. Chemical systems are studied to compare this approach to the more traditional grid based approaches. The grid-free approach is found to be an effective method of calculating energies and geometries, provided an adequate auxiliary basis set is used.

CHAPTER 1: INTRODUCTION

I. Overview of topics

IA. General overview

Transition metals are a vital part of chemistry due to the extensive and varied reactivity resulting from their partially filled d orbitals. Fe^+, a ^6D (3d64s1) metal cation, has been studied extensively as a catalyst for many different reactions of interest. Fe^+ is generally not used as a catalyst alone, usually a complexed form is utilized. A good candidate for such complexes is $FeCO^+$, because CO is important in the chemistry of many transition metals, playing a role in many chemical processes and industrial procedures. In both the oxidative addition of H_2 to metals and the reductive elimination of H_2 from metals, CO is important because it is effective in stabilizing transition metals, even those which carry negative charges. $FeCO^+$ in particular has been studied as a catalyst for reactions involving polyhalogenated methane and halogens both in a microwave discharge and without microwaves. This makes $FeCO^+$ of particular interest given the role that halogens play in the atmospheric destruction of the ozone layer. Gas phase studies and theoretical calculations have shown that $FeCO^+$ has significantly different reactivity and selectivity than Fe^+ and other Fe^+ complexes such as $Fe(H_2O)_n^+$. Armentrout and Tjelta found that $Fe(CO)^+$ activates both C-C and C-H bonds in ethane, while $Fe(H_2O)^+$ preferentially activates the C-H bonds. This can be partially explained by the observation that R groups must interact with the 3dσ orbital in $Fe(H_2O)^+$ instead of the empty 4s orbital in $Fe(CO)^+$. The 4s orbital in $FeCO^+$ is unoccupied in the quartet states, but occupied in the sextet states. Therefore the ^6D Fe^+ must undergo a conversion to quartet upon forming $FeCO^+$. Unfortunately, calculations on such systems have been difficult, because transition metals

often have many low lying states and computationally demanding approaches are usually necessary to produce accurate results.

As alluded to above, chemists often find adding "correlation" to electronic structure calculations to be essential. The correlation energy is defined as the difference between the Hartree-Fock energy and the exact full configuration interaction (CI) energy in a complete one–electron basis. Correlation corrections are provided by all methods that are more accurate than a single-reference Hartree-Fock. This improved accuracy requires the use of more computer resources. The correlation energy can be obtained in a number of ways: perturbation or cluster expansions of the correction carried out to finite order, modified Hamiltonians as in Density Functional Theory (DFT), and variationally as in Configuration Interaction (CI) methods. DFT is advantageous because its computational requirements are relatively low.

IB. $FeCO^+$

At dissociation the lowest state of $Fe^+ + CO$ is naturally the sextet, since the ground state for a Fe^+ ion is ^6D and CO is a $^1\Sigma^+$. Experimentally the $FeCO^+$ complex is known to be a quartet, so a state crossing must occur. Studying the low lying states of a transition metal complex such as $FeCO^+$ generally requires the use of a multi-configurational wavefunction. Occupation numbers for orbitals are often found to differ significantly from the single-reference values of 1.0, 2.0 and 0.0. The simultaneous existence of effects such as "sigma donation" and "pi backbonding" forces electrons that are nominally non-bonding to weakly interact. Such weak interactions are often a driving force for fractional natural orbital occupation numbers. If one does not use a multi-reference wavefunction in such systems, the underlying wavefunction will be incorrect and all results are suspect. Getting

the correct wavefunction for degenerate states can require state-averaging (SA). A pair of delta states will lose their symmetry if only one is optimized, whereas optimizing the pair of states yields occupation numbers of 1.5 and 1.5 for the degenerate delta orbitals. Some excited states might not converge, because the variational principle forces the wavefunction to collapse to a lower energy state.

Additional correlation must be added to the $FeCO^+$ wavefunction in order to obtain quantitatively correct results. In this work, this is accomplished by using a perturbation expansion to calculate correlation energy. The multi-configuration quasi-degenerate perturbation theory to the second order (MC-QDPT2) method is used. This method assumes that the correlation energy is a small perturbation to the MCSCF energy and that the correlation energy is a property of the MCSCF wavefunction. MC–QDPT2 is able to properly treat states in which a single–reference wavefunction is not a close approximation to the exact wavefunction. It can also handle states that are degenerate or nearly degenerate.

IC. Grid-free DFT

Density Functional Theory (DFT) has been used for several decades. Recently, the advent of much tighter integration grids and much better gradient-corrected functionals has resulted in a surge in its utilization among chemists. DFT can provide electron correlation with a computational expense that is little more than Hartree-Fock. This is achieved by changing the underlying Hamiltonian to one that has terms that depend directly on the electron density. The resulting integrals are so complicated that they must be evaluated using approximations. Traditionally, this has meant evaluating the integrals using a numerical grid. A grid-free approach to DFT that relies on basis set completeness rather than grid completeness has been developed and implemented and is reported in this thesis.

Whatever approach is used to evaluate the DFT integrals, it is important that a numerically stable and efficient approach be chosen. The grid-based methods have been shown to suffer from numerical instability. Just as a poorly designed grid can introduce problems, a poorly designed basis set can introduce problems. A significant portion of this research deals with the issue of designing an auxiliary basis set. An entire chapter is devoted to properly handling the density derivatives. Parts of several chapters are devoted to efficient integral computation and screening algorithms.

Although single-point energies provide a great deal of useful information, in general one does not know *a priori* at what points to calculate energies. Gradients of the energy with respect to nuclear coordinates provide a useful insight, allowing one to search efficiently for a energy minima or saddle point, by minimizing the energy gradient with respect to nuclear position. Gradients have been implemented in a general method for the grid-free DFT approach. The gradients also rely on basis set completeness.

II. Thesis Organization

Chapters 2 through 5 are papers accepted, submitted to, or prepared for submission to peer reviewed journals with me as primary author.

Chapter 2 presents initial results of the grid-free DFT approach without the use of auxiliary basis sets. A detailed derivation of the method is presented. The need for the use of auxiliary basis sets is shown.

Chapter 3 presents research into properly treating the density gradient terms within the grid-free DFT approach. A numerically stable method is presented and compared to several unstable methods.

Chapter 4 presents further research into the grid-free DFT approach. Additional implementation details are presented with an emphasis on auxiliary basis sets. Results using auxiliary basis sets are presented.

Chapter 5 provides an in depth study of the low lying states of $FeCO^+$. The need for electron correlation is shown, and results using correlated methods are presented.

Chapter 6 is a general conclusion based on the research presented in chapters 2 through 5.

III. Theoretical Background

IIIA. Quantum mechanics

Quantum mechanics models the microscopic world using equations to describe the underlying physics and the wavefunction Ψ to describe the physical system. The ultimate goal of all quantum mechanical calculations is to achieve a solution for the time-dependent Schrödinger[1] equation:

$$-\frac{h}{2\pi i}\frac{\partial \Psi(\vec{x},t)}{\partial t} = \hat{H}\Psi(\vec{x},t), \qquad (1)$$

where h is Planck's constant, t is time, $\vec{x}$ is position, $\hat{H} = \hat{T} + \hat{V}(\hat{x},t)$ is the Hamiltonian of the system of interest, and Ψ is the wavefunction for the system. $\hat{T}$ is the kinetic energy portion and $\hat{V}$ is the potential energy portion of the Hamiltonian. $\Psi^*\Psi$ describes the probability of finding the object Ψ at any point in space. Therefore, even if Ψ has imaginary values, the probability will be real valued. All work presented within this thesis is based on Ψ's that are real valued. Eq. (1) describes the basic underlying quantum physics of the problem. If the solution to Eq. (1) could be found for a given system (not necessarily molecular), then we would have a complete picture of the system. $\hat{H}$

interconnects all particles at all times, therefore the equations describing the interdependencies are too complicated to solve. Well-defined, systematic assumptions must be made in order to find solutions. With each of these subsequent approximations, the problem presented in Eq. (1) is simplified, but the quality of the answer Ψ suffers.

The first approximation is to remove the time dependence from Eq. (1). This requires assuming that the potential $\hat{V}$ is independent of t. Therefore for most quantum chemistry calculations performed, the time-independent Schrödinger[1] equation is utilized:

$$\hat{H}\Psi(\bar{x}) = E\Psi(\bar{x}), \tag{2}$$

where E is the total energy of the system, $\hat{H}$ is the time-independent Hamiltonian, and Ψ describes both the electrons and nuclei. Eq. (2) is an eigenvalue problem with multiple solutions. For each eigenvalue E_ξ, there is a corresponding eigenfunction Ψ_ξ. The Ψ with the lowest value of E is the ground state. Eq. (2) can only be solved exactly for a one or two body system, such as the hydrogen atom. For molecular systems, it is necessary to make a distinction between nuclei and electrons based on their different properties.

The Born-Oppenheimer[2] approximation assumes that the nuclei move on a time scale much longer than that of electrons. Therefore it is a reasonable assumption that the nuclei are fixed in space when treating the electrons. The nuclear-nuclear interactions become a constant for a given geometry, and therefore only the Hamiltonian for the electrons H_{elec} must be solved (with nuclear repulsion merely acting as a fixed potential):

$$\hat{H}_{elec} = -\tfrac{1}{2}\sum_{i}^{n}\left(\nabla_i^2 - \sum_{A}^{N}\frac{Z_A}{r_{iA}}\right) + \sum_{i>j}^{n}\frac{1}{r_{ij}}, \tag{3}$$

where n is the number of electrons, N is the number of atoms, r_{ij} is the distance between i and j, Z_A is the nuclear charge of atom A, and ∇_i^2 is the laplacian for the i^{th} electron. The

first term in the brackets is kinetic energy and the second term is the nuclear-electron attraction; both of these terms are relatively simple to evaluate. The third term of Eq. (3), which represents electron-electron repulsion, is a multi-body term, and therefore analytically solving the equations that result from applying this term to a Ψ is impossible for systems with more than one electron. All calculations presented within this thesis are performed within the time-independent Born-Oppenheimer framework.

The troublesome third term in Eq. (3) is simplified within the orbital approximation. The Hamiltonian is not approximated, but restrictions are put on the wavefunction that simplify the application of Eq. (3). Each electron is assumed to have a well–defined spin orbital that defines its position in space. Each electron feels a space averaged repulsion from all of the other electrons. Therefore the n electron Hamiltonian can be replaced with n one-electron effective Hamiltonians (each of which can be solved exactly):

$$\hat{F}\psi_j = \varepsilon_j \psi_j, \text{ with } j = 1,\ldots, n, \tag{4}$$

where $\hat{F}$ is the Fock operator, ε_j is an orbital energy, and ψ_j is a variationally optimized orbital. This method is called Hartree-Fock theory.[3]

The total wavefunction Ψ is required to be an antisymmetrized product of the spin-orbitals, therefore interchanging any two electrons changes the overall sign: $\Psi(1,2)=-\Psi(2,1)$. This requirement enforces the Pauli exclusion principle, which keeps two electrons from being in the same place at the same time. This is a form of correlation, but it only applies to the interaction between electrons with the same spin. The requirement is met by making Ψ a Slater determinant of the ψ's:

$$\Psi = (n!)^{-1/2} \begin{vmatrix} \psi_1(e_1) & \psi_2(e_1) & \cdots & \psi_n(e_1) \\ \psi_1(e_2) & \psi_2(e_2) & \cdots & \psi_n(e_2) \\ \vdots & \vdots & & \vdots \\ \psi_1(e_n) & \psi_2(e_n) & \cdots & \psi_n(e_n) \end{vmatrix}, \tag{5}$$

instead of the much simpler Hartree product of the molecular spin orbitals:

$$\Psi = \psi_1(e_1) \cdot \psi_2(e_2) \cdot \psi_3(e_3) \cdot \ldots \cdot \psi_n(e_n), \tag{6}$$

where n is the number of electrons, e_i is the i^{th} electron, and ψ_i is the i^{th} molecular spin orbital. The Slater determinant is often written compactly using the bra-ket notation:

$$\Psi = |\psi_1 \psi_2 \psi_3 \cdots \psi_n\rangle, \ \Psi^* = \langle \psi_1 \psi_2 \psi_3 \cdots \psi_n|, \tag{7}$$

where all of the permutations of all of the electrons in all of the occupied molecular orbitals is implied.

The Fock operator $\hat{F}$ depends upon the orbitals $\{\psi\}$ and the orbitals $\{\psi\}$ are pseudo–eigenfunctions of $\hat{F}$, therefore Eq. (4) must be solved in an iterative manner. An initial guess at $\{\psi\}$ must be made, and then the resulting $\hat{F}$ is used to generate an improved $\{\psi\}$. This improved $\{\psi\}$ is then used to generate a new $\hat{F}$ and the process continues until $\{\psi\}$ and $\hat{F}$ do not change to some prescribed tolerance. This iterative process is called the self-consistent field (SCF) process. If the $\{\psi\}$ are allowed to be different for alpha and beta electrons, then this is called the unrestricted Hartree-Fock (UHF)[4] method. If the $\{\psi\}$ are the same for alpha and beta electrons then this is called the restricted Hartree-Fock (RHF)[5] method for closed shell systems and the restricted open-shell Hartree-Fock (ROHF)[6] method for systems with different numbers of alpha and beta electrons. Spin is often not a well-defined quantum number within the UHF formalism, so although it does remove a restriction and thus lowers the energy, unrestricted wavefunctions have not been used

extensively within this thesis.

Within this work, the $\{\psi\}$ are chosen to be linear combinations of atomic orbitals.[7] Although there is nothing in the Hartree-Fock formalism to force this choice, it is a very convenient choice:

$$\psi_j = \sum_{\mu} C_{\mu j} \chi_{\mu}, \tag{8}$$

where C's are the LCAO (linear combination of atomic orbital) coefficients and the χ's are atomic orbitals. Within this work, to allow fast evaluation of integrals over the orbitals, linear combinations of gaussian functions[8] are utilized as the atomic basis:

$$\chi_{\mu} = x^{l} y^{m} z^{n} \sum_{i} N_i e^{-\alpha (x^2 + y^2 + z^2)}, \tag{9}$$

where N_i is a contraction coefficient, *l,m,n* are integers that provide angular momentum, and α is the exponent that determines the diffuseness of the gaussian. The contractions allow several gaussian functions to be combined to form a single atomic orbital.

Hartree-Fock is size-consistent. In order for a method to be size-consistent, the energy for A + B at a very large distance must be the same as the sum of the energies for the two systems A and B. This does not mean that Hartree-Fock can properly treat the breaking of bonds, because breaking bonds would involve the unpairing of electrons. All Hartree-Fock methods are invariant with respect to any transformation of the molecular orbitals that does not change the total electron density. The energy therefore depends only on the electron density and not the choice of molecular orbitals.[9]

Hartree-Fock is often inadequate for molecules such as $FeCO^+$. This failure is partially due to its inability to correlate electrons with opposite spin. This results in electron-electron repulsions that are too large. By adding correlation to the Hartree-Fock wavefunction these deficiencies can be overcome.

IIIB. Density functional theory (DFT)

DFT is a method of calculating the correlation energy by replacing the underlying Hamiltonian $\hat{H}$ with a modified $\hat{H}^{DFT}$ that contains terms that are functions of the electron density.[10] DFT can be based on a converged Hartree-Fock density or on a density optimized using $\hat{H}^{DFT}$. Because $\hat{H}^{DFT}$ is not the correct Hamiltonian, it is possible to get energies that are lower than the exact answer. Therefore, DFT is not truly variational. DFT is often referred to as "semi-variational", because within the $\hat{H}^{DFT}$ framework, energies are never lower than the correct $\hat{H}^{DFT}$ answers. Like Hartree-Fock, DFT is orbitally invariant and size-consistent. Within this work, DFT is implemented as a single-reference method, where the density is required to be represented by a set of single-reference orbitals.

IIIC. Configuration Interaction(CI)

A full CI calculation will give the correct solution within the basis set used for Eq. (2) ($\hat{H}$ is the Hamiltonian presented in Eq. (3)) [9]. Therefore in the limit of a complete basis set, a full CI gives the correct Born-Oppenheimer energy. A full CI is generated by taking the optimum linear combination of all possible arrangements of electrons in the molecular orbitals. Because all combinations are used, the choice of zeroth-order wavefunction is irrelevant, but the Hartree-Fock Ψ is a convenient choice for Ψ_0 and used in Eq. (10).

$$\left|\Psi_{\text{full CI}}\right\rangle = c_{0,1}\left|\Psi_0\right\rangle + \sum_{i}^{\substack{\text{All single}\\ \text{excitations}}} c_{1,i}\left|\Psi_{1,i}\right\rangle + \sum_{i}^{\substack{\text{All double}\\ \text{excitations}}} c_{2,i}\left|\Psi_{2,i}\right\rangle + \sum_{i}^{\substack{\text{All triple}\\ \text{excitations}}} c_{3,i}\left|\Psi_{3,i}\right\rangle \ldots, \quad (10)$$

Where $\{c_{n,m}\}$ are the CI coefficients, and $|\Psi_{j,k}>$ is the k^{th} possible way of exciting j electrons out of the Ψ_0 occupied orbitals into the Ψ_0 virtual orbitals. The CI coefficients provide weights of each $|\Psi_{l,k}>$ in the CI wavefunction, and are chosen to minimize the total energy.

The full CI calculation is computationally demanding. Therefore, the CI expansion is often truncated to single and double excitations (CISD).[11] CISD is not size-consistent because simultaneous double excitation in both A and B is a quadruple excitation on the A + B supermolecule. The energy of A + B would therefore be higher than the energy of A and B calculated separately. Although CISD works well for small molecules, larger molecules often require higher order excitations.

Another approach is to do a full CI, but only for the "chemically important" or "active" orbitals. If both the orbitals and CI coefficients are optimized, then this method is called the Fully Optimized Reaction Space Multi-Configurational Self-Consistent Field (FORS-MCSCF)[12] method. Mixing virtual, active, or core orbitals separately does not change the energy, therefore FORS-MCSCF is orbitally invariant. If the active orbitals are chosen properly, then the FORS-MCSCF can properly treat the breaking of bonds. The FORS-MCSCF method is size-consistent, although the active space on the A + B supermolecule must correspond to the active spaces on the separated A and B systems.

IIID. Coupled-Cluster (CC).

CC methods[13] provide a way to approximate a full CI, but CC is not variational. CC approximates the exact wavefunction Ψ with an exponential operator acting on the zero-order wavefunction (usually Hartree-Fock).

$$\left|\Psi_{exact}\right\rangle = e^{\hat{T}}\left|\Psi_{O}\right\rangle, \text{ where } \hat{T} = \hat{T}_1 + \hat{T}_2 + \cdots + \hat{T}_n, \tag{11}$$

n is the number of electrons and $\hat{T}_m$ depends upon m-electron excitations. The exact form of $\hat{T}$ will depend on how high of an order the expansion is carried out to. The complicated nature of $\hat{T}$ makes this method computationally expensive, but efficient compared to a full CI provided that $\hat{T}$ is truncated to a low order. All CC methods used in this work are

derived to be orbitally invariant and size-consistent. Usually $\hat{T}$ consists of single and double replacements, together with some method of approximating the triples.

IIIE. Perturbation Theory.

Another approach is to assume that the correlation energy is a perturbation to the zero-order wavefunction. The Hamiltonian is written as the zero-order Hamiltonian of Eq. (4) plus everything that was left out of the Hamiltonian in Eq. (3) to generate Eq. (4).

$$\hat{H} = \hat{H}_0 + \hat{H}_{1,\ldots,n} \tag{12}$$

For closed shell singlet Hartree-Fock the correction is:

$$\hat{H}_{1,\ldots,n} = \sum_{i>j}^{n} \frac{1}{r_{ij}} - \sum_{i}^{n/2} \sum_{j}^{n/2} (2J_{ij} - K_{ij}), \tag{13}$$

where {J} are the coulomb integrals and {K} are the exchange integrals. $\hat{H}_{1,\ldots,n}$ is expanded in a Taylor series and usually only the first two terms are used. For a converged Hartree-Fock wavefunction the first-order term vanishes although this is not always true for perturbations based on a converged SA–MCSCF wavefuction.[14,15] The underlying wavefunction must be close to the exact wavefunction for this expansion to be valid. This method is not variational. The perturbation methods used in this work are all size-consistent. The multi-reference method used within this thesis is called Multi-Configurational Quasi-Degenerate Perturbation Theory to the second-order (MC-QDPT2).[16] It can perturb multiple states simultaneously, including degenerate or nearly degenerate states.

All these correlation methods have advantages and disadvantages. The choice of correlation method is determined by the available computer resources, the accuracy required, and the nature of the problem. In this work, the methods used are chosen to provide chemical accuracy for the problem at hand.

References

1. a. E. Schrödinger, Ann. Physik. **79**, 361 (1926). b. E. Schrödinger, Ann. Physik. **79**, 489 (1926). c. E. Schrödinger, Ann. Physik. **79**, 734 (1926). d. E. Schrödinger, Ann. Physik. **80**, 437 (1926). e. E. Schrödinger, Ann. Physik. **81**, 109 (1926).
2. M. Born and J.R. Openheimer, Ann. Physik. **84**, 457 (1927).
3. a. D.R. Hartree, Proc. Cambridge Phil Soc. **24**, 89 (1929). b. D.R. Hartree, Proc. Cambridge Phil Soc. **24**, 111 (1929). c. D.R. Hartree, Proc. Cambridge Phil Soc. **24**, 426 (1929). d. V. Fock, Physik **61**, 126 (1930).
4. J.A. Pople and R.K. Nesbet, J. Chem. Phys. **22**, 571 (1954).
5. C.C.J. Roothan, Rev. Mod. Phys. **23**, 69 (1954).
6. a. R. McWeeny, G. Diercksen, J. Chem. Phys. **49**, 4852 (1968). b. J.S. Binkley, J.A. Pople, and P.A. Dobosh, Mol. Phys. **38**, 1423 (1974). c. E.R. Davidson, Chem. Phys. Lett. **21**, 565 (1973).
7. C.C.J. Roothan, Rev. Mod. Phys. **32**, 179 (1970).
8. S.F. Boys, Proc. R. Soc. London Ser. A **200**, 542 (1950).
9. A. Szabo and N.S. Ostlund in *Modern Quantum Chemisty*, McGraw-Hill, New York, 1989.
10. R.J. Parr and W. Yang in *Density-Functional Theory of Atoms and Molecules*, Oxford University Press, New York, 1989.
11. a. B.Brooks and H.F.Schaefer, J.Chem. Phys. **70**, 5092 (1979). b. T. Helgaker, J. Gauss, P. Jørgensen and J. Olsen, J. Chem. Phys. **106**, 6430 (1997).

12. a. L.M. Cheung, K.R. Sunberg, and K. Ruedenberg, Int. J. Quantum Chem. **16**, 1103 (1979). b. B.O. Roos, P. Taylor, and P.E.M. Siegbahn, Chem. Phys. **48**, 157 (1980).

13. a. G.E. Scuseria, C.L. Janssen, and H.F. Schaefer III, J. Chem. Phys. **89**, 7382 (1988). b. J.F. Stanton, Chem. Phys. Lett. **281**, 130 (1997).

14. a. J.A. Pople, J.S. Binkley, and R. Seeger, Int. J. Quantum Chem. **S10**, 1 (1976). b. P. Carsky, B.A. Hess, and L.J. Schaad, J. Comp. Chem. **5**, 280 (1984).

15. Z. Konkoli, Z. He, and D. Cremer, Theor. Chem. Acc. **96**, 71 (1997).

16. a. K. Hirao, Chem. Phys. Lett. **190**, 374 (1992). b. K. Hirao, Chem. Phys. Lett. **196**, 397 (1992). c. K. Hirao, Chem. Phys. Lett. **201**, 59 (1993). d. K. Hirao, Int. J. Quantum Chem. **S26**, 517 (1992). e. H. Nakano, J. Chem. Phys. **99**, 7983 (1993). f. H. Nakano, Chem. Phys. Lett. **207**, 372 (1993). g. H. Nakano, K. Hirao, and M.S. Gordon, J. Chem. Phys. **108**, 5660 (1998).

CHAPTER 2: INVESTIGATION OF A GRID-FREE DENSITY FUNCTIONAL THEORY (DFT) APPROACH

A paper that has been published in the Journal of Chemical Physics.
Reprinted with permission from *Journal of Chemical Physics* **108**(24),
June 22, 1998, pp 9959-9969.

Kurt R. Glaesemann and Mark S. Gordon

Abstract

Density functional theory (DFT) has gained popularity, because it can frequently give accurate energies and geometries. Because evaluating DFT integrals fully analytically is usually impossible, most implementations use numerical quadrature over grid points, which can lead to numerical instabilities. To avoid these instabilities the Almlöf-Zheng(AZ) grid-free approach was developed. This approach involves application of the resolution of the identity (RI) to evaluate the integrals. The focus of the current work is on the implementation of the AZ approach into the electronic structure code GAMESS, and on the convergence of the resolution of the identity with respect to basis set in the grid-free approach. Both single-point energies and gradients are calculated for a variety of functionals and molecules. Conventional atomic basis sets are found to be inadequate for fitting the RI, particularly for gradient corrected functionals. Further work on developing auxiliary basis set approaches is warranted.

I. Introduction.

In recent years, density functional theory (DFT), formulated in terms of the spin densities (n_α,n_β) representing all electrons, has gained popularity as a method for

determining molecular properties and structures as an alternative to *ab initio* wavefunctions. Functionals of the density have been fit to the uniform electron gas,[1,2] and have incorporated corrections that depend upon the density gradient.[3,4,5] "Hybrid functionals" that mix in Hartree-Fock exchange can help correct for the inadequacies of a single-reference wavefunction, although the meaning of terms such as single-reference and multi-reference are not entirely clear for density functionals.[6,7] Nonetheless, a multi-reference wavefunction is still necessary for some problems, e.g., to describe bond breaking, and to obtain the correct electronic spin and space symmetry.[8,9] DFT can frequently give energies, relative energies and geometries more accurately than second-order perturbation theory, with significantly less computational expense.[10] DFT can also give results in qualitative agreement with coupled cluster methods,[11] although reports of failures of DFT are not uncommon in the literature,[12,13,14] partially because DFT is not strictly variational.[15,16,17]

Integrating the functionals over the spin densities to obtain energies would require a computational effort of order N^4 or higher, where N is the size of the atomic basis set. Because evaluating integrals over the functionals in a closed analytic form is usually impossible, most DFT implementations evaluate the integrals using numerical quadrature over a finite set of grid points:

$$\int_{\text{All space}} f(n_\alpha, n_\beta)\,d\vec{r} \approx \sum_{\text{Grid points}} f(n_\alpha, n_\beta)\,\Delta\vec{r}. \qquad (1)$$

These grids are usually organized in atom centered Lebedev spheres.[18,19,20] Dunlap *et. al.* eloquently discussed how the use of grids can lead to numerical instabilities.[21,22] Recently, grid-free approaches have been developed to avoid these difficulties.[21,22,23,24,25] However, these analytic approaches involve their own approximations, and their convergence with respect to basis set has not been explored extensively. The primary focus

of the current work is on these basis set convergence properties of grid-free DFT. In section II the Almlöf-Zheng (AZ) grid-free approach to DFT is discussed, with emphasis on its implementation into the electronic structure code GAMESS.[26] This will require calculating several types of integrals and doing several types of matrix manipulations. The derivation and implementation of analytic energy gradients are also discussed in this section. In section III results based on the AZ approach are presented. Several prototypical systems are studied to explore the convergence of properties (geometries, dipole moments, singlet-triplet splittings, isomerization energies) as a function of the basis set. These results will demonstrate in detail the basis set dependence of the grid-free approach.

II. A Grid-Free approach to DFT.

IIA. Single point energies.

In this section the AZ approach of using matrix relations to evaluate the complicated DFT integrals is explained. Initially methods of simplifying the integrals using approximations will be examined. This will result eventually in exactly evaluating a four-center integral and a gradient integral. The initial integral simplification uses the resolution of the identity(RI).[27] Consider the product of two arbitrary functions, f(x,y,z) and g(x,y,z). In matrix representation the resolution of the identity can be expressed as:

$$M_0[f \cdot g] \approx M_1[f] M_2[g], \qquad (2)$$

where M_r are matrix representations in terms of some atomic basis set $\{\chi_i\}$. In terms of individual elements of the matrices (and therefore integrals),

$$M_0[f\cdot g]_{i,j} = \int \chi_i (f\cdot g)\chi_j \, d\vec{r} \tag{3a}$$

$$\approx \sum_m \int \chi_i \, f\theta_m \, d\vec{r} \cdot \int \theta_m \, g\, \chi_j \, d\vec{r} \tag{3b}$$

$$= \sum_m M_1[f]_{i,m} M_2[g]_{m,j}. \tag{3c}$$

The foregoing expressions are exact if $\{\theta_m\}$ is a complete orthonormal set; otherwise, one expects some dependence of the calculations on the size of the basis set. Within GAMESS, the average of f•g and g•f is used, to preserve matrix symmetry . One well-defined choice for $\{\theta_m\}$ is the set of orthonormal molecular orbitals from the current SCF cycle. This choice appears to maintain a proportionality between the accuracy of the resolution of the identity and the accuracy of the wavefunction (the RI basis set and the atomic orbital basis set are the same size). As will be shown in section III, this is unfortunately not the case.

As an example of using the resolution of the identity, consider the DePristo-Kress gradient corrected exchange functional,[28] which multiplies the uniform electron gas limit of $n^{4/3}$ times a term that depends on the gradient of the density. After substituting the density matrix D for one factor of n in Eq. (4a) and applying the resolution of the identity in Eq. (4b), this functional simplifies to:

$$\int n^{\frac{1}{3}} y^2 \frac{1+a_1 y}{1+b_1 y^2} d\vec{r} = \sum_{\mu\nu}^{AO's} D_{\mu\nu} \cdot \int \chi_\mu n^{\frac{1}{3}} y^2 \frac{1+a_1 y}{1+b_1 y^2} \chi_\nu d\vec{r} \tag{4a}$$

$$\approx \sum_{\mu\nu}^{AO's} D_{\mu\nu} \sum_m^{Orthonormal} \int \chi_\mu n^{\frac{1}{3}} \theta_m d\vec{r} \cdot \int \theta_m y^2 \frac{1+a_1 y}{1+b_1 y^2} \chi_\nu \, d\vec{r} \tag{4b}$$

where, a_i, b_i = fitted parameters

$$y = \left| \frac{\nabla n}{n^{4/3}} \right|$$

f(n) in Eq. (3) $= n^{\frac{1}{3}}$

g(y) in Eq. (3) $= y^2 \frac{1 + a_i y}{1 + b_i y^2}$.

This leaves complicated integrals involving functions of the density n and the dimensionless density gradient y. Another resolution of the identity is used,[29] to evaluate these integrals, because they cannot be solved directly. This new resolution of the identity will rely upon the special properties of diagonalized matrices.

This resolution of the identity will transform M[n] into M[f(n)] for an arbitrary function f. Any function of the density, f(n), may be represented in matrix form as follows. M[n] is transformed into a new matrix M´[n] using an orthonormal basis set.

$$M'[n] = \tilde{V} M[n] V \qquad (5)$$

The matrix of LCAO coefficients is chosen for V, for which $\tilde{V}SV = I$, with S=overlap matrix in the atomic orbital basis set. M´[n] is then diagonalized by a unitary transformation U, yielding eigenvalues λ.

$$M'[n] = U \lambda \tilde{U} \qquad (6)$$

The function f is then evaluated at the eigenvalues, and incorporated into M´:

$$M'[f(n)] = U f(\lambda) \tilde{U}. \qquad (7)$$

Eq. (7) is exact in a complete basis (see appendix A). Finally, M´[n] is transformed back to the atomic basis, giving:

$$M[f(n)] = (\tilde{V})^{-1} \left(U f(\lambda) \tilde{U} \right) (V)^{-1} = SVU f(\lambda) \tilde{U}\tilde{V}S. \qquad (8)$$

Therefore, once the matrix representation of the density is determined, the matrix

representation of any function of the density can be readily obtained. Similarly, this can be shown to be true for the matrix representations of y, n_α, or n_β.

The matrix representation of the density M[n] is calculated from the first-order density matrix D and atomic orbitals i, j, k and l, by

$$M[n]_{i,j} = \int \chi_i n \chi_j \, d\vec{r} = \sum_{k,l} D_{kl} \int \chi_i \chi_k \chi_l \chi_j \, d\vec{r} = \sum_{k,l} D_{kl} (ikl j). \tag{9}$$

The four-center one-electron integrals $(ikl j) = \int \chi_i \chi_k \chi_l \chi_j d\vec{r}$ can be evaluated using a recursion formula similar to recursion formulae used by others[30,31]

$$\int \chi_a \chi_b \chi_c \chi_d \, d\vec{r} = (abcd) = \left(\frac{\alpha_a A_x + \alpha_b B_x + \alpha_c C_x + \alpha_d D_x}{\alpha_a + \alpha_b + \alpha_c + \alpha_d} - \alpha_a A_x \right) (a - 1_x | bcd) +$$

$$\frac{a_x (a - 2_x | bcd) + b_x (b - 1_x | acd) + c_x (c - 1_x | abd) + d_x (d - 1_x | abc)}{2(\alpha_a + \alpha_b + \alpha_c + \alpha_d)} \tag{10}$$

where $\alpha_a, \alpha_b, \alpha_c, \alpha_d$ = Gaussian exponents

A_x, B_x, C_x, D_x = X positions of atoms with orbitals a, b, c and d

a_x, b_x, c_x, d_x = exponents of the x^0, x^1, x^2, etc. part of the orbital

(for a = f_{x^2y} orbital: $a_x = 2, a_y = 1, a_z = 0$).

Here, the integral (b-1_x|acd) is the integral (abcd) with the x component of the angular momentum of orbital b decreased by one. Although the 4-center 1-electron integrals are unusual, they do appear in other contexts, such as the density based orbital localization method.[32,33] These one-electron integrals are analogous to the two-electron integral $\int \chi_i(1) \chi_k(1) (1/r_{12}) \chi_l(2) \chi_j(2) d\vec{r}$ and are equivalent to the two-electron integral $\int \chi_i(1) \chi_k(1) \, \delta_{12} \, \chi_l(2) \chi_j(2) d\vec{r}$. The one-electron (i k l j) integrals formally scale

computationally as order N^4, as do the corresponding two-electron integrals. Screening, parallelization, vectorization, direct, and symmetry techniques used to reduce the N^4 dependence of the two-electron $(i(1)\ k(1)|1/r_{12}|l(2)\ j(2))$ integrals[34] are easily extended to the $(i\ k\ l\ j)$ integrals. For example, $(i\ k\ l\ j)$ integrals can be screened to avoid their evaluation by using the Schwarz inequalities.

$$(iklj) \le \sqrt{(iikk)(lljj)} \tag{11a}$$

$$(iklj) \le \sqrt{(iill)(kkjj)} \tag{11b}$$

$$(iklj) \le \sqrt{(iijj)(kkll)} \tag{11c}$$

Evaluation of the *set* of one-electron integrals takes less time than the set of two-electron integrals, because the index symmetries ($(i\ k\ l\ j)=(i\ l\ k\ j)=\ldots$) allow fewer unique integrals to be computed. Note, however, that the dominant time bottleneck is the number of indices, not whether the integral involves one or two electrons. The notion that one-electron integrals are significantly faster than two-electron integrals is historical, since usually one-electron integrals are of the type $(i\ \hat{h}\ j)$, where $\hat{h}$=one electron part of Hamiltonian operator. In the work of Almlöf and Zheng, these four-center one-electron integrals were approximated with three-center one-electron integrals, whose number grows as order N^3, using the resolution of the identity:

$$(iklj) = \sum_m (ik\theta_m)(\theta_m lj). \tag{12}$$

This application of the resolution of the identity is computationally equivalent to expanding the density n in the $\{\theta_m\}$ basis and then calculating M[n] (see appendix B). This would result in a computational savings by reducing the number of integrals that have to be computed. In this work, $(i\ j\ k\ l)$ integrals are evaluated directly, although an option to use

the three-center integral approximation has been implemented in GAMESS. Although the integrals scale as order N^4, the matrix multiplications and diagonalizations in the AZ grid-free approach scale as order N^3.

The more popular DFT functionals involve terms that depend upon the gradient of the density. Integrals over $|\nabla n| \cdot n^{-4/3}$ are computed as follows.

$$\int \chi_\mu \left(n^{-4/3}\frac{dn}{dx}\right)\chi_\nu d\vec{r} = \int \chi_\mu \left(n^{-4/3}\frac{dn}{dx} - 3n^{-1/3}\frac{d}{dx}\right)\chi_\nu d\vec{r}$$

$$+ \int \chi_\mu \left(3n^{-1/3}\frac{d}{dx}\right)\chi_\nu d\vec{r} \qquad (13a)$$

$$= -3\int \chi_\mu \frac{d}{dx}\left(n^{-1/3}\cdot\chi_\nu\right)d\vec{r} + 3\int \chi_\mu n^{-1/3}\frac{d}{dx}\chi_\nu d\vec{r} \qquad (13b)$$

$$\approx 3 \sum_{m}^{\text{Orthonormal}} - \left\{ \int \chi_\mu \frac{d}{dx}\theta_m d\vec{r} \cdot \int \theta_m n^{-1/3}\chi_\nu d\vec{r} \right.$$

$$\left. + \int \chi_\mu n^{-1/3}\theta_m d\vec{r} \cdot \int \theta_m \frac{d}{dx}\chi_\nu d\vec{r} \right\} \qquad (13c)$$

$$= -3 \sum_{m}^{\text{Orthonormal}} \left\{ \int \chi_\mu \frac{d}{dx}\theta_m d\vec{r} \cdot \int \theta_m n^{-1/3}\chi_\nu d\vec{r} \right.$$

$$\left. + \int \chi_\nu \frac{d}{dx}\theta_m d\vec{r} \cdot \int \theta_m n^{-1/3}\chi_\mu d\vec{r} \right\} \qquad (13d)$$

The last step follows, because d/dx is anti-hermitian and $n^{-1/3}$ is hermitian. The $\int \chi_i \frac{d}{dx}\chi_j d\vec{r}$ are dipole velocity integrals. The d/dy and d/dz contributions are calculated similarly. We only study the gradient of the energy, because no popular functional uses higher order derivatives, due to numerical stability problems.[35,36]

In order to calculate energies, the wavefunction must be optimized using a self-consistent-field (SCF) method. This requires calculating Fock matrix elements, which are the derivatives of the energy with respect to changing the orbitals. The contribution of functional $f(n_\alpha, n_\beta, \nabla n_\alpha, \nabla n_\beta)$ to the alpha Fock matrix is computed from the spin densities (n_α, n_β), and atomic orbitals χ_i, χ_j.[37]

$$F_{ij}^{DFT,\alpha} = \int \left(\frac{\partial f}{\partial n_\alpha}(\chi_i\chi_j) + \frac{\partial f}{\partial \nabla n_\alpha} \nabla(\chi_i\chi_j) + \frac{\partial^2 f}{\partial \nabla n_\alpha^2} \nabla^2(\chi_i\chi_j) + \ldots \right) d\vec{r} \qquad (14a)$$

A more easily coded, but less transparent formulation for the first two terms is[10]

$$F_{ij}^{DFT,\alpha} = \int \left(\frac{\partial f}{\partial n_\alpha}(\chi_i\chi_j) + \left(2\frac{\partial f}{\partial(\nabla n_\alpha \cdot \nabla n_\alpha)} \nabla n_\alpha + \frac{\partial f}{\partial(\nabla n_\alpha \cdot \nabla n_\beta)} \nabla n_\beta \right) \nabla(\chi_i\chi_j) \right) d\vec{r}. \qquad (14b)$$

It is important to note that (unlike traditional Hartree-Fock) the dot product of F^{DFT} with the density matrix does not give the DFT energy contribution; the DFT contribution to the energy must be explicitly calculated. For example, the dot product of the X-α Fock matrix with the density matrix would overestimate exchange by 1/3 (see appendix C).

IIB. Analytic Nuclear Gradients of the Energy.

Chemists usually not only want the energy for a single arbitrary geometry, but the geometry at a stationary point on the potential energy surface as well. To efficiently search for these geometries, the derivative of the energy with respect to nuclear coordinates is needed. Although many DFT codes calculate these nuclear gradients, the potential energy surfaces sometimes suffer from grid noise.[21,22,24] Because the grid moves with the atoms, derivatives with respect to the grid are needed, but many DFT codes neglect these terms.[10,38,39] Such irregularities make determining saddle points and energy minima difficult. Methods for eliminating these effects have been developed.[40,41] However, the corrections can introduce numerical difficulties of their own, and therefore other research groups now advocate relying on tighter grids to eliminate these problems.[41,42]

The grid-free DFT approach can be extended to the computation of gradients as follows . The Hartree-Fock formalism for the derivative with respect to nuclear coordinate X_A for restricted closed shell non-complex wavefunctions is:

$$\frac{\partial E}{\partial X_A} = \left\langle \Psi \left| \frac{\partial H}{\partial X_A} \right| \Psi \right\rangle + 4 \sum_{i}^{occ} \left\langle \psi_i' \left| (\hat{V} + \hat{T} + \hat{J} - \hat{K}) - \varepsilon_i \right| \psi_i \right\rangle, \tag{16}$$

where $\psi_i' = \sum_{r}^{AO} C_{ri} \frac{\partial \chi_r}{\partial X_A}$

and the other operators and symbols have their usual meaning: operators $\hat{V}$=nuclear-electron attraction, $\hat{T}$=kinetic energy, $\hat{J}$=Coulomb, $\hat{K}$=exchange; χ=atomic orbitals, Ψ=molecular wavefunction, ψ=spin-orbitals, and ε_i=orbital energy. The sum of Eq. (16) is over occupied spin-orbitals. Only the exchange term $\hat{K}$ in the resulting integral

$$\int \left(\frac{\partial \chi_r}{\partial X_A} \right) \hat{K} \chi_s \, d\vec{r}, \tag{17}$$

must be modified to calculate DFT gradients. $\hat{K}$ is replaced with the DFT exchange-correlation term $\hat{K}^{DFT}$. If atomic orbital χ_r is not on atom A, then the derivative is zero, because χ_r has no dependence on the position of atom A. If χ_r is centered on atom A, then the nuclear coordinate X_A is replaced by the negative of the electronic coordinate x. This is because X_A appears in the gaussian basis function χ_r as $(x-X_A)$.

$$\int \left(\frac{\partial \chi_r}{\partial X_A} \right) \hat{K}^{DFT} \chi_s d\vec{r} = - \int \left(\frac{\partial \chi_r}{\partial x} \right) \hat{K}^{DFT} \chi_s d\vec{r} \tag{18}$$

The resolution of the identity is then applied, giving

$$\int \left(\frac{\partial \chi_r}{\partial X_A} \right) \hat{K}^{DFT} \chi_s d\vec{r} \approx - \sum_{m}^{Orthonormal} \int \left(\frac{\partial \chi_r}{\partial x} \right) \theta_m d\vec{r} \cdot \int \theta_m \hat{K}^{DFT} \chi_s d\vec{r}. \tag{19}$$

Evaluation of both integrals in Eq. (19) is possible, because these are related to dipole velocity and the DFT contribution to the Fock matrix. It is important to realize that this

approach is independent of the functional chosen. Once the grid-free gradients are implemented, they are available for all functionals for which single point energies are available. The resolution of the identity in Eq. (19) can introduce problems, if the basis set $\{\theta_m\}$ is inadequate. For example, the exchange-correlation contribution to a translation of the entire molecule in the x direction clearly must be zero:

$$\delta T_x = 4 \sum_i^{occ} \int \left(\sum_A^{atom} \frac{\partial \psi_i}{\partial X_A} \right) \hat{K}^{DFT} \psi_i \, d\vec{r} = -4 \sum_i^{occ} \int \left(\frac{\partial \psi_i}{\partial x} \right) \hat{K}^{DFT} \psi_i \, d\vec{r} = 0. \qquad (20)$$

With the application of the resolution of the identity, this becomes

$$\delta T = -4 \sum_i^{occ} \int \left(\frac{\partial \psi_i}{\partial x} \right) \hat{K}^{DFT} \psi_i \, d\vec{r} \approx -4 \sum_i^{occ\ orthonormal} \sum_m \int \left(\frac{\partial \psi_i}{\partial x} \right) \theta_m \, d\vec{r} \cdot \int \theta_m \hat{K}^{DFT} \psi_i \, d\vec{r} \quad (21)$$

which is not necessarily zero. This also applies to translations in the y and z directions, and to net rotations about the molecule's center of mass. These variances (which vanish in symmetric molecules), are projected out in GAMESS. This is done by summing all the contributions to a translation or torque and then subtracting it back out. This emphasizes the need for an adequate basis set $\{\theta_m\}$ to ensure that the resolution of the identity has been sufficiently converged. These variances are also present in the grid-based approach, but are reported not to occur in the X-α specific approach of Werpetinski and Cook.[25] The sizes of the variances δT_x, δT_y,δT_z,δR_x, δR_y,δR_z can be used as diagnostics for the adequacy of the basis set's capability to resolve the identity.

IIC. The Grid connection.

Now that the implementation of the grid-free approach is clearly laid out, it is worthwhile to examine its relationship to the grid based approach. Careful analysis reveals that the grid based approach may be thought of as a special case of the grid-free approach.

Consider the generic integral $\int\chi_i\, f(n_\alpha)\cdot g(n_\beta)\,\chi_j d\vec{r}$. An auxiliary basis set of non-overlapping normalized step functions $\{\theta_m\}$ is used for the resolution of the identity. The resolution of the identity as in Eq. (3), which is exact in a complete basis $\{\theta_m\}$, is applied, to give

$$\int\chi_i\, f(n_\alpha)\cdot g(n_\beta)\,\chi_j d\vec{r} \approx \sum_m \int\chi_i\, f(n_\alpha)\,\theta_m d\vec{r}\cdot\int\theta_m\, g(n_\beta)\,\chi_j d\vec{r}. \qquad (22)$$

The atomic orbitals $\{\chi\}$ are assumed to vary insignificantly over an individual step function θ_m, therefore the atomic orbitals act like step functions in the region of θ_m. This gives:

$$\int\chi_i\, f(n_\alpha)\cdot g(n_\beta)\,\chi_j d\vec{r} \approx \sum_m \xi_{i,m}\int\theta_m\, f(n_\alpha)\,\theta_m d\vec{r}\cdot\xi_{j,m}\int\theta_m\, g(n_\beta)\,\theta_m d\vec{r}, \qquad (23)$$

where $\xi_{i,m}$ is a grid-size weighted overlap. For a fine grid, this is the value of the orbital χ_i at the step function θ_m multiplied by the size of θ_m. Now, the matrix function representation in Eq. (8), which is exact in a complete basis $\{\theta\}$, is used. Because $M[f(n_\alpha)]$ and $M[g(n_\beta)]$ are diagonal in the θ basis, U=I in Eq. (8), so

$$\int\chi_i\, f(n_\alpha)\cdot g(n_\beta)\,\chi_j d\vec{r} \approx \sum_m \xi_{i,m}\xi_{j,m}\, f(\int\theta_m n_\alpha\,\theta_m d\vec{r})\cdot g(\int\theta_m n_\beta\,\theta_m d\vec{r}\,). \qquad (24)$$

If the grid of step functions is very tight, then the step function is a single grid point. This gives the integral in terms of a grid:

$$\int\chi_i\, f(n_\alpha)\cdot g(n_\beta)\,\chi_j d\vec{r} \approx \sum_m \xi_{i,m}\xi_{j,m}\, f(n_\alpha \text{ at grid point m})\cdot g(n_\beta \text{ at grid point m}). \qquad (25)$$

This is the grid based approach to evaluation of the integrals that arise in DFT.

III. Grid-Free DFT Results

IIIA. Functionals and methods

The grid-free approach outlined in Sections II and III is used to implement several DFT functionals in GAMESS:

1. Local exchange: X-α[1] which is exact in the limit of a uniform electron gas for

α=2/3. The more popular empirical value of α=0.7 is also available if no gradient correction to exchange is present.

2. Local correlation: VWN5[2,10] and the PW local,[43] which are designed to interpolate between the ferromagnetic limit and paramagnetic limit of the Ceperley and Alder[44] Monte Carlo results. The PW local approach is a newer more accurate fit that is reported to give overall better energetics and structures than the VWN fits.

3. Local exchange and correlation: three Wigner forms,[43,45,46,47] which are designed to model exchange and correlation simultaneously. These are modifications of the simple, yet effective, equation:

$$E_{xc} = \int \frac{C_1 n^{4/3}}{1 + C_2 n^{1/3}} d\vec{r}, \qquad (26)$$

which in the limit of C_2=0 is X-α. The Wigner form does not involve any terms that depend upon the spin-polarization $\xi=(n_\alpha - n_\beta)/(n_\alpha + n_\beta)$; therefore, the portion of correlation that results from α–β interaction is not included.

4. Gradient-corrected exchange: DePristo-Kress,[28] Becke88[48] and the CAMA[43] and CAMB[43] modifications to Becke88. These all multiply a local exchange term by functions of the dimensionless density gradient $y = |\nabla n| / n^{4/3}$. Becke88 is by far the most popular functional.

5. Closed-shell gradient-corrected correlation: LYP[49,50] which is designed to reformulate the correlation formulas of Colle and Salvetti[51] in terms of the electron density and the local kinetic energy density. This functional is not based upon adding a correction term to a local correlation functional.

Naturally, combinations of these functionals, such as BVWN with Becke88 exchange and VWN correlation are available to the user. Hybrid functionals such as mixing

half Hartree-Fock exchange and half Becke88 exchange are available also.

All comparisons presented below are made to the grid based DFT code in Gaussian 92/DFT[52]. A pruned (75,302) grid of approximately 7000 points per atom[53] is used, because looser grids gave off-axis dipole components for NH_3 and a net dipole moment for planar NH_3. Both GAMESS and Gaussian92/DFT calculate all non-exchange/correlation terms explicitly from Ψ, rather than from n and the dimensionless gradient y:

$$E = \int \left[C_{kinetic} n^{5/3} + C_{potential} n + C_{exchange} n^{4/3} \cdot f(y) \right] d\vec{r}, \text{ where } y = \left| \frac{\nabla n}{n^{4/3}} \right| \qquad (27)$$

as was done in older purely DFT implementations. The current implementation of grid-free DFT in GAMESS does not use an auxiliary basis set, so the same basis that is used for the LCAO expansion is also used for the resolution of the identity. Consequently, as the basis set size is increased, both the accuracy of the wavefunction and the accuracy of the resolution of the identity are increased. Of course, use of an auxiliary basis set for the resolution of the identity would be more efficient and will be implemented in a subsequent version.

IIIB. Energies of atoms

Small closed shell atoms provide a good initial test case. Absolute energies for atoms are calculated using even tempered uncontracted basis sets.[54,55] He, Be and Ne are studied here. As can be seen in Tables 1 and 2, the Slater functional (X-α with α=2/3) energy converges with relatively small basis sets. Tables 3-5 show that gradient corrected functionals require basis functions of one higher angular momentum quantum number, because of the resolution of the identity introduced in Eq. (13d). When i and j are on the same atom, the integral $\int \chi_i \frac{d}{dx} \chi_j d\vec{r}$ vanishes if i and j do not differ by exactly one in x angular momentum. Even though s functions on Ne provide a gradient correction to the p

functions, the addition of d functions greatly enhances the accuracy of the calculation, by providing an additional gradient correction as can be seen clearly in Table 5. Although adding d functions to helium would make the basis set more complete (and therefore make the resolution of the identity more exact), it would not improve the accuracy of the calculation, unless the functional includes second derivatives of the density. This is because the second derivative of the density would involve $\int \chi_i \frac{d^2}{dx^2} \chi_j d\vec{r}$ integrals and these vanish unless i and j have the same x angular momentum or differ by exactly two in x angular momentum.

IIIC. Energies and dipole moments of diatomics

The bond distances, dipole moments, and binding energies for CO and N_2 calculated with the B-null (Becke88 exchange, no correlation) functional using uncontracted even tempered basis sets[54,55] are given in Table 6. The isolated atoms are calculated using unrestricted wavefunctions. The basis sets used are 20s13p10d3f for N, 20s13p10d1f for C and 20s13p10d1f for O. The grid and grid-free results for both N_2 and CO are very comparable, differing by only 0.001Å. Both approaches predict CO dipole moments that are within 2% of each other. B-null overestimates the N_2 bond length compared to the experimental[56] value of 1.098Å, and underestimates the experimentally predicted[56] N_2 binding energy of 9.90eV. This functional also overestimates the CO bond length compared to the experimental value of 1.128Å,[57] and underestimates the experimentally predicted[58] CO binding energy of 11.1 eV. The sign of the CO dipole moment is predicted correctly (difficult to do[59,60]) and close to the experimental[61,62] value of 0.112 D.

IIID. Energies and dipole moments

Dipole moments and energies for H_2O and NH_3 are examined with B-null using correlation consistent[63] basis sets in Table 7. The water geometry is fixed at R(OH)=0.95781Å, θ(HOH)=104.4776°, and that of ammonia is fixed at R(NH)=1.012Å , A(HNH)=106.7°. As the basis set size increases, the dipole moments converge to the same answer. For the grid-free approach, a triple zeta basis set is necessary to adequately represent the resolution of the identity, based on the agreement of grid and grid-free approaches. A quadruple zeta basis for water and a pentuple zeta basis for ammonia is necessary to converge the dipole moment and energy. So, for these species, the resolution of the identity is converged with respect to basis set before the dipole moment is. These dipole moments are within 0.04 D of the experimentally observed[62] dipole moments of 1.85 D for H_2O and 1.47 D for NH_3.

IIIE. The ammonia bend potential

The bend potential of NH_3 was studied initially with the B-null exchange functional and the 6-311++G(3d,3p) basis set.[64] The N-H bond distance was constrained to the optimal X-α (α=2/3) value of 1.0496Å to match the previous work by Werpetinski and Cook.[22] Because the NH bond is optimized for the X-α functional, the gradient will never go to zero. The energy, net dipole moment, and root-mean-square (RMS) cartesian gradient at each point along the bend angle from 55° to 90° in 0.5° increments are presented in Figures 1-3, respectively. The dipole moments (Fig. 1) differ by no more than 0.116 D and 5.95%. The grid-free and grid based energies (Fig. 2) differ by 0.0606 Hartree, but the shapes of the surfaces are very similar (the standard deviation of the energy difference between the curves is 0.00073 h). This suggests that for this size basis set the grid-free

approach gives reliable relative energies, even though the absolute energies are too high. The RMS gradient is significantly different (Fig 3); this is probably a result of errors introduced by the resolution of the identity, particularly applying it to derivatives in Eq. (13) and (19). Uncontracting the 6-311++G(3d,3p) basis set improves the fitting of the resolution of the identity, and therefore the quality of the grid-free results. To further explore these issues, the systematic correlation consistent basis sets of Dunning are utilized.[63] The energy for basis sets that fail to adequately resolve the identity can be too low (Fig. 4). Therefore, just as an inadequate grid can give non-variational and erratic energies and properties, an inadequate basis set to represent the resolution of the identity can suffer from the same problem. Grid-free results for all but the cc-QZVP basis set give incorrectly shaped RMS gradient curves (Fig. 5). To further explore the resolution of the identity, the cc-TZVP basis set is systematically uncontracted (Fig. 6 and 7), because cc-TZVP gave the worst RMS gradient curves. By uncontracting the valence p shell on the nitrogen the resolution of the identities in Eq. (13) and (19) are more correctly represented. By further uncontracting the s shell on the hydrogen the resolution of the identity is better fit and the curves become more reasonable, although the minimum RMS gradient is mispositioned by five degrees.

IIIF. Electronic states of triatomics

The $^1A_1$ and $^3B_1$ states of CH_2[65] are compared in Table 8 for both B-VWN5 and Hartree-Fock using an aug-cc-pVTZ[63] basis set. The $^3B_1$ state is optimized with a restricted open shell wavefunction. Table 8 shows that a basis set that is well designed for modelling occupied molecular orbitals, is not necessarily well designed to converge the resolution of the identity. For CH_2, the aug-cc-pVTZ basis set is too contracted to adequately represent

the resolution of the identity. Uncontracting the s functions and then the p functions results in more sensible predicted properties. Additional sets of polarization functions (one set of more diffuse d's and one set of tighter d's on C and one set of more diffuse p's and one set of tighter p's on H), improves the resolution of the identity in Eq. (13) and (19). Results for the quadruple zeta basis set show a similar trend, with the additional polarization functions agreeing with the grid-based approach. Unlike Hartree-Fock, the B-VWN5 results agree with the experimentally observed splitting of 0.369-0.390eV (8.5-9.0 kcal/mol)[67], and the experimental geometries[66] of 1.11Å, 102° for $^1A_1$ and 1.07Å, 134° for $^3B_1$.

IIIG. Isomers of polyatomics

The geometries and energies of cyclopropane and propene[68] are compared in Table 9 using both Hartree-Fock and B-VWN5 with a 6-311++G(3d,3p) basis set[64]. Although the grid-free approach gives reasonable geometries, it badly underestimates the energy difference. By uncontracting the basis set, and thus increasing the accuracy of the resolution of the identity, the grid-free approach, gives reasonable geometries and energy differences. The experimental $\Delta H_{298..15}$ is about 1.7 eV, with zero point energy (ZPE) corrections predicted to be significant.[68] While direct comparison with experimental values is not entirely appropriate, both the grid based and the grid-free results appear to be poor.

IV. Conclusions

The grid-free approach to DFT provides an alternative to the grid based approach to DFT. The resolution of the identity[69] (especially for gradient corrected functionals and energy gradient calculations) requires a more accurate basis set than does the wavefunction.

The use of such large basis sets results in the calculation of a large number of two-electron integrals that are not otherwise needed. A more efficient approach will be to augment the atomic basis set with auxiliary functions only during the DFT part of the calculation. The vast knowledge base available for dealing with *wavefunction* basis set completeness in DFT[70] appears to be inadequate for addressing this issue, particularly for gradient corrected functionals. Previous work on auxiliary basis sets have dealt with the fitting of the $n^{1/3}$ X-α potential[71] or the Coulomb potential.[72] Little or no work has been done on fitting the gradient of the density as in Eq. (13) or fitting the resolution of the identity between the alpha density and the beta density as in Eq. (15).

Appendix A. Proof of equation 7

$\tilde{M}[f(n)]$ is in an orthonormal basis in which $\tilde{M}[n]$ is diagonal (i.e. $\tilde{M}[n]=\lambda$)

$$\tilde{M}[f(n)] = \tilde{M}\left[\sum_m \alpha_m n^m\right], \text{series expansion of the function}$$

$$= \sum_m \alpha_m \tilde{M}[n^m]$$

$$= \sum_m \alpha_m (\tilde{M}[n])^m, \text{by the resolution of the identity (exact in complete basis)}$$

$$= \sum_m \alpha_m \lambda^m, \text{ since } \tilde{M}[n] \text{ is diagonal}$$

$$\tilde{M}[f(n)] = f(\lambda)$$

This should not be confused with the commonly used relationship, which is true in any basis:

$$f(\tilde{M}[n]) = f(\lambda)$$

Appendix B. Approximate three-center approach

Expand the density in an orthonormal basis set:

$$M[n] \approx M\left[\sum_{m=1}^{K} C_m \theta_m\right]$$

$$M[n]_{i,j} = \int \chi_i \sum_{m=1}^{K} C_m \theta_m \chi_j d\vec{r}.$$

Because $\{\theta\}$ is orthonormal, the expansion coefficients are given by,

$$C_m = \int n \cdot \theta_m d\vec{r}.$$

$$C_m = \sum_{r,s}^{AO} D_{r,s} \int \chi_r \chi_s \theta_m d\vec{r}.$$

Substituted into $M[n]_{i,j}$ gives:

$$M[n]_{i,j} = \int \chi_i \sum_{m=1}^{K} \left(\sum_{r,s}^{AO} D_{r,s} \int \chi_r \chi_s \theta_m d\vec{r} \right) \theta_m \chi_j d\vec{r},$$

which rearranges to give:

$$M[n]_{i,j} = \sum_{r,s}^{AO} \sum_{m=1}^{K} D_{r,s} \int \chi_i \chi_j \theta_m d\vec{r} \cdot \int \theta_m \chi_r \chi_s d\vec{r},$$

Which is equivalent to just applying the resolution of the identity.

Appendix C. X-α Functional Energy

For the closed shell $X-\alpha$ functional f, with molecular orbitals ψ.

$$\hat{K}_{u,v}^{DFT} = \int \psi_u \psi_v \frac{\partial f}{\partial n} d\vec{r}$$

$$\hat{K}_{u,v}^{DFT} = C_\alpha \tfrac{4}{3} \int \psi_u \psi_v n^{1/3} d\vec{r}$$

Forming the dot product of the DFT fock matrix with the diagonal density matrix yields:

$$\hat{K}^{DFT} \bullet D = \sum_{u}^{occupied} 2 \cdot C_\alpha \tfrac{4}{3} \int \psi_u \psi_u n^{1/3} d\vec{r}$$

$$\hat{K}^{DFT} \bullet D = C_\alpha \tfrac{4}{3} \int n^{4/3} d\vec{r}$$

$$\hat{K}^{DFT} \bullet D = \tfrac{4}{3} \cdot E^{DFT}$$

This is not the DFT energy.

References

1. J.C. Slater, Adv. Quant. Chem. **6**, 1 (1972).

2. S.H. Vosko, L. Wilk and M. Nusair, Can. J. Phys. **58**, 1200 (1980).

3. D.C. Langreth and M.J. Mehl, Phys. Rev. B **28**, 1909 (1983).

4. M. Rasolt and D.J.W. Geldhart, Phys. Rev. B **34**, 1325 (1986).

5. P. Hohenberg and W. Kohn, Phys. Rev. **136** B864 (1964).

6. J.P. Perdew, K. Burke and M. Ernzerhof, J. Chem. Phys. **105**, 9982 (1996).

7. A.D. Becke, J. Chem. Phys. **104**, 1040 (1996).

8. B.I. Dunlap, Chem. Phys. **125**, 89 (1988).

9. B.I. Dunlap, Phys. Rev. A **19**, 2902 (1984).

10. B.G. Johnson, P.M.W. Gill and J.A. Pople, J. Chem. Phys. **98**, 5612 (1993).

11. G.E. Scuseria, J. Chem. Phys. **97**, 7528 (1992).

12. T.G. Wright, J. Chem. Phys. **105**, 7579 (1996).

13. S. Gronert, G.N. Merrill and S.R. Kass, J. Org. Chem. **60**, 488 (1995).

14. H.M. Sulzbach, H.F. Schaefer III, W. Klopper and H.P. Lüthi, J. Am. Chem. Soc. **118**, 3519 (1996).

15. R.G. Parr and W. Wang, Section 3 of *Density-Functional Theory of Atoms and Molecules* (Oxford, New York, 1989).

16. A.I.M. Rae, Chem. Phys. Lett. **18**, 574 (1972).

17. B.G. Johnson, C.A. Gonzales, P.M.W. Gill and J.A. Pople, Chem. Phys. Lett. **221**, 100 (1994).

18. V.I. Lebedev, Zh. Vychisl. Mat. Mat. Fiz. **15**, 48 (1975).

19. V.I. Lebedev, Zh. Vychisl. Mat. Mat. Fiz. **16**, 293 (1975).

20. P.M.W. Gill, B.G. Johnson, J.A. Pople and M.J. Frisch, Chem. Phys. Lett. **197**, 499 (1992).

21. B.I. Dunlap, J. Phys. Chem. **90**, 5524 (1986).

22. K.S. Werpetinski and M. Cook, Phys. Rev. A **52**, R3397 (1995).

23. Y.C. Zheng and J. Almlöf, Chem. Phys. Lett. **214**, 397 (1993).

24. Y.C. Zheng and J. Almlöf, J. Mol. Struct. (Theochem) **288**, 277 (1996).

25. K.S. Werpetinski and M. Cook, J. Chem. Phys. **106**, 7124 (1997).

26. M.W. Schmidt, K.K. Baldridge, J.A. Boatz, S.T. Elbert, M.S. Gordon, J.H. Jensen, S. Koseki, N. Matsunaga, K.A. Nguyen, S. Su, T.L. Windus, M. Dupuis, and J.A. Mongomery Jr., J. Comp. Chem. **14**, 1347 (1993).

27. O. Vahtras, J. Almlöf and M.W. Feyereisen, Chem. Phys. Lett. **213**, 514 (1993).

28. A.E. DePristo and J.D. Kress, J. Chem. Phys. **86**, 1425 (1987).

29. B.A. Hess, R.J. Buenker and P. Chandra, Int. J. of Quant. Chem. **29**, 737 (1986).

30. S. Obara and A. Saika, J. Chem. Phys. **84**, 3963 (1986).

31. A.M. Köster, J. Chem. Phys. **104**, 4114 (1996).

32. W. von Niessen, Theoret. chim. Acta. (Berl) **27**, 9 (1972).

33. W. von Niessen, J. Chem. Phys. **56**, 4290 (1971).

34. J. Almlöf in *Modern Electron Structure Theory Part 1*, edited by D.R. Yarkony (World Scientific Publishing, River Edge NJ, 1995).

35. F. Herman, I.B. Ortenburger and J.P. van Dyke, Int. J. Quant. Chem. **IIIS**, 827 (1970).

36. R. Neumann and N.C. Handy, Chem. Phys. Lett. **266**, 16 (1997).

37. K. Kobayashi, N. Kurita, H. Kumahora and K. Tago, Phys. Rev. A **43**, 5810 (1991).

38. R. Fournier, J. Chem. Phys. **92**, 5422 (1990).

39. J.P. Perdew and Y. Wang, Phys. Rev. B **45**, 13244 (1992).

40. B.G. Johnson, P.M.W. Gill and J.A. Pople, Chem. Phys. Lett. **220**, 377 (1994).

41. J. Baker, J. Andzelm, A. Scheiner, and B. Delley, J. Chem. Phys. **101**, 8894 (1994).

42. V. Termath, D.J. Tozer and N.C. Handy, Chem. Phys. Lett. 228, 239 (1994).

43. Eq. (4) and (5) of Q. Zhao and R.G. Parr, Phys. Rev. A **46**, R5320 (1992).

44. D.M. Ceperley and B.J. Alder, Phys. Rev. Lett. **45**, 466 (1980).

45. Eq. (24) of G.J. Laming, V. Termath and N. Handy, J. Chem. Phys. **99**, 8765 (1993).

46. E.P. Wigner, Phys. Rev. 46, 1002 (1934).

47. E.P. Wigner, Trans. Faraday. Soc. 34, 678 (1938).

48. A.D. Becke, Phys. Rev. A **38**, 3098 (1988).

49. B. Miehlich, A. Savin, H. Stoll and H. Preuss, Chem. Phys. Lett. **157**, 200 (1989).

50. C. Lee, W. Yang and R.G. Parr, Phys. Rev. B **37**, 785 (1988).

51. R. Colle and D. Salvetti, Theor. Chim. Acta **37**, 329 (1975).

52. Gaussian 92/DFT, Revision G.3, M.J. Frisch, G.W. Trucks, H.B. Schlegel, P.M.W. Gill, B.G. Johnson, M.W. Wong, J.B. Foresman, M.A. Robb, M.Head-Gordon, E.S. Replogle, R. Gomperts, J.L. Andres, K. Raghavachari, J.S. Binkley, C. Gonzalez, R.L. Martin, D.J. Fox, D.J. Defrees, J. Baker, J.J P. Stewart, and J.A. Pople, Gaussian, Inc., Pittsburgh PA, 1993.

53. Int=FineGrid and SCF=tight. It is worth noting that this is the default grid in Gaussian 94.

54. M.W. Schmidt and K. Ruedenberg, J. Chem. Phys. **71**, 3951 (1979).

55. Exponents for higher angular momentum (d,f) were generated using the outermost shell exponents.

56. K.P. Huber and G. Herzberg, Constants of Diatomic Molecules, Van Nostrand Reinhold, New York, 1979.

57. D. Sundholm, P. Pyykko and L. Laaksonen, Mol. Phys. **56**, 1411 (1985).

58. L.A. Curtiss, K. Raghavachari,G.W. Trucks and J.A. Pople, J. Chem. Phys. **94**, 7221 (1991).

59. X.W. Fan, X.J. Chen, S.J. Zhou, Y. Zheng, C.E. Brion, R. Frey and E.R. Davidson, Chem. Phys. Lett. **276**, 346 (1997).

60. M.P.C.M. Krijn and D. Feil, Chem. Phys. Lett. **150**, 45 (1988).

61. J.S. Muenter, J. Mol. Spectrosc. **55**, 490 (1975).

62. Handbook of Chemistry and Physics, edited by D.R. Lide, 72nd ed (CRC, Boca Raton, FL, 1991).

63. T.H. Dunning, Jr., J. Chem. Phys. **90**, 1007 (1989).

64. R. Krishnan, J.S. Binkley, R. Seeger and J.A. Pople, J. Chem. Phys. **72**, 650 (1980).

65. N. Matsunaga, S. Koseki and M.S. Gordon, J. Chem. Phys. **104**, 7988 (1996).

66. A.R.W. McKellar, P.R. Bunker, T.J. Sears, K.M. Evenson, R.J. Saykally and S.R. Langhoff, J. Chem. Phys. **79**, 5251 (1983).

67. D.G. Leopold, K.K. Murray, A.E. Stevens Miller and W.C. Lineberger, J. Chem. Phys. **83**, 4849 (1985).

68. K.-N. Fan, Z.-H. Li, W.-H. Li, W.-N. Wang, H.-H Huang and W. Huang, Chem. Phys. Lett. **277**, 257 (1997).

69. In this work, Eq. (3b), (7), (13c), and (19).

70. J.M. Martell, J.D. Goddard and L.A. Eriksson, J. Phys. Chem. A **101**, 1927 (1997).

71. N. Godbout, D.R. Salahub, J. Andzelm and E. Wimmer, Can. J. Chem. **70**, 560 (1992).

72. K. Eichkorn, O. Treutler, H. Öhm, M. Häser and R. Ahlrichs, Chem. Phys. Lett. **240**, 283 (1995).

Acknowledgements

This work was supported in part by grants from the Air Force Office of Scientific Research (F49-620-95-1-0073) and by the Ames Laboratory, US-DOE. The authors would like to thank Dr. Mike Schmidt for many enlightening conversations. We would also like to thank the late Professor Jan Almlöf and Mr. Y. C. Zheng for providing us with an early version of the grid-free code in SUPERMOLECULE for comparisons to the GAMESS grid-free code.

Table 1: He energies in Hartrees with the Slater exchange functional

Basis Set	Hartree-Fock	Grid	Grid-Free
5s	-2.858589	-2.719253	-2.722985
10s	-2.861647	-2.723547	-2.723952
15s	-2.861679	-2.723630	-2.723731
20s	-2.861680	-2.723638	-2.723674

Table 2: Be energies in Hartrees with the Slater exchange functional

Basis Set	Hartree-Fock	Grid	Grid-Free
5s	-14.479361	-14.131597	-14.156690
10s	-14.571727	-14.221960	-14.224846
15s	-14.572985	-14.223236	-14.223890
20s	-14.573021	-14.223284	-14.223487
25s	-14.573023	-14.223289	-14.223369

Table 3: He energies in Hartrees with the Becke88 exchange functional

Basis Set	Grid	Grid-Free (+1p)	Grid-Free (+3p)	Grid-Free (+5p)	Grid-Free (+10p)	Grid-Free (+15p)	Grid-Free (+20p)
5s	-2.859231	-2.801225	-2.845034	-2.857012			
10s	-2.863302	-2.797241	-2.848139	-2.860223	-2.863275		
15s	-2.863373	-2.796592	-2.846943	-2.860447	-2.862979	-2.863351	
20s	-2.863378	-2.796338	-2.846451	-2.858871	-2.862903	-2.863271	-2.863366

Table 4: Be energies in Hartrees with the Becke88 exchange functional.

Basis set	Grid	Grid-Free (+1p)	Grid-Free (+3p)	Grid-Free (+5p)	Grid-Free (+10p)	Grid-Free (+15p)	Grid-Free (+20p)	Grid-Free (+25p)
10s	-14.564943	-14.415043	-14.500901	-14.541349	-14.565649			
15s	-14.566296	-14.417206	-14.502231	-14.540217	-14.564638	-14.566347		
20s	-14.566353	-14.415954	-14.502004	-14.538576	-14.564523	-14.565936	-14.566589	
25s	-14.566362	-14.414982	-14.501644	-14.537827	-14.564432	-14.565804	-14.566240	-14.566420

Table 5: Neon energies in Hartrees with the Becke88 exchange functional.

Basis set	Grid	Grid-Free (+0d)	Grid-Free (+1d)	Grid-Free (+3d)	Grid-Free (+5d)	Grid-Free (+10d)
10s10p	-128.580485	-128.337180	-128.424312	-128.538924	-128.578138	-128.584228
15s10p	-128.589469	-128.351221	-128.436205	-128.548799	-128.582479	-128.588480
15s15p	-128.589771	-128.352051	-128.438204	-128.549564	-128.583082	-128.589235
20s10p	-128.589749	-128.353294	-128.438981	-128.549593	-128.582621	-128.588607
20s15p	-128.590051	-128.354483	-128.440131	-128.550023	-128.583751	-128.589404
20s20p	-128.590069	-128.354434	-128.440120	-128.548917	-128.583121	-128.589297
25s10p	-128.589767	-128.354170	-128.440521	-128.549615	-128.582726	-128.588583
25s15p	-128.590069	-128.355356	-128.441362	-128.550457	-128.583821	-128.589407
25s20p	-128.590087	-128.355502	-128.441220	-128.548636	-128.583303	-128.589306
25s25p	-128.590090	-128.355500	-128.441166	-128.548669	-128.583157	-128.589280

Table 6: CO and N_2 results with the Becke88 functional

Atomic and Molecular Energies (Hartree)	Grid	Grid-Free
C	-37.69044	-37.68825
O	-74.83315	-74.82951
CO	-112.87314	-112.87204
N	-54.40088	-54.40026
N_2	-109.08620	-109.08526
Binding Energies (eV)		
N_2	7.68	7.75
CO	9.51	9.64
Bond Lengths (Å)		
CO	1.147	1.148
N_2	1.113	1.113
Dipole Moments (Debye)		
CO	0.1655	0.1621

Table 7: NH_3 and H_2O dipole moments with the Becke88 functional

	H_2O grid-free	H_2O grid dipole	NH_3 grid-free	NH_3 grid
cc-VDZ	1.6675 D	1.8016 D	1.3818 D	1.5027 D
cc-VTZ	1.8415 D	1.8379 D	1.4935 D	1.5084 D
cc-VQZ	1.8057 D	1.8086 D	1.4912 D	1.4832 D
cc-VPZ	1.8140 D	1.8099 D	1.4690 D	1.4661 D

Table 8: CH_2 geometry optimizations with B-VWN5 functional

	Singlet energy (hartree)	Singlet bond distance(Å)	Singlet HCH Angle	Triplet energy (hartree)	Triplet bond distance(Å)	Triplet HCH Angle	Splitting (eV)
aug-cc-pVTZ Basis							
Hartree-Fock	-38.89271	1.096	103.6°	-38.93268	1.070	129.5°	-1.09
Grid	-39.37803	1.115	101.0°	-39.39197	1.079	134.0°	-0.38
Grid-Free	-39.45045	1.411	60.5°	-39.45521	1.253	82.3°	-0.13
Uncontracted S							
Grid	-39.37888	1.115	101.0°	-39.39271	1.079	133.9°	-0.38
Grid-Free	-39.23749	1.134	93.8°	-39.26604	1.079	136.6°	-0.78
Uncontracted							
Grid	-39.37895	1.115	101.0°	-39.39276	1.079	133.9°	-0.38
Grid-Free	-39.34417	1.121	98.8°	-39.35817	1.081	134.6°	-0.38
+2 more polarization							
Grid	-39.38012	1.114	101.2°	-39.39319	1.079	134.0°	-0.36
Grid-Free	-39.35578	1.119	100.0°	-39.36999	1.080	135.3°	-0.39
aug-cc-pVQZ Basis							
Grid	-39.38232	1.113	101.4°	-39.39567	1.079	134.0°	-0.36
Grid-Free	-39.31940	1.111	102.7°	-39.33494	1.079	134.2°	-0.42
Uncontracted							
Grid	-39.38243	1.113	101.4°	-39.39577	1.079	134.1°	-0.36
Grid-Free	-39.36437	1.122	98.7°	-39.37746	1.081	132.5°	-0.36
+2 more polarization							
Grid-Free	-39.37065	1.115	101.1°	-39.38426	1.079	133.8°	-0.37

Table 9: C_3H_6 geometry optimizations with B-VWN5 functional

	Propene energy (hartree)	Propene C=C bond distance (Å)	Propene C-C bond distance (Å)	Cyclopropane energy (hartree)	Cyclopropane C-C bond distance (Å)	Cyclopropane H-C bond distance (Å)	Energy Difference (eV)
Hartree-Fock	-117.108688	1.317	1.511	-117.096518	1.498	1.073	-0.33
Grid	-118.604631	1.338	1.524	-118.588178	1.521	1.083	-0.45
Grid-Free	-118.457918	1.328	1.544	-118.456606	1.544	1.084	-0.04
Uncontracted							
Grid	-118.607912	1.339	1.524	-118.591789	1.520	1.083	-0.44
Grid-Free	-118.540559	1.339	1.526	-118.523173	1.525	1.088	-0.47

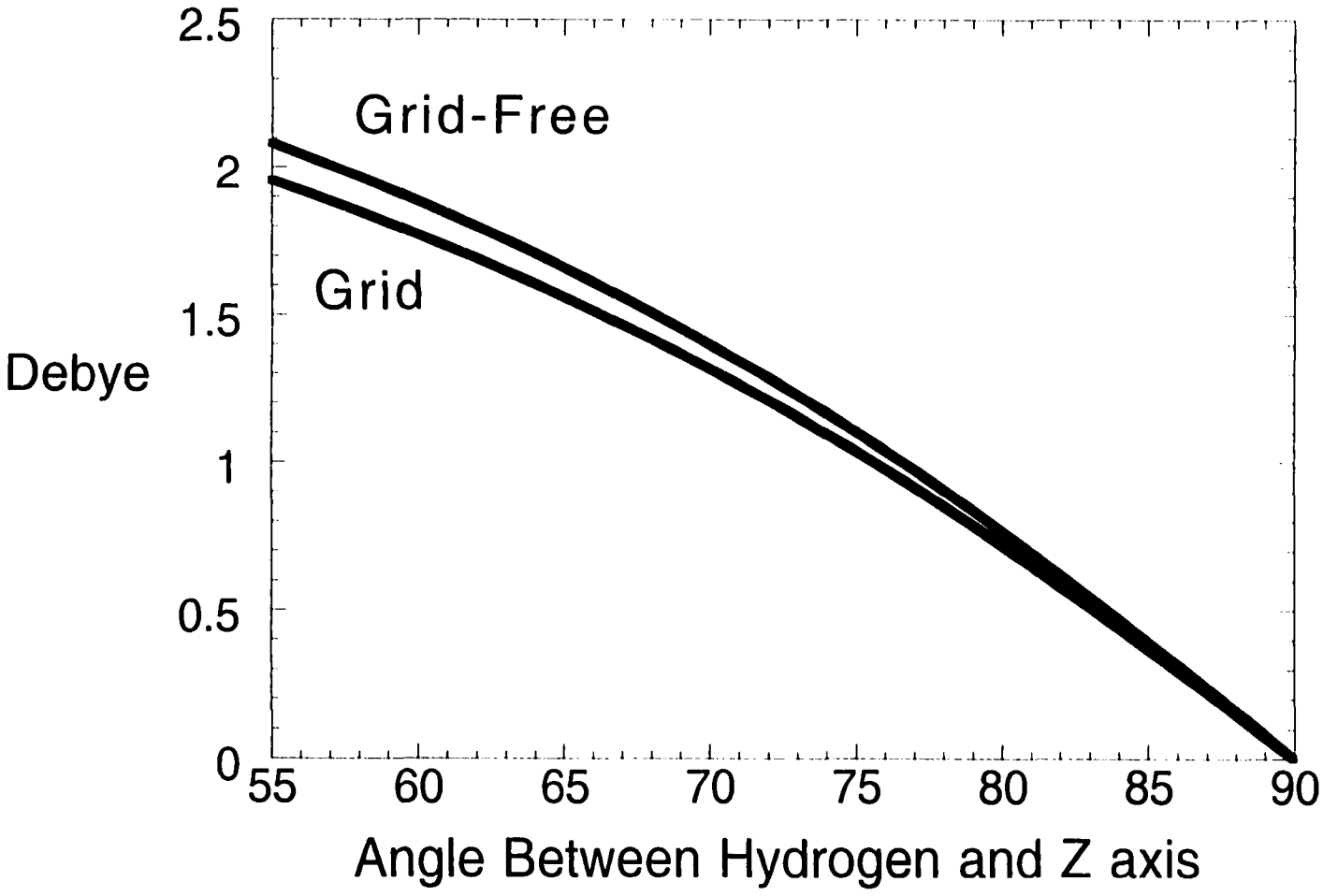

Figure 1: NH3 dipole with the Becke88 and 6-311++G(3d,3p)

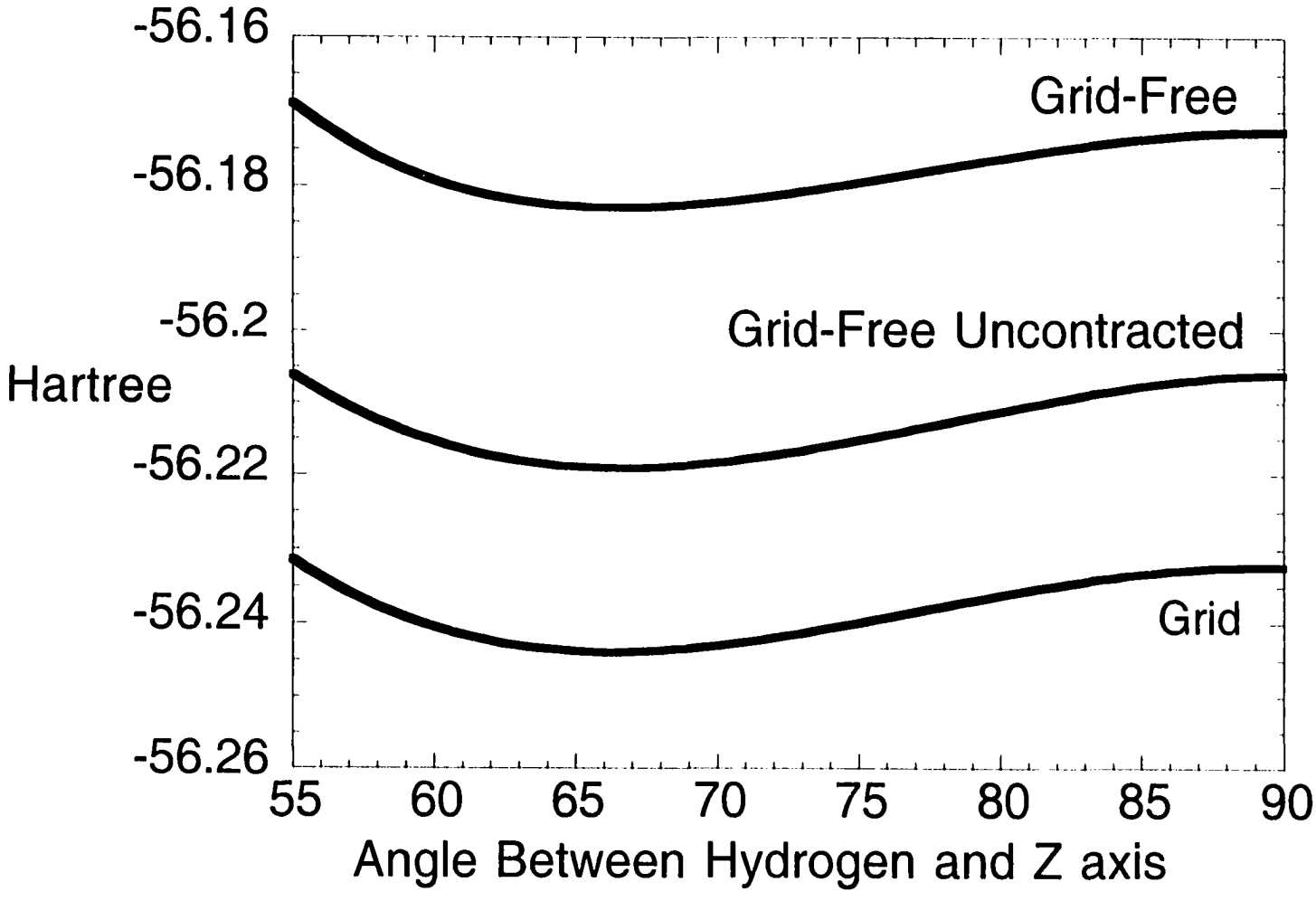

Figure 2: NH3 bend potential with the Becke88 and 6-311++G(3d,3p)

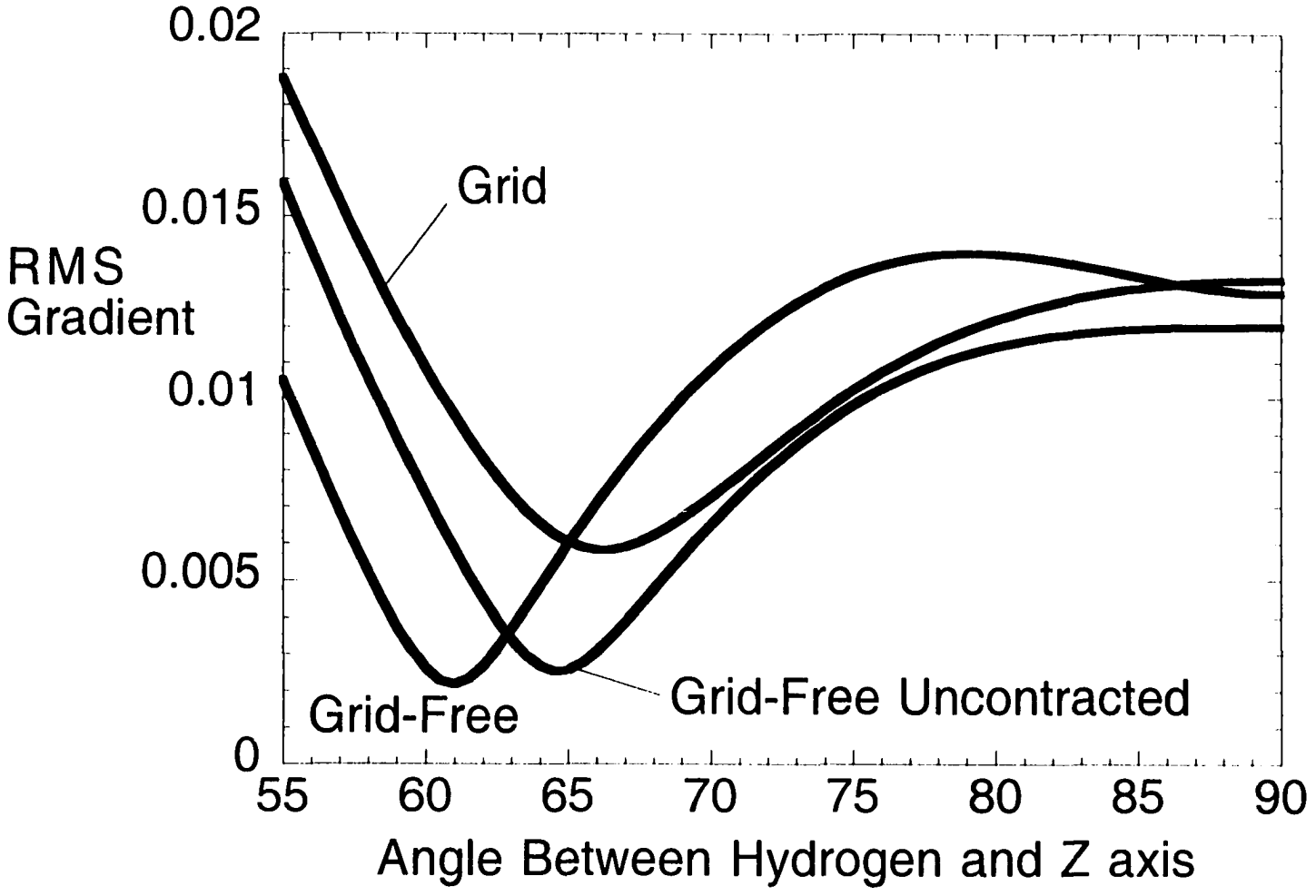

Figure 3: NH3 RMS gradient with the Becke88 and 6-311++G(3d,3p)

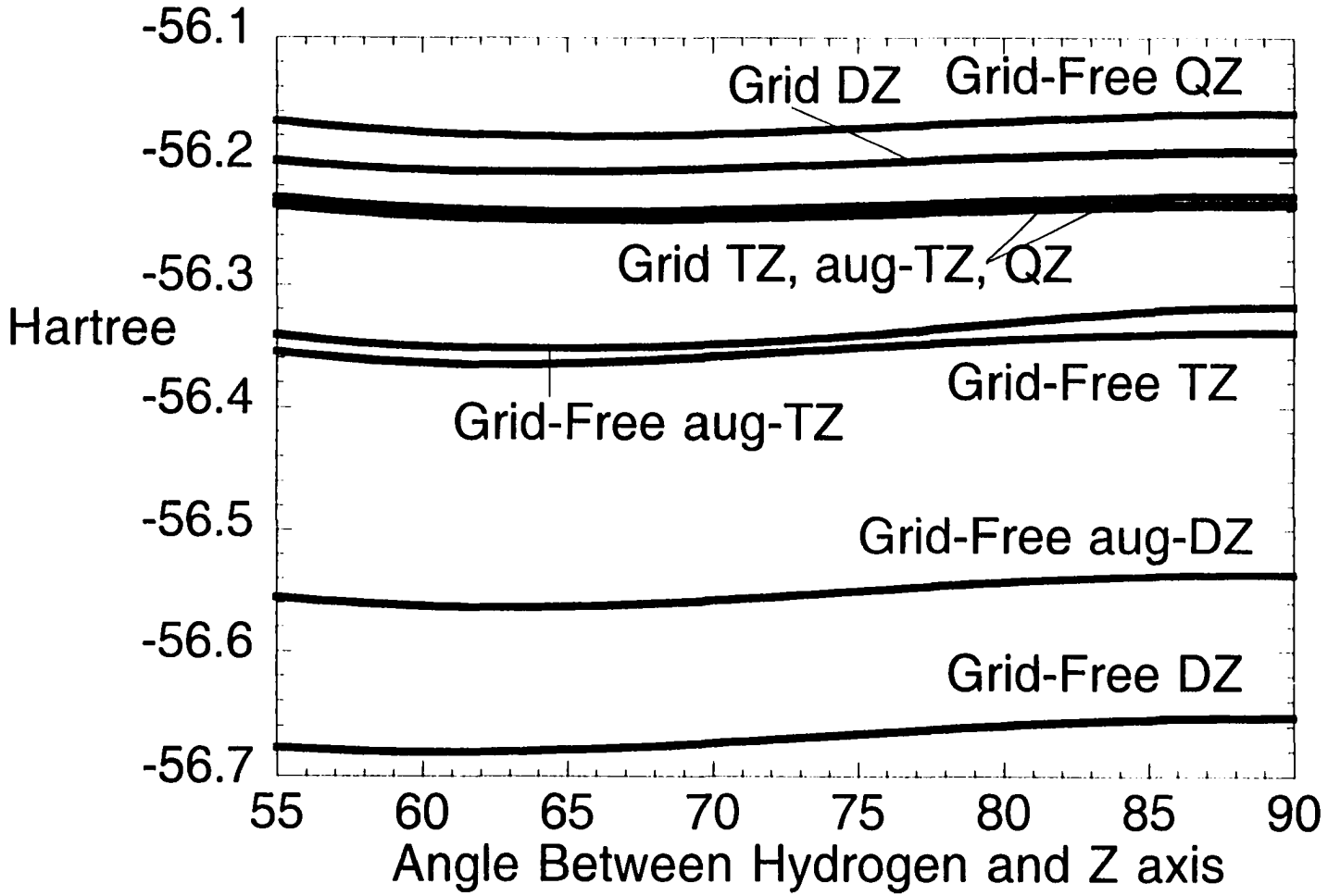

Figure 4: NH3 bend potential with the Becke88 functional

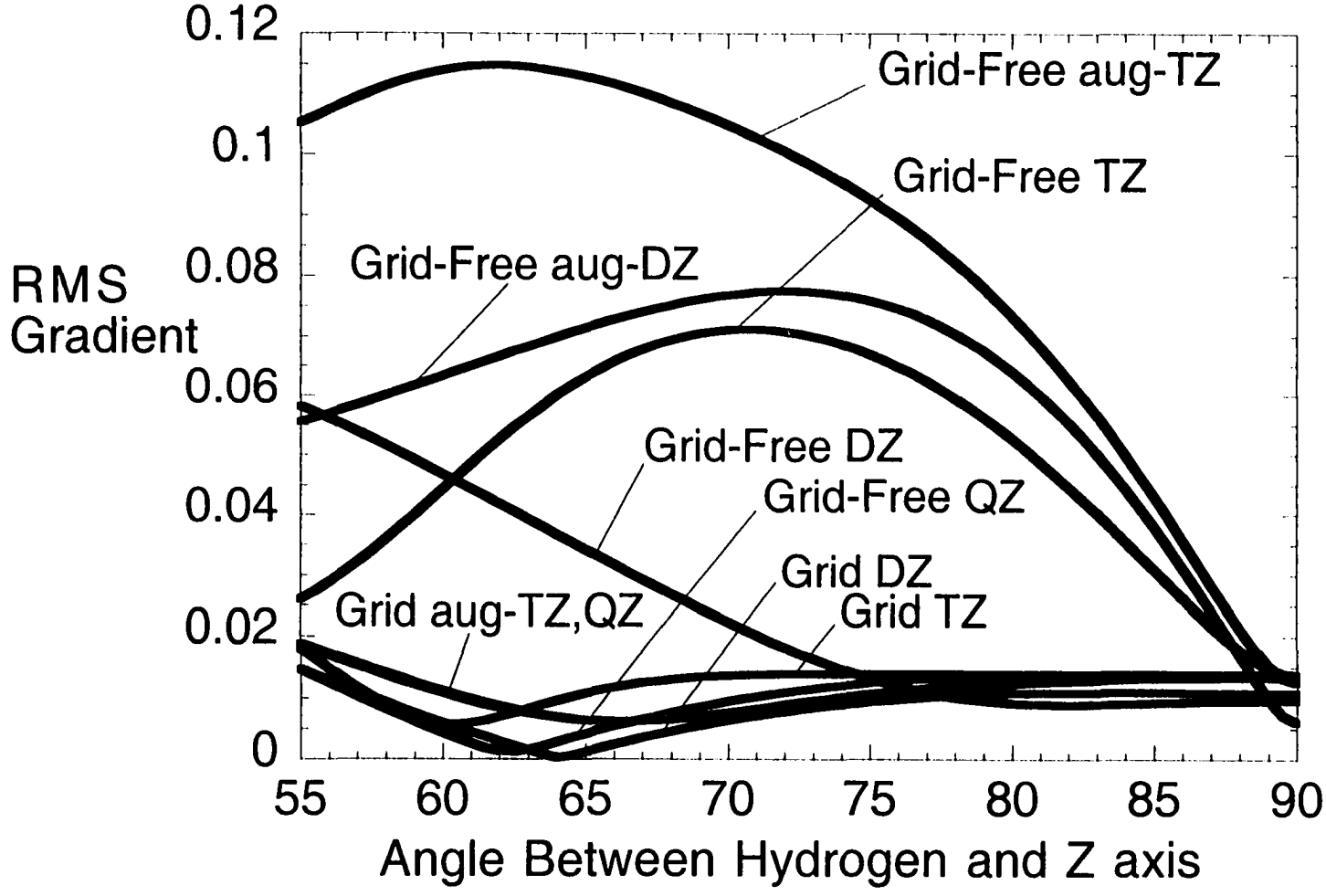

Figure 5: NH3 RMS gradient with the Becke88 functional and correlation consistent basis sets

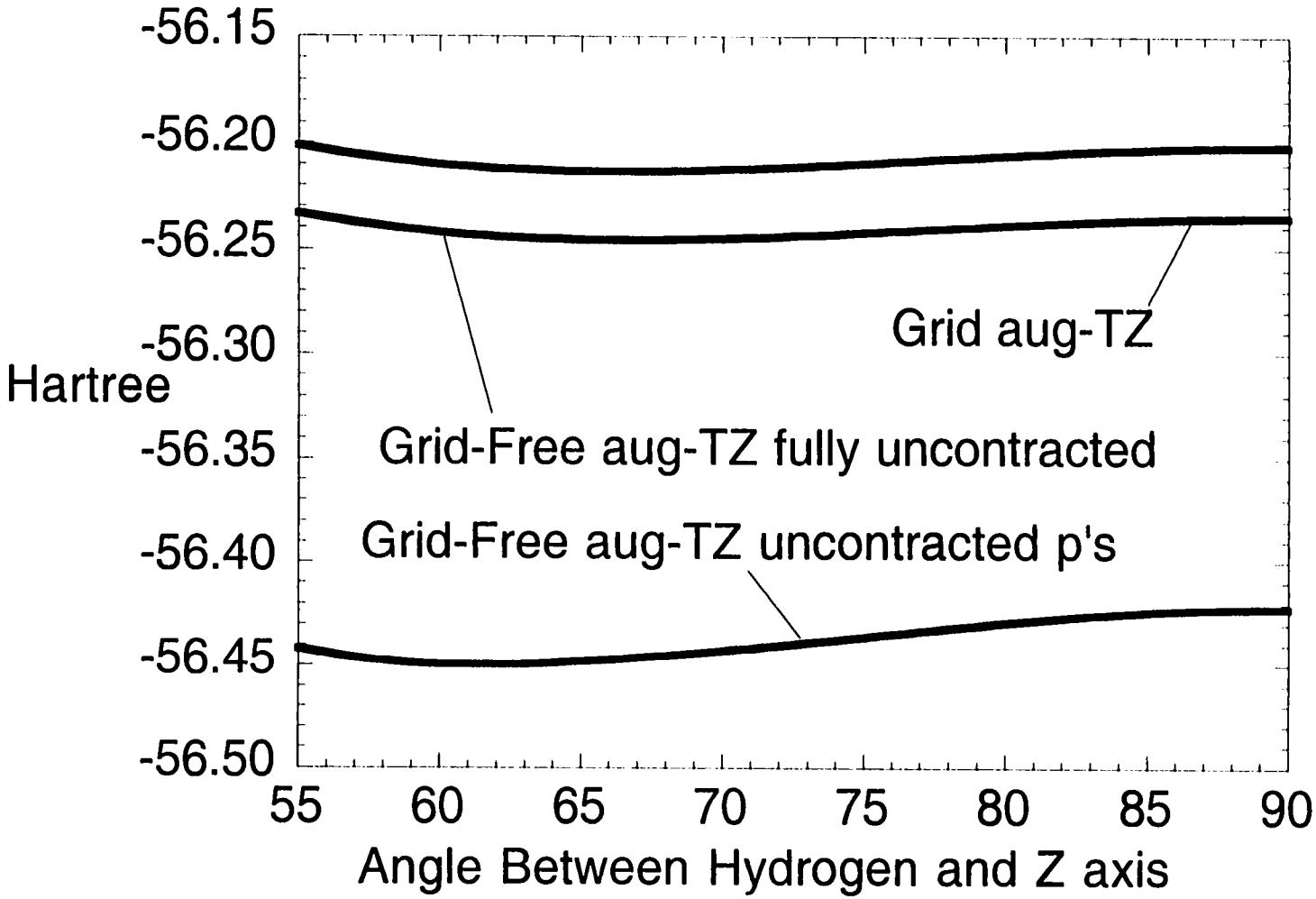

Figure 6: NH3 Energy with the Becke88 functional and correlation consistent basis sets

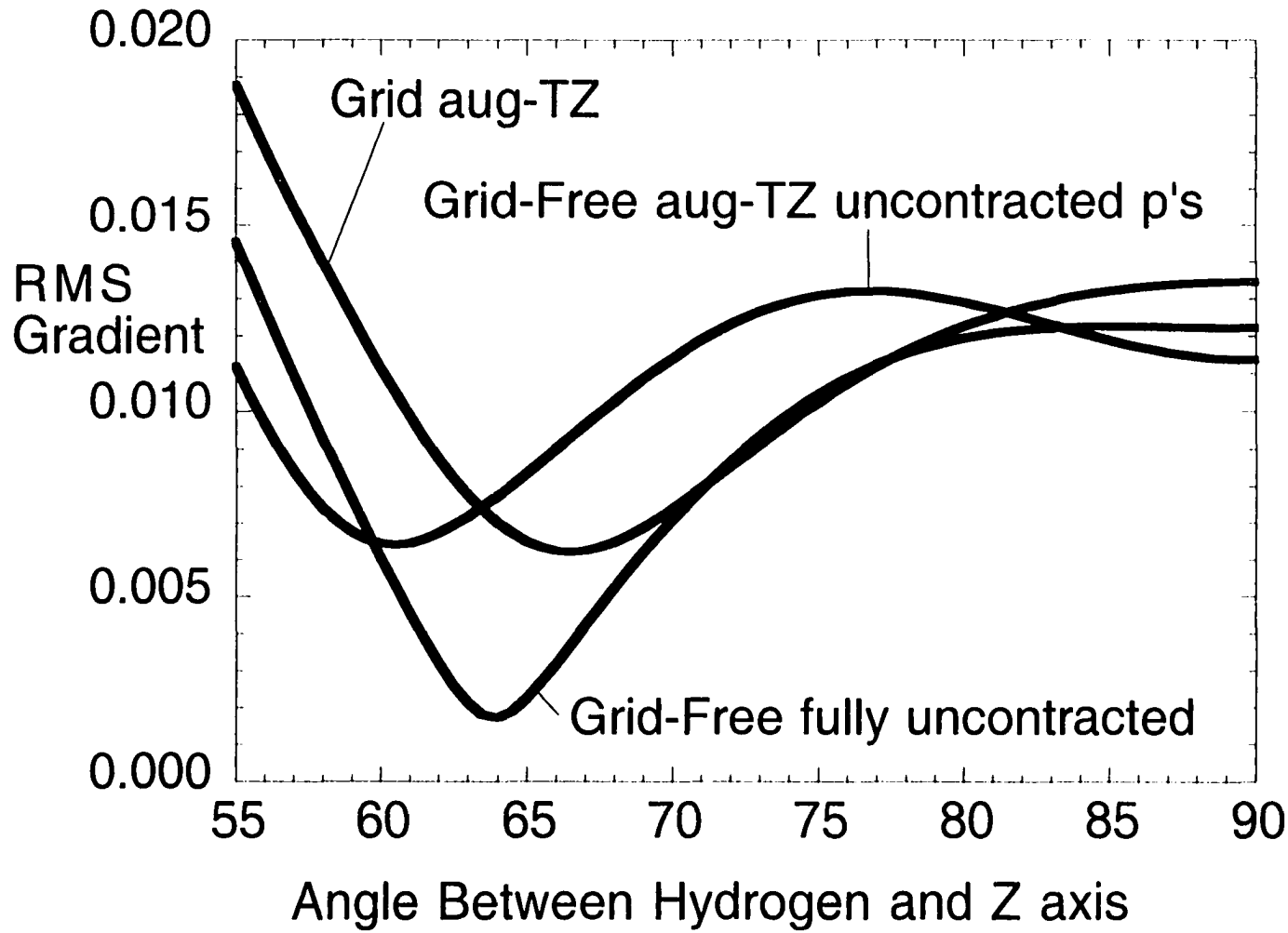

Figure 7: NH3 RMS gradient with the Becke88 functional and correlation consistent basis sets

CHAPTER 3: EVALUATION OF GRADIENT CORRECTIONS IN GRID-FREE DENSITY FUNCTIONAL THEORY

A paper submitted to the Journal of Chemical Physics

Kurt R. Glaesemann and Mark S. Gordon

Abstract

The Almlöf–Zheng approach to grid-free density functional theory (DFT) uses the resolution of the identity (RI) instead of a finite grid to evaluate the integrals. Application of the RI can lead to stability problems, particularly when gradients are involved. The focus of the current work is on choosing a stable method of evaluating the gradient correction using the RI. A stable method is compared to several unstable methods.

I. Introduction.

In recent years, density functional theory (DFT), formulated in terms of the spin densities (n_α, n_β), has gained popularity as an alternative to *ab initio* wavefunctions for determining molecular properties and structures. Functionals were originally fit to the uniform electron gas,[1,2] but accurate energetics usually require density gradient terms.[3,4,5,6,7,8] Integrals over density functionals are generally complicated; therefore, the standard procedure is to evaluate the integrals using a numerical grid:

$$\int_{\text{All space}} f(n_\alpha, n_\beta, \nabla n_\alpha, \nabla n_\beta)d\vec{r} \approx \sum_{i}^{\text{Grid points}} f(n_\alpha(i), n_\beta(i), \nabla n_\alpha(i), \nabla n_\beta(i)) \triangle \vec{r}(i). \qquad (1)$$

One grid–free approach has been developed as an alternative to the standard grid–based approach specifically for the uniform electron gas-based X–α exchange functional.[9,10,11] Other functionals require the more general approach proposed by Almlöf

and Zheng (AZ).[12,13,14,15,16] Both grid–free approaches involve approximations of their own. The AZ grid–free approach is based on the resolution of the identity (RI).[17] The primary focus of the current work is on properly treating density gradient terms within the AZ approach. In Section II the AZ approach is discussed; the resulting derivations demonstrate the need for careful application of the RI.

II. A Grid–Free approach to gradient corrected DFT.

The initial integral simplification uses the RI. Consider the product of two arbitrary functions, f and g. The RI can be utilized as follows, with $\{\chi\}$ being an arbitrary basis set and $\{\theta_m\}$ being a set of orthonormal functions:

$$\int \chi_i \, f \cdot g \, \chi_j \, d\vec{r} \approx \sum_m \int \chi_i \, f \, \theta_m \, d\vec{r} \cdot \int \theta_m \, g \, \chi_j \, d\vec{r} \qquad (2)$$

The foregoing expression is exact only if $\{\theta_m\}$ completely spans the f•g function space (which is often smaller than a complete basis).[15,16,18] One should therefore expect dependence of the calculation on the size of the $\{\theta_m\}$ basis set; the molecular orbitals are usually an inadequate basis.[15,18] The functions f and g must also be "well–behaved" in order for the decomposition in Eq. (2) to be reliable. A well-behaved function is single-valued and defined in the entire relevant space. The relevant space of functions of n is $\{0 \ldots \infty\}$, and of functions of the spin polarization $\zeta=(n_\alpha-n_\beta)/(n_\alpha+n_\beta)$ is $\{-1 \ldots 1\}$. For example, consider decomposing the well–behaved function $f•g=1$ into $f=x^2-1$ and the poorly behaved $g=1/(x^2-1)$. $f=x^2-1$ is smooth and defined over all space. For $g=1/(x^2-1)$, the limit as x approaches +1 is ∞ from the left and $-\infty$ from the right. Another example of a poorly behaved function is $h=\sin(1/n)$, because h oscillates wildly as n approaches zero.

Application of the RI in Eq. (2) to DFT integrals will leave integrals involving functions of the spin–densities and the density gradient. The "spectral" resolution of the identity is used,[19] to evaluate these integrals. This method (see Eq. (3) below) assumes that the matrix of integrals over the density has been transformed to an orthonormal basis set in which this matrix is diagonal. No generality is lost, since this is just a basis transformation. The function of the integral is assumed to be the integral of the function:

$$\int \theta_i f(n) \theta_j d\vec{r} \approx f\left(\int \theta_i n \theta_j \, d\vec{r} \right) = f(\lambda_i)\delta_{ij} \qquad (3)$$

where λ_i is an eigenvalue of the matrix $M[n]_{ij} = \int \theta_i \; n \; \theta_j \; d\vec{r}$. Eq. (3) is exact in a complete basis, provided f is well–behaved.[15] In DFT, n is the density, although Eq. (3) does not assume this. Therefore, once the integrals over n are determined, the integrals over any well–behaved function of n can be readily obtained.

The more popular DFT functionals involve terms that depend upon the gradient of the density, to allow for "non-local" effects. The 1988 exchange functional of Becke:[20]

$$[B88X] = n^{4/3} \frac{-c_1 y^2}{1 + 6 \cdot c_1 \cdot y \cdot \sinh^{-1} y}, \; c_1 = 0.0042, \qquad (4)$$

like many functionals, is a function of the dimensionless density gradient $y = |\nabla n| / n^{4/3}$ or $y^2 = (\nabla n)^2 / n^{8/3}$.

There are many different ways to apply Eq. (2) and (3) to calculate the gradient corrections. The AZ papers suggest two approaches to calculating ∇n and $n^{-4/3}$ separately, then combining the results using Eq. (2). The first paper[13] suggested using the commutator relationship $(\nabla n)^2 = [[n, \nabla^2], n]$ to calculate y^2, and the second paper[14] suggested using the commutator relationship $\nabla n = [\nabla, n]$ to calculate y. Implementing these approaches causes numerical stability problems.[21] Although the ∇n terms are calculated properly, the resulting

y terms are not numerically stable. For example, the expectation value $\langle n^{-4/3} \rangle$ is infinite for the exact hydrogen wavefunction.[22] Thus, the condition that f is well-behaved in Eq. (3) is not met for $n^{-4/3}$. There are reports in the literature of stability problems while evaluating the derivative this way.[12] Therefore, within the AZ method, the ∇n and $n^{4/3}$ terms need to be calculated together as either y or y^2.

The first choice might be to directly evaluate $y^2=(\nabla n/n^{4/3})^2$, because y^2 and not y is the dimensionless gradient originally proposed.[23] This is similar to the approach taken in the first paper by AZ and that proposed by others.[22] The RI presented in Eq. (2) is used in Eq. (5c).

$$\left(\frac{\nabla n}{n^{4/3}}\right)^2 = 9\left[\left[n^{-1/3}, \nabla^2\right], n^{-1/3}\right] \tag{5a}$$

$$\int \chi_\mu \left(\frac{\nabla n}{n^{4/3}}\right)^2 \chi_\nu d\vec{r} = 9\int \chi_\mu \left(2n^{-1/3}\nabla^2 n^{-1/3} - \nabla^2 n^{-2/3} - n^{-2/3}\nabla^2\right)\chi_\nu d\vec{r} \tag{5b}$$

$$\approx 9 \sum_{m,n}^{\text{Orthonormal}} \left\{ \int \chi_\mu 2n^{-1/3}\theta_m d\vec{r} \cdot \int \theta_m \nabla^2 \theta_n d\vec{r} \cdot \int \theta_n n^{-1/3}\chi_\nu d\vec{r} \right. \tag{5c}$$

$$- \int \chi_\mu \nabla^2 \theta_m d\vec{r} \cdot \int \theta_m n^{-2/3}\chi_\nu d\vec{r}$$

$$\left. - \int \chi_\mu n^{-2/3}\theta_m d\vec{r} \cdot \int \theta_m \nabla^2 \chi_\nu d\vec{r} \right\}$$

The derivation can be conveniently completed in the orthonormal basis set in which n is diagonal. Since this is only a basis transformation, no generality is lost, provide that $\{\chi\}$ and $\{\theta\}$ span the same space. This must be the case in order for $\int \chi_\mu n^{-1/3}\theta_m d\vec{r}$ to be evaluated using the RI presented in Eq. (3). The eigenvalues of the matrix of $\int \chi_\mu\, n\, \chi_\nu d\vec{r}$ that appear in Eq. (3) are denoted λ_υ. Eq. (5c) simplifies greatly, since integrals of the type $\int \chi_\mu n^a \chi_\nu d\vec{r}$ are evaluated using the $\{\lambda_\upsilon\}$ and many indices collapse due to the Kronecker-δ in Eq. (3). Eq. (5c) becomes:

$$\int \chi_\mu \left(\frac{\nabla n}{n^{4/3}}\right)^2 \chi_\nu d\vec{r} = 9\{2\lambda_\mu^{-1/3} \cdot \int \chi_\mu \nabla^2 \chi_\nu d\vec{r} \cdot \lambda_\nu^{-1/3} - \int \chi_\mu \nabla^2 \chi_\mu d\vec{r} \cdot \lambda_\nu^{-2/3} \qquad (6a)$$

$$-\lambda_\mu^{-2/3} \cdot \int \chi_\nu \nabla^2 \chi_\nu d\vec{r}\}$$

$$= -9(\lambda_\mu^{-1/3} - \lambda_\nu^{-1/3})^2 \cdot \int \chi_\mu \nabla^2 \chi_\nu d\vec{r}. \qquad (6b)$$

Clearly, $\int \chi_\upsilon \left(\frac{\nabla n}{n^{4/3}}\right)^2 \chi_\upsilon d\vec{r} = 0$ for all υ after this application of the RI. Therefore, the sum of all the eigenvalues of this representation of $(\nabla n/n^{4/3})^2$ is zero, since a unitary transformation will change the diagonal elements but not their sum. But $(\nabla n/n^{4/3})^2$ is certainly positive definite, so all of its eigenvalues must be positive, even though this is clearly not the case after applying the RI in Eq. (5c). Thus, this application of the RI is flawed and produces an inconsistent result, because increasing the size of the basis set will not converge to the correct value. In other words, the condition that f and g be well–behaved in Eq. (2) is not satisfied as applied in Eq. (5c).

Therefore, the density gradient in GAMESS[24] is evaluated using $y=|\nabla n|/n^{4/3}$ rather than $y^2=(\nabla n/n^{4/3})^2$. The commutator relationship used is similar to that proposed in the second paper by AZ. The RI presented in Eq. (2) is used in Eq. (7c).

$$\left(\frac{\nabla n}{n^{4/3}}\right) = 3\left[n^{-1/3}, \nabla\right] \qquad (7a)$$

$$\int \chi_\mu \left(\frac{\nabla n}{n^{4/3}}\right) \chi_\nu d\vec{r} = 3\int \chi_\mu (n^{-1/3}\nabla - \nabla n^{-1/3}) \chi_\nu d\vec{r} \qquad (7b)$$

$$\approx 3 \sum_m^{\text{Orthonormal}} \{\int \chi_\mu n^{-1/3} \theta_m d\vec{r} \cdot \int \theta_m \nabla \chi_\nu d\vec{r} \qquad (7c)$$

$$- \int \chi_\mu \nabla \theta_m d\vec{r} \cdot \int \theta_m n^{-1/3} \chi_\nu d\vec{r}\}$$

As in Eq. (5), choosing the orthonormal basis set in which n is diagonal yields,

$$\int \chi_\mu \left(\frac{\nabla n}{n^{4/3}}\right)\chi_\nu d\vec{r} = 3\left\{\lambda_\mu^{-1/3}\cdot\int \chi_\mu \nabla\chi_\nu d\vec{r} - \int \chi_\mu \nabla\chi_\nu d\vec{r}\cdot\lambda_\nu^{-1/3}\right\} \quad (8a)$$

$$= 3\left(\lambda_\mu^{-1/3} - \lambda_\nu^{-1/3}\right)\cdot\int \chi_\mu \nabla\chi_\nu d\vec{r}. \quad (8b)$$

Eq. (8b) results in the diagonal values of $\int \chi_\mu \left(\frac{\nabla n}{n^{4/3}}\right)\chi_\nu d\vec{r}$ all being zero, but note that $\nabla n/n^{4/3}$ and not the positive definite quantity $y=|\nabla n|/n^{4/3}$ has been calculated in Eq. (7) and (8). The RI presented in Eq. (2) is used to generate integrals over y^2 with all positive eigenvalues.

$$\int \chi_\mu \left(\frac{\nabla n}{n^{4/3}}\right)^2 \chi_\nu d\vec{r} = \sum_m \int \chi_\mu \left(\frac{\nabla n}{n^{4/3}}\right)\chi_m d\vec{r}\cdot\int \chi_m \left(\frac{\nabla n}{n^{4/3}}\right)\chi_\nu d\vec{r} \quad (9)$$

This matches the proper physics of the system. Although a large basis set is needed for this RI to be accurate, this RI does converge with an adequate auxiliary basis set.[16] This method involves integrals over $n^{-1/3}$, which is well-behaved with $\langle n^{-1/3}\rangle = 4.943$ for the exact hydrogen wavefunction.[22] This method was successfully used previously,[15] and it is proving useful in additional cases.[16] It is therefore recommended for implementations of the AZ grid–free approach to DFT.

Acknowledgements

This work was supported in part by grants from the Air Force Office of Scientific Research (F49–620–97–1–0522) and by the Ames Laboratory, US–DOE. Special thanks to W.M. Klopper, J. Hutter and D.E. Bernholdt for enlightening discussions.

References

1. J.C. Slater, Adv. Quant. Chem. **6**, 1 (1972).
2. S.H. Vosko, L. Wilk and M. Nusair, Can. J. Phys. **58**, 1200 (1980).
3. D.C. Langreth and M.J. Mehl, Phys. Rev. B **28**, 1909 (1983).
4. M. Rasolt and D.J.W. Geldhart, Phys. Rev. B **34**, 1325 (1986).
5. P. Hohenberg and W. Kohn, Phys. Rev. **136** B864 (1964).
6. J.P. Perdew, K. Burke and M. Ernzerhof, J. Chem. Phys. **105**, 9982 (1996).
7. A.D. Becke, J. Chem. Phys. **104**, 1040 (1996).
8. B.G. Johnson, P.M.W. Gill and J.A. Pople, J. Chem. Phys. **98**, 5612 (1993).
9. B.I. Dunlap, J. Phys. Chem. **90**, 5524 (1986).
10. K.S. Werpetinski and M. Cook, Phys. Rev. A **52**, R3397 (1995).
11. K.S. Werpetinski and M. Cook, J. Chem. Phys. **106**, 7124 (1997).
12. G. Berghold, J. Hutter and M. Parrinello, Theor. Chem. Acc. **99**, 344 (1998).
13. Y.C. Zheng and J. Almlöf, Chem. Phys. Lett. **214**, 397 (1993).
14. Y.C. Zheng and J. Almlöf, J. Mol. Struct. (Theochem) **288**, 277 (1996).
15. K.R. Glaesemann and M.S. Gordon, J. Chem. Phys. **108**, 9959 (1998).
16. K.R. Glaesemann and M.S. Gordon, to be submitted.
17. O. Vahtras, J. Almlöf and M.W. Feyereisen, Chem. Phys. Lett. **213**, 514 (1993).
18. D.E. Bernhold and R.J. Harrison, J. Chem. Phys. **109**, 1593 (1998).
19. B.A. Hess, R.J. Buenker and P. Chandra, Int. J. of Quant. Chem. **29**, 737 (1986).
20. A.D. Becke, Phys. Rev. A **38**, 3098 (1988).
21. K.R. Glaesemann and M.S. Gordon, unpublished results.
22. W.M. Klopper, personal correspondence.

23. F. Herman, I.B. Ortenburger and J.P. van Dyke, Int. J. Quant. Chem. **IIIS**, 827 (1970).

24. M.W. Schmidt, K.K. Baldridge, J.A. Boatz, S.T. Elbert, M.S. Gordon, J.H. Jensen, S. Koseki, N. Matsunaga, K.A. Nguyen, S. Su, T.L. Windus, M. Dupuis, and J.A. Mongomery Jr., J. Comp. Chem. **14**, 1347 (1993).

CHAPTER 4: FURTHER INVESTIGATION OF A GRID-FREE DENSITY FUNCTIONAL THEORY (DFT) APPROACH

A paper prepared for submission to the Journal of Chemical Physics

Kurt R. Glaesemann and Mark S. Gordon

Abstract

Density functional theory (DFT) has gained popularity because it can frequently give accurate energies and geometries. The evaluation of DFT integrals in a fully analytically manner is generally impossible, thus most implementations use numerical quadrature over grid points, which can lead to numerical instabilities. To avoid these particular instabilities, the grid-free approaches were developed. The approach in this work involves application of the resolution of the identity (RI) to evaluate the integrals. Of particular concern is the convergence of the RI with respect to basis set in the grid-free approach. Conventional atomic basis sets are inadequate for fitting the RI, particularly for gradient corrected functionals (J. Chem. Phys. **108**, 9959 (1998)). The focus of this work is on implementation of and selection of auxiliary basis sets.

I. Introduction.

In recent years, density functional theory (DFT), formulated in terms of the spin densities (n_α,n_β), has gained popularity as a method for determining molecular properties and structures as an alternative to *ab initio* wavefunctions. Functionals of the density have been fit to the uniform electron gas,[1,2] and have incorporated corrections that depend upon the density gradient.[3,4,5] "Hybrid functionals" that mix in Hartree-Fock exchange are reported to help correct for the inadequacies of a single-reference wavefunction.[6,7] DFT

can frequently give energies, relative energies and geometries more accurately than second-order perturbation theory, with significantly less computational expense,[8] although reports of failures of DFT are not uncommon in the literature.[9,10,11]

Evaluating integrals over functions of the density in a closed analytic form is usually impossible, because the functional forms involve very complicated functions of the density. Most DFT implementations evaluate the integrals using numerical quadrature over a finite set of grid points often organized in atom centered Lebedev spheres:[12,13,14]

$$\int_{\text{All space}} f(n_\alpha, n_\beta, \nabla n_\alpha, \nabla n_\beta)d\vec{r} \approx \sum_{i}^{\text{Grid points}} f(n_\alpha(i), n_\beta(i), \nabla n_\alpha(i), \nabla n_\beta(i)) \Delta \vec{r}(i). \qquad (1)$$

Dunlap discussed how integrating over a finite grid can lead to numerical instabilities.[15] An X-α specific grid-free approach was developed to avoid these difficulties.[15,16,17] Recently, a more general grid-free approach has been proposed by Almlöf-Zheng (AZ)[18,19] and has been further developed by us and others.[20,21,22] These grid-free approaches involve approximations that introduce errors that can be systematically eliminated by increasing the basis set size, and are independent of the coordinate system chosen.

The primary focus of the current work is on the basis set convergence properties of auxiliary basis sets within AZ grid-free DFT. The auxiliary basis sets are used to converge the resolution of the identity (RI).[23] Several prototypical systems are studied to explore the convergence of properties as a function of the basis set. These results will demonstrate in detail the basis set dependence of the grid-free approach. In the previous work convergence of the RI was approached by enlarging the atomic basis set. This was successful, but it made separating basis set convergence from RI convergence difficult and resulted in extensive use of computational resources, because expensive two-electron integrals grew with the basis set. Bernholdt and Harrison have recently considered auxiliary basis sets for

fitting RI-MP2.[24]

II. A Grid-Free approach to DFT.

The several approximations used within the grid-free approach implemented in GAMESS[25] are briefly reviewed here. The accuracy of these approximations will always be directly related to the completeness of the basis. The initial simplification will be to split portions that depend on functions of the density, such as n_α ,n_β, ∇n_α, and ∇n_β. This integral simplification uses the RI. The resolution of the identity is utilized as follows:

$$\int \chi_i \, f \cdot g \, \chi_j \, d\vec{r} \approx \sum_m \int \chi_i \, f \, \theta_m \, d\vec{r} \cdot \int \theta_m \, g \, \chi_j \, d\vec{r} \qquad (2)$$

The foregoing expression is exact if $\{\theta_m\}$ is a complete orthonormal set; otherwise, one expects some dependence of the calculation on the size of the basis set. One choice for $\{\theta_m\}$ is the set of molecular orbitals from the current SCF cycle. This choice is the simplest to implement, but inadequate.[20,24] Calculating the spin-polarization $\zeta=(n_\alpha-n_\beta)/(n_\alpha+n_\beta)$ requires using the RI in Eq. (2) to combine $(n_\alpha+n_\beta)^{-1}$ and $(n_\alpha-n_\beta)$ to form ζ.

A second "spectral" RI must be used to evaluate the resulting complicated integrals involving functions of the density and the density gradient.[26] This method (see Eq. (3) below) assumes that the matrix of integrals over the density has been transformed to an orthonormal basis set in which this matrix is diagonal. No generality is lost, since this is just a basis transformation. The function of the integral is assumed to be the integral of the function:

$$\int \theta_i \, f(n) \theta_j \, d\vec{r} \approx f(\int \theta_i \, n \theta_j \, d\vec{r}) = f(\lambda_i)\delta_{ij} \qquad (3)$$

where λ_i is an eigenvalue of the matrix $M[n]_{ij} = \int \theta_i \, n \, \theta_j \, d\vec{r}$. Eq. (3) is exact in a complete basis. In DFT, n is the density, although Eq. (3) does not assume this. Therefore, once the

integrals over n are determined, the integrals over any well–behaved function of n can be readily obtained, such as $n^{-1/3}$.

The matrix representation of the density M[n] is calculated from the first-order density matrix D and atomic orbitals i, j, k and l without using the RI.

$$M[n]_{i,j} = \int \chi_i n \chi_j d\vec{r} = \sum_{k,l} D_{kl} \int \chi_i \chi_k \chi_l \chi_j d\vec{r}. \tag{4}$$

The density gradient is evaluated dimensionlessly using the commutator $n^{-4/3} \cdot \nabla n = 3[n^{-1/3}, \nabla]$.

$$\int \chi_\mu \left(\frac{\nabla n}{n^{4/3}} \right) \chi_\nu d\vec{r} = 3 \left\{ \int \chi_\mu n^{-1/3} \nabla \chi_\nu d\vec{r} - \int \chi_\mu \nabla \left(n^{-1/3} \chi_\nu \right) d\vec{r} \right\} \tag{5a}$$

$$\approx 3 \sum_{m}^{\text{Orthonormal}} \left\{ \int \chi_\mu n^{-1/3} \theta_m d\vec{r} \cdot \int \theta_m \nabla \chi_\nu d\vec{r} - \right. \tag{5b}$$

$$\left. \int \chi_\mu \nabla \theta_m d\vec{r} \cdot \int \theta_m n^{-1/3} \chi_\nu d\vec{r} \right\}$$

Squaring the matrix of integrals using the RI in Eq. (3) generates the integrals over $(\nabla n)^2/n^{8/3}$. Due to the presence of derivative terms, basis functions of one higher angular momentum are needed in order for this application of the RI to be accurate.

The AZ grid-free DFT approach is extended to the computation of nuclear gradients.[19,20] The RI is only applied once in Eq. (6).

$$\int \left(\frac{\partial \chi_r}{\partial x} \right) \hat{K}^{DFT} \chi_s d\vec{r} \approx \sum_{m}^{\text{Orthonormal}} \int \left(\frac{\partial \chi_r}{\partial x} \right) \theta_m d\vec{r} \cdot \int \theta_m \hat{K}^{DFT} \chi_s d\vec{r} \tag{6}$$

As in Eq. (5), higher angular momentum functions are necessary to properly treat the derivative terms.

III. Auxiliary basis sets for fitting the resolution of the identity.

Since a large basis set is necessary for the RI to be accurate, during the DFT portion of the calculation, all matrices are augmented with sets of auxiliary functions. Before the

SCF procedure is begun, the auxiliary basis set is built. Each atom is given a set of even tempered basis functions[54] that include angular momentum functions from zero to one higher than that of the valence space. The valence space is defined as s for H-He, sp for Li-Ar, and spd for K-Xe. The latter angular momentum has been previously shown to be essential for functionals contain density derivative terms or when calculating nuclear gradients. The two index one-electron dipole velocity and overlap integrals are calculated over both the AO basis and the auxiliary basis and stored to disk. Using the overlap matrix S, the matrix W is generated (analogous to the linear combination of atomic orbitals matrix V). W transforms both AO and the auxiliary orbitals to an orthonormal set, because $W^{\dagger}SW=I$ (analogous to $V^{\dagger}SV=I$). During the generation of W, the MO's are not allowed to contain any auxiliary character. This is done by fixing the MO coefficients and forcing the auxiliary space to be orthogonal to the entire MO space. Due to the size of the auxiliary basis set, it is crucial to test for linear dependencies. Linearly dependent functions are moved to the end of the W matrix and zeroed out. This is summarized in the pictorial representation of the W matrix in Figure (1).

The matrix representation of the density M[n] is generated every SCF cycle according to Eq. (4). The k and l run only over the AO basis because the auxiliary basis functions contain no electron density, but indices i and j run over the entire basis. This requires the calculation of N^2M^2 integrals, where N is the number of AO's and M is the number of AO's plus the number of auxiliary functions. At the end of each SCF cycle, only the parts of the resulting matrices that correspond to the MO space are saved. For gradient calculations the entire exchange-correlation potential is saved for use later in Eq. (6).

IV. Grid-Free DFT Results

IV. A. Functionals and methods

The grid-free approach outlined in Sections II and III has been used to implement the following DFT functionals in GAMESS. Different functionals will be used to examine different applications of the RI. Energy gradients will be calculated to demonstrate the RI in Eq. (6), which is independent of the functional.

1. X-α[1] has neither n_α n_β cross-terms nor gradient dependence. It only involves that use of the RI in Eq. (3). For the uniform electron gas value of α=2/3, this is called the Slater functional.

2. VWN5[2,8,27,28] has no gradient dependence. It uses the RI in Eq. (2) to multiply together terms that depend on $\zeta=(n_\alpha-n_\beta)/(n_\alpha+n_\beta)$ and terms depending on n. Functions of ζ and n are generated using the RI presented in Eq. (3).

3. Becke88[29] gradient corrected exchange functional relies on the RI in Eq. (5) to generate $y^2=(\nabla n)^2/n^{8/3}$, the dimensionless density gradient. The RI in Eq. (3) is used to generate functions of both n and y^2. Finally, the RI in Eq. (2) is used to combine all the terms. The Depristo-Kress functional[30] is a predecessor to Becke88 that is similar in design and use of the RI.

All comparisons presented below are made to the grid based DFT code in Gaussian 94.[31] The grid used in all calculations is a pruned grid of (75, 302), in which there are 75 radial shells and 302 angular points per shell. This results in about 7000 points per atom. This is the default integration grid in Gaussian 94. Both GAMESS and Gaussian94 calculate all non-exchange-correlation terms explicitly from Ψ, rather than from n.

The auxiliary basis sets presented are based on the correlation-consistent basis sets

of Dunning *et al.*[32] It has been shown that by using large auxiliary basis sets RI-MP2 can be made exact, but one needs much smaller basis sets to get accurate energy differences.[24,33] The initial choice of auxiliary functions was a set of even tempered[34] functions that spanned the same exponent range as the aug-cc-pVDZ basis. This is different than the initial RI-MP2 basis set used by Bernholdt and Harrison, which are uncontracted correlation consistent basis sets. The basis sets in this work are augmented in an even tempered manner. The auxiliary basis set notation is as follows: "5s3p" means that there are 5 s gaussians and 3 sets of p gaussians that span the same exponent range as the s and p shells of the aug-cc-pVDZ basis set of Dunning. "5s++3p-" means that there are 2 additional diffuse s gaussians and 1 additional set of tight p gaussians. When multiple atoms are present, the heavy atom will be listed first and the hydrogen atom last, as in 10s5p2d/5s2p. This notation is used throughout the remainder of this work. In our previous work, the even tempered basis set approach was very slow to converge the RI, because the basis was not augmented with diffuse or tight functions. Therefore, 10 s functions and 20 s functions spanned nearly the same range of exponents and gave similar results.

IV. B. Hydrogen atom

Hydrogen was first studied as an atom with the Slater functional and the cc-pVDZ atomic basis set (Table 1). Note that the "exchange" energy for single electron systems is present to cancel out the self-repulsion terms. The addition of 5 s (to match aug-cc-pVDZ) gaussians is found to reduce the difference from the grid based approach by over an order of magnitude to 0.15 kcal/mol, but the error is still larger than would be preferred. Adding an additional s gaussian between each gaussian of the 5s yields the 9s auxiliary basis set and

9s differs from the grid based approach by less than 0.01 kcal/mol. Because most calculations involve H within molecules, an additional diffuse s function is added to help account for longer range interactions, even though 9s and 9s+ give the same results for the H atom. Therefore, the RI presented in Eq. (3) is found to converge very quickly, as was found in our previous work. All further calculations will focus on more complicated applications of the RI.

Gradient-corrected calculations on H with the Becke88 functional are summarized in Table 2. This functional requires that the auxiliary basis set contain p functions due to the use of the RI in Eq. (5). The initial auxiliary basis set is the one optimized for the Slater functional (9s+) plus 3 additional sets of p functions to yield the 9s+3p auxiliary basis set. This basis set differs from the grid based approach by over 1 kcal/mol, but the difference is only one sixth that of the grid-free approach with no auxiliary basis set. A set of diffuse p functions reduces the difference to an order of magnitude smaller than that with no auxiliary basis set. Adding a set of tight p functions (without the diffuse set of p functions) reduces the difference to %0.11 percent. Therefore, these are combined to form the 9s+3p+- auxiliary basis set and the difference between the grid and grid-free methods is reduced to %0.10.

IV. C. Nitrogen atom

Atomic N was studied with an unrestricted wavefunction, the Becke88 functional and the cc-pVDZ atomic basis set (Table 3). The initial auxiliary basis is 10s5p2d, because it involves the same number of gaussians as aug-cc-pVDZ. This auxiliary basis set corrects the non-variational behavior that occurs if no auxiliary basis set is used, and the RI is poorly represented. The difference from the grid based method is still 40 kcal/mol, so chemical

accuracy will require a larger auxiliary basis set. Because the aug-cc-pVDZ basis does not provide p functions for the 1s orbital, two tight sets of p functions are added and the difference from the grid method is reduced by 34 kcal/mol to 6.5 kcal/mol. The p functions improve the accuracy of the RI in Eq. (5) for atomic s functions and the RI in Eq. (2) and (3) for atomic p functions. A third set of p functions only results in the slight improvement of 0.15 kcal/mol, so no additional sets of p functions are added. Tight d functions are added, because polarization functions present in atomic basis sets have exponents designed for the bonding region and not near the atomic center. The first set of d functions reduces the difference from the grid by 1 kcal/mol to 5.3 kcal/mol. The second set of tight d functions reduces the difference from the grid method to 1.8 kcal/mol. This difference is only 0.18 kcal/mol the addition of the third set of tight d functions. The difference between the grid and grid-free method is reduced to 0.02 kcal/mol with the addition of a fourth set of tight d functions. Therefore the RI presented in Eq. (2), (3) and (5) are converged with the 10s5p---2d---- auxiliary basis set. The only RI not investigated is Eq. (6), since nuclear gradients are not relevant to an atom.

IV. D. NH_3 bend potential

For extremely loose grids, Werpetinski and Cook[16] found that the NH_3 bend potential obtained with grid-based DFT approaches could become disturbingly asymmetrical. For small basis sets, the AZ grid-free approach gave symmetrical, but inaccurate curves.[20] As the basis set was increased, the grid-free bend potential approached the correct behavior. The atomic basis set used in the present calculations is cc-pVDZ basis set.[32] The NH bond distance is fixed at 1.0496Å, to allow easy comparison to previous work.[16,20] Because the NH bond distance is optimized for the X-α functional, the gradient

will never go to zero for other functionals. The functional used is Becke88, so that all of the RI's can be investigated.

Potential energy surfaces as a function of angle are presented in Figure 2. With no auxiliary basis set the curve is off by 0.5 Hartree, and the shape does not match the shape of the grid based curve. Adding the initial 10s5p2d/5s2p basis set (even tempered uncontracted aug-cc-pVDZ) yields a properly shaped curve; the energy differs from the grid curve by an average of 38 kcal/mol. Enlarging the auxiliary basis set to 10s5p---2d--/9s+3p+-, reduces the average difference across the entire PES to 3 kcal/mol. As was found in RI-MP2, accurate relative energies are obtained with smaller basis sets than absolute energies. Using the auxiliary basis set optimized for H and N of 10s5p---2d----/9s+3p+-, the maximum difference anywhere on the PES is reduced to 1.0 kcal/mol. The range of the differences between the grid and the grid-free approaches is -0.25 to 1.01 kcal/mol.

The cartesian RMS gradient of NH_3 provides insight into the RI in Eq. (6). These results are presented in Figure 3. Without an auxiliary basis set, the curve is completely misshaped. The RI is so poorly converged that the gradient is little more than random numbers. This is to be expected, since the agreement of the energies was poor. Using the 5s2p/10s5p2d auxiliary basis set moves the minimum to within 2° of the grid minimum, but the grid-free RMS gradient has a smaller drop than that of the grid RMS gradient. The 9s+3p+-/10s5p---2d-- basis set gives a curve that is very similar to the grid based curve, except for the lowest portions of the curve, which has RMS values that are larger than the grid based values. The 9s+3p+-/10s5p---2d---- basis set was optimized for the N and H atoms, and it gives the same minimum RMS gradient as the grid method. The curves are

almost indistinguishable. Therefore convergence of the nuclear gradient RI in Eq. (6) requires tight auxiliary basis functions near the nucleus. Several sets of d functions were needed for the RI to be accurately represented. This can be explained by the bonding in NH_3. The atomic p orbitals on N are important in bonding and therefore d functions (one higher angular momentum) are needed in order for the nuclear gradient resulting from these bonds to be accurate.

IV. E. Nitrogen molecule

N_2 was shown in our previous work to require a large and cumbersome atomic basis set to get accurate results because an auxiliary basis set was not used. In the current work, the aug-cc-pVDZ basis set and unrestricted wavefunctions are used for atomic N. The Becke88 functional is used in order to allow easy comparison to our previous work. Results are presented in Table 4. With no auxiliary basis set, the geometry differs from the grid method by 0.26 Å and the binding energy differs by 38 kcal/mol. Obviously, a auxiliary basis set is needed to get accurate geometries and relative energies. Although the 5s2p/10s5p2d auxiliary basis set predicts geometries to within 0.010 Å of the grid method, the binding energies differ by 7 kcal/mol. The 9s+3p+-/10s5p---2d-- basis set predicts geometries within 0.002 Å of the grid method and binding energies to within 0.3 kcal/mol of the grid method. The 9s+3p+-/10s5p---2d---- auxiliary basis set gives the same geometry as the grid but the binding differs by 2.4 kcal/mol.

IV. F. Extension to other systems.

The auxiliary basis sets developed for NH_3 are generalized to elements up to Ne. The aug-cc-pVDZ basis sets are used to provide the exponents for the tightest and most diffuse gaussian function of the initial 5s2p/10s5p2d auxiliary basis sets. Results for both

5s2p/10s5p2d auxiliary basis set and the larger auxiliary basis sets are presented.

The $^1A_1$ and $^3B_1$ states of CH_2 are compared in Table 5 with the Becke88, Depristo-Kress, and B-VWN5 functionals. In our previous work, the RI only converged after the atomic basis set was uncontracted and augmented with additional functions. The AO basis set is cc-pVTZ.[32] The $^3B_1$ state is optimized with a restricted open shell wavefunction. Experimental values are presented in Table 5 for comparision.[35,36] Using no auxiliary basis set results in H-C-H bend angles that differ from the grid based approach by over 50° for all three functionals studied. The C-H bond distances differ from the grid based predictions by 0.3 Å. The predicted $^1A_1$ - $^3B_1$ splittings differ from the grid based values by as much as 0.33 eV. As is to be expected, the RI is not adequately represented by the CH_2 atomic basis set. The 10s5p2d/5s2p auxiliary basis set reduces the difference of the grid-free from the grid results for all of all the angles, with the largest difference being 8° for the B-VWN5 triplet. The largest difference in bond lengths between the grid and grid-free approaches is reduced to 0.016 Å with the addition of an auxiliary basis set. The grid/grid-free agreement on splitting energies is improved, with the largest difference being 0.09 eV. Enlarging the auxiliary basis set to 10s5p---2d--/9s+2p+- predicts angles that are all within 0.4° of the values predicted with the grid. The largest difference in predicted bond distances is reduced to 0.004 Å. The predicted splittings all agree to within 0.06 eV of the grid-based predictions. The largest auxiliary basis set of 10s5p---2d----/9s+2p+- has the same maximum bond difference of 0.004 Å, a slightly larger splitting difference of 0.07 eV for B-VWN5, and a larger angle difference of 1.7° for the triplet B-VWN5. In all calculations, the $^3B_1$ was correctly found to be the ground state. The DePristo-Kress and Becke88 functionals are both gradient corrected exchange functionals, and they are found to

have similar convergence properties with respect to the RI. For both the grid and grid-free approaches, the addition of electron correlation by the VWN5 functional is needed in order to avoid overestimating the $^1A_1$ - $^3B_1$ splitting. For CH_2, auxiliary basis sets are found to be effective for functionals that depend on n_α, n_β, ζ, ∇n_α, and ∇n_β. Nuclear derivatives are also found to be reliable, because the grid and grid-free approaches predicted similar geometries.

The geometry of the ground state of water is optimized with the 6-31G** basis set[37] and the Becke88 functional. Results are presented in Table 6. Without any auxiliary basis functions, the O is predicted to be sp^2 hybridized with a H - O - H angle of 120.1°. The predicted H-O bond distances are found to differ from the grid based value by 0.023 Å. Addition of the 10s5p2d/5s2p auxiliary basis set yields a H - O - H angle that differs from the grid by 4.2°. The bond distance is found to differ from the grid by 0.013 Å. The 10s5p---2d--/9s+2p+- auxiliary basis set reduces the difference in the predicted angle to 1.2° and the difference in the predicted bond distance to 0.004 Å. The 10s5p---2d----/9s+2p+- auxiliary basis set predicts a geometry that differs from the 10s5p---2d--/9s+2p+- auxiliary basis set by only 0.001 Å and 0.2°.

Given the success in these previous systems, these auxiliary basis sets are applied to several additional molecules with the Becke88 functional. High spin cases are all treated with unrestricted wavefunctions. O_2, F_2, and B_2H_6 use the cc-pVTZ basis set as the atomic basis set. BeH_2 and LiH use the 6-31G** basis set, because the cc-pVTZ basis set is not currently available for Be and Li. All molecules are geometry optimized using nuclear gradients. Inter-atomic distances are presented in Table 7. With no auxiliary basis sets, the largest variance from the grid based result is 0.6 Å for the B - B distance in B_2H_6. The

smallest difference from the grid based approach is 0.009Å for the terminal H in B_2H_6. The 10s5p2d/5s2p auxiliary basis set reduces the B - B distance predicted to 1.870 Å which differs from the grid prediction by 0.055 Å. The agreement of the inter-atomic distances predicted by the grid and grid-free approaches is improved for all distance in Table 7 upon adding the 10s5p2d/5s2p auxiliary basis set. Extending the auxiliary basis set to 10s5p---2d--/9s+2p+- reduces the largest difference between the grid predicted and the grid-free predicted distance to 0.014 Å. Other grid-free predicted distances differ from the grid predicted distances by as little as 0.001 Å. The larger 10s5p---2d----/9s+2p+- auxiliary basis set predicts all intra-atomic distances to within 0.013 Å of the grid predicted distances. Clearly, structures are not predicted properly without an auxiliary basis set, but the largest auxiliary basis sets predict structures that agree with the grid to within 0.013 Å.

Binding energies are predicted using the Becke88 functional for the same systems studied above in Table 7. Binding energies are calculated relative to isolated atoms and are presented in Table 8. Since geometries are unreliable without an auxiliary basis set, the binding energies are not reliable without an auxiliary basis set. The largest difference from the grid based prediction is 6.0 eV for B_2H_6. The 10s5p2d/5s2p auxiliary basis set reduces the largest difference by an order of magnitude to 0.6 eV. The 10s5p---2d--/9s+2p+- auxiliary basis has a difference of 0.69 eV for F_2. For the other molecules studied, this auxiliary basis set reduces the difference to 0.19 eV or less. The larger 10s5p---2d----/9s+2p+- basis set predicts a binding energy that differs from the grid approach by 0.82 eV for F_2.

IV. G. F_2 binding energies

F_2 has an obvious difference in predicted binding energies for the grid and grid-free approaches. This is issue was investigated further. The Slater functional was used, because in order for an auxiliary basis set to work for the Becke88 functional, it must also work for the simpler Slater functional. Results of these additional calculations are summarized in Table 9. The 10s5p2d auxiliary basis set predicts an F_2 bond distance that is 0.02 Å different from the grid prediction. The 10s5p---2d--/9s+2p+- auxiliary basis gets a bond distance that is within 0.0001 Å of the grid predicted bond distance. The predicted binding energies differ by 0.66 eV. Since the geometries agree, this auxiliary basis set is used as the starting point of all additional calculations. The addition of a single tight s or diffuse s function does not change the predicted properties. To verify that an insufficient number of s functions in the auxiliary basis set is not the problem, 5 tight and 5 diffuse s functions are simultaneously added to the auxiliary basis set and the predicted properties are not changed. The addition of an extra set of tight or diffuse p functions also does not change the predicted properties. Therefore, an extra 3 sets of tight and an extra 3 sets of diffuse p functions were added simultaneously to the auxiliary basis set. The predicted properties remained unchanged. 2 additional sets of tight d functions and 2 additional sets of diffuse d functions are added, and the bond distance shifted slightly (0.0009 Å), but the binding energy did not change. This is not unexpected, since Slater energies do not require higher angular momentum, but Slater nuclear gradients do require higher angular momentum. The number of s functions spanning the aug-cc-pVDZ space is doubled and an extra diffuse s is added, since this proved useful in building the auxiliary basis set for H. Neither binding energies nor properties changed. The number p functions is doubled, and

no change in the properties predicted occurs. Clearly the grid and grid-free approaches agree on the Slater predicted bond length of 1.404 Å. The grid and grid free approaches consistently predict Slater binding energies that differ by 0.66 eV. To verify that this is not a result of an interaction between the specific atomic basis set used and the grid or the auxiliary basis set used, results for the 6-31G basis set are presented in Table 9. The grid and the grid-free 10s5p---2d-- auxiliary basis set predict the same bond length, but different binding energies. Clearly their is a fundamental difference in the energetics predicted by the grid based approach and the grid-free approach.

IV. H. The next row of the periodic table: SiH_2

The auxiliary basis sets are extended to the next row of the periodic table. The smallest auxiliary basis set is 13s9p2d, because that matches the aug-cc-pVDZ basis set. The larger 10s5p---2d-- auxiliary basis set is extended to the Lithium row as 13s+9p---2d--. SiH_2 is investigated to see if these simple extensions are adequate. The atomic basis set is a modified version of the double ζ basis set of Dunning and Hay.[38] A single set of d polarization is added to the Si (ζ=0.395). This is (3s)/[2s] for H and (11s,7p,1d)/[6s,4p,1d] for Si. Results are presented in Table 10. When no auxiliary basis sets are used, the triplet is incorrectly predicted to be the ground state. Bond lengths differ by 0.04 Å and angles differ by 6° from the grid based results . With the addition of the 13s9p2d/5s2p auxiliary basis set, the grid-free approach correctly predicts the singlet as the ground state. Bond lengths are predicted to with 0.01 Å of the grid approach, and the H - Si - H angle is predicted to within 2.7° of the grid approach. The larger 13s+9p--2d--/9s+3p+- auxiliary basis set improves the agreement of bond lengths to within 0.007 Å, both angles to within 1.9°, and the triplet-singlet splitting to within 2.6 kcal/mol. Since the

agreement is not as good as was achieved for the Lithium row, the basis set was investigated further. Adding two additional diffuse s functions has no significant effect on any of the predicted values. Adding two additional sets of tight d functions to the auxiliary basis set, improves the agreement on the splitting by 0.67 kcal/mol to 2.0 kcal/mol. The triplet angle is 1.4° closer to the grid value, but the singlet angle is 0.3° farther away from the value predicted by the grid approach. The singlet bond distance is 0.0037 Å closer and the triplet bond distance is 0.0019 Å closer to the grid prediction. Adding a fifth set of tight d functions improves the agreement with grid for both the singlet and the triplet bonds by 0.0014 Å and 0.0006 Å, respectively. The extra set of d functions causes the singlet angle to be 0.3° closer to the grid value, but the triplet angle to be 0.3° farther away from the grid value. The triplet-singlet splitting values is 0.16 kcal/mol closer to the grid value. Adding a sixth set of tight d functions to the auxiliary basis set on Si only makes the singlet SiH bond agree less with the grid, while leaving all other predicted values the same. Therefore, the five sets of tight d functions are adequate. To this 13s+9p---2d----- / 9s+3p+- auxiliary basis set, an additional set of tight p functions were added, and no predicted values changed. A set of diffuse p functions was therefore added instead, and the agreement of the grid is worse by 0.15 kcal/mol for the binding. The only predicted value that was closer to the grid predicted value after adding this set of p functions was the singlet bond by 0.0004 Å. A second set of diffuse p functions was added to the auxiliary basis set, and the singlet bond is the only predicted property that agrees better with the grid than before the diffuse p functions were added. Therefore, diffuse p functions are not included in the auxiliary basis set. 13s+9p---2d----- / 9s+3p+- is therefore chosen as the optimized auxiliary basis set for SiH_2.

IV. I. Timing comparisons

For several different auxiliary basis sets, timing comparisons are made to the grid based method (Table 11). Timing comparisons are not made to the grid-free approach without an auxiliary basis set, since the results are poor enough to render timings irrelevant. The 10s5p2d/5s2p auxiliary basis set is not adequate for many molecules, so it is not used either. The 10s5p---2d--/9s+3p+- and the 10s5p---2d----/9s+3p+- both give reliably give reasonable results, therefore they are used for comparisons. In all cases, the CPU time of the entire calculation is compared. The grid used is the default grid described above, which provides about 7000 points per atom. Both atoms and molecules are studied. All calculations are run in direct mode. The N^3 matrix manipulations dominate the timings for the smaller molecules, and therefore the grid-free approach is significantly slower for small molecules such as O_2. The N^4 integral calculations dominate the calculation for larger molecules, and therefore the grid-free approach only took twice as long as the grid approach for larger molecules like B_2H_2.

IV. Conclusions

The grid-free approach to DFT provides an alternative to the grid based approach to DFT. The resolution of the identity (especially for gradient corrected functionals and energy gradient calculations) requires a more accurate basis set than does the wavefunction, therefore an approach that utilizes auxiliary basis sets has been developed. Previous work on auxiliary basis sets have dealt with the fitting of the $n^{1/3}$ X-α potential (Dunlap *et al*) or the Coulomb potential (RI-MP2). The gradient integrals terms that appear in Eq. (5) and (6), present a unique problem of requiring orbitals of higher angular momentum than that of

the AO basis set. An even tempered basis set is used to allow for the easy and systematic enlargement of the auxiliary basis set. By using the Dunning basis sets as a guide for what the range of exponents should be, an effective auxiliary basis set is presented for the elements through argon is developed.

Acknowledgements

This work was supported in part by grants from the Air Force Office of Scientific Research (F49–620–97–1–0522) and by the Ames Laboratory, US–DOE.

References:

1. J.C. Slater, Adv. Quant. Chem. **6**, 1 (1972).
2. S.H. Vosko, L. Wilk and M. Nusair, Can. J. Phys. **58**, 1200 (1980).
3. D.C. Langreth and M.J. Mehl, Phys. Rev. B **28**, 1909 (1983).
4. M. Rasolt and D.J.W. Geldhart, Phys. Rev. B **34**, 1325 (1986).
5. P. Hohenberg and W. Kohn, Phys. Rev. **136** B864 (1964).
6. J.P. Perdew, K. Burke and M. Ernzerhof, J. Chem. Phys. **105**, 9982 (1996).
7. A.D. Becke, J. Chem. Phys. **104**, 1040 (1996).
8. B.G. Johnson, P.M.W. Gill and J.A. Pople, J. Chem. Phys. **98**, 5612 (1993).
9. T.G. Wright, J. Chem. Phys. **105**, 7579 (1996).
10. S. Gronert, G.N. Merrill and S.R. Kass, J. Org. Chem. **60**, 488 (1995).
11. H.M. Sulzbach, H.F. Schaefer III, W. Klopper and H.P. Lüthi, J. Am. Chem. Soc. **118**, 3519 (1996).
12. V.I. Lebedev, Zh. Vychisl. Mat. Mat. Fiz. **15**, 48 (1975).

13. V.I. Lebedev, Zh. Vychisl. Mat. Mat. Fiz. **16**, 293 (1975).

14. P.M.W. Gill, B.G. Johnson, J.A. Pople and M.J. Frisch, Chem. Phys. Lett. **197**, 499 (1992).

15. B.I. Dunlap, J. Phys. Chem. **90**, 5524 (1986).

16. K.S. Werpetinski and M. Cook, Phys. Rev. A **52**, R3397 (1995).

17. K.S. Werpetinski and M. Cook, J. Chem. Phys. **106**, 7124 (1997).

18. Y.C. Zheng and J. Almlöf, Chem. Phys. Lett. **214**, 397 (1993).

19. Y.C. Zheng and J. Almlöf, J. Mol. Struct. (Theochem) **288**, 277 (1996).

20. K.R. Glaesemann and M.S. Gordon, J. Chem. Phys. **108**, 9959 (1998).

21. G. Berghold, J. Hutter and M. Parrinello, Theor. Chem. Acc. **99**, 344 (1998)

22. W.M. Klopper, personal correspondence.

23. O. Vahtras, J. Almlöf and M.W. Feyereisen, Chem. Phys. Lett. **213**, 514 (1993).

24. D.E. Bernhold and R.J. Harrison, J. Chem. Phys. **109**, 1593 (1998).

25. M.W. Schmidt, K.K. Baldridge, J.A. Boatz, S.T. Elbert, M.S. Gordon, J.H. Jensen, S. Koseki, N. Matsunaga, K.A. Nguyen, S. Su, T.L. Windus, M. Dupuis, and J.A. Mongomery Jr., J. Comp. Chem. **14**, 1347 (1993).

26. B.A. Hess, R.J. Buenker and P. Chandra, Int. J. of Quant. Chem. **29**, 737 (1986).

27. Eq. (4) and (5) of Q. Zhao and R.G. Parr, Phys. Rev. A **46**, R5320 (1992).

28. D.M. Ceperley and B.J. Alder, Phys. Rev. Lett. **45**, 466 (1980).

29. A.D. Becke, Phys. Rev. A **38**, 3098 (1988).

30. A.E. Depristo and J. D. Kress, J. Chem. Phys. **86**, 1425 (1987).

31. Gaussian 94, Revision E.2, M. J. Frisch, G. W. Trucks, H. B. Schlegel, P. M. W. Gill, B. G. Johnson, M. A. Robb, J. R. Cheeseman, T. Keith, G. A. Petersson, J. A. Montgomery, K. Raghavachari, M. A. Al-Laham, V. G. Zakrzewski, J. V. Ortiz, J. B. Foresman, J. Cioslowski, B. B. Stefanov, A. Nanayakkara, M. Challacombe, C. Y. Peng, P. Y. Ayala, W. Chen, M. W. Wong, J. L. Andres, E. S. Replogle, R. Gomperts, R. L. Martin, D. J. Fox, J. S. Binkley, D. J. Defrees, J. Baker, J. P. Stewart, M. Head-Gordon, C. Gonzalez, and J. A. Pople, Gaussian, Inc., Pittsburgh PA, 1995.

32. a) T.H. Dunning, Jr. J. Chem. Phys. **90**, 1007 (1989). b) R.A. Kendall, T.H. Dunning, Jr. and R.J. Harrison, J. Chem. Phys. **96**, 6769 (1992). c) D.E. Woon and T.H. Dunning, Jr. J. Chem. Phys. **98**, 1358 (1993). d) D.E. Woon and T.H. Dunning, Jr. J. Chem. Phys. **100**, 2975 (1994). e) T.H. Dunning, Jr. J. Chem. Phys. **103**, 4572 (1995). f) A. K. Wilson, T. v. Mourik and T. H. Dunning, Jr., J. Mol. Struct. (THEOCHEM) **388**, 339 (1997).

33. D.E. Bernholdt, personal correspondence.

34. M.W. Schmidt and K. Ruedenberg, J. Chem. Phys. **71**, 3951 (1979).

35. A.R.W. McKellar, P.R. Bunker, T.J. Sears, K.M. Evenson, R.J. Saykally and S.R. Langhoff, J. Chem. Phys. **79**, 5251 (1983).

36. D.G. Leopold, K.K. Murray, A.E. Stevens Miller and W.C. Lineberger, J. Chem. Phys. **83**, 4849 (1985).

37. a. R. Ditchfield, W.J. Hehre, and J.A. Pople, J. Chem. Phys. **54**, 724 (1971). b. W.J. Hehre, R. Ditchfield, and J.A. Pople, J. Chem. Phys. **56**, 2257 (1972). c. J.D. Dill, and J.A. Pople, J. Chem. Phys. **62**, 2921 (1975). d. J.S. Binkley, and J.A. Pople, J. Chem. Phys. **66**, 879 (1977). e. P.C. Hariharan, and J.A. Pople, Theor. Chim. Acta **28**, 213 (1973).

38. T.H. Dunning, Jr., and P.J. Hay, Chapter 1 in *Methods of Electronic Structure Theory*, H.F. Shaefer III, Ed. Plenum Press, N.Y. 1977, pp 1-27. Note that GAMESS uses inner/outer scale factors of 1.2 and 1.15 for DH's hydrogen (since at least 1983).

Table 1: Hydrogen atom with the Slater functional

Auxiliary Basis set	Energy (Hartree)	Difference from grid (kcal/mol)	Percent difference from grid
Grid	-0.455670	0.00	0.00
None	-0.462003	-3.97	-1.39
5s	-0.455904	-0.15	-0.05
9s	-0.455684	-0.01	-0.00
9s+	-0.455684	-0.01	-0.00

Table 2: Hydrogen atom with the B-null functional

Auxiliary Basis set	Energy (Hartree)	Difference from grid (kcal/mol)	Percent difference from grid
Grid	-0.496403	0.00	0.00
None	-0.479810	10.49	3.37
9s+3p	-0.493721	1.68	0.54
9s+3p+	-0.494663	1.09	0.35
9s+3p-	-0.495862	0.34	0.11
9s+3p+-	-0.495869	0.33	0.10

Table 3: Nitrogen atom with the B-null functional

Auxiliary Basis set	Energy (Hartree)	Difference from grid (kcal/mol)	Percent difference from grid
Grid	-54.381408	0.00	0.000
None	-54.833381	-283.62	-0.831
10s5p2d	-54.316204	40.92	0.120
10s5p--2d	-54.371032	6.51	0.019
10s5p---2d	-54.371275	6.36	0.019
10s5p---2d-	-54.373005	5.27	0.015
10s5p---2d--	-54.378489	1.83	0.005
10s5p---2d---	-54.381700	-0.18	0.000
10s5p---2d----	-54.381436	0.02	0.000

Table 4: N_2 with the B-null functional and aug-cc-pVDZ

Auxiliary Basis set	Binding energy (kcal/mol)	Bond length (Ångstroms)
Grid	178.5	1.113
None	140.7	1.376
10s5p2d	185.7	1.123
10s5p---2d--	178.2	1.115
10s5p---2d----	175.8	1.113

Table 5: CH_2 with cc-pVTZ

Auxiliary Basis set	$^1A_1$ CH bond (Ångstroms)	$^1A_1$ H - C - H angle	$^3B_1$ CH bond (Ångstroms)	$^3B_1$ H - C - H angle	$^1A_1$ - $^3B_1$ splitting (eV)
Experimental	1.11	102°	1.07	134°	0.369-0.390
Becke88 functional					
Grid	1.135	100.6°	1.096	131.8°	0.88
None	1.420	61.1°	1.259	83.5°	0.55
10s5p2d / 5s2p	1.151	96.7°	1.100	131.7°	0.97
10s5p---2d-- / 9s+3p+-	1.139	100.2°	1.098	132.0°	0.93
10s5p---2d---- / 9s+3p+-	1.137	100.7°	1.098	132.1°	0.92
DePristo functional					
None	1.416	62.0°	1.283	81.2°	0.29
10s5p2d / 5s2p	1.144	99.1°	1.099	132.0°	0.91
10s5p---2d-- / 9s+3p+-	1.136	100.6°	1.094	132.5°	0.89
10s5p---2d---- / 9s+3p+-	1.133	101.4°	1.094	132.1°	0.89
b-vwn functional					
Grid	1.115	101.0°	1.079	134.0°	0.38
None	1.411	60.5°	1.253	82.3°	0.13
10s5p2d / 5s2p	1.129	97.5°	1.091	125.9°	0.37
10s5p---2d-- / 9s+3p+-	1.118	100.7°	1.077	134.4°	0.32
10s5p---2d---- / 9s+3p+-	1.116	101.3°	1.075	135.7°	0.31

Table 6: H_2O with B-null functional and 6-31G**

Auxiliary Basis set	O - H bond (Ångstroms)	H - O - H angle
Grid	0.987	102.1°
None	0.964	120.6°
10s5p2d / 5s2p	1.000	97.9°
10s5p---2d-- / 9s+3p+-	0.991	100.9°
10s5p---2d---- / 9s+3p+-	0.990	100.7°

Table 7: Bond lengths in several systems with B-null functional in Ångstroms

Auxiliary Basis set:	Grid	None	10s5p2d/5s2p	10s5p---2d--/ 9s+3p+-	10s5p---2d----/ 9s+3p+-
O_2 bond	1.249	1.320	1.292	1.254	1.249
F_2 bond	1.460	1.589	1.517	1.455	1.446
Terminal H - B bond in B_2H_6	1.207	1.198	1.210	1.208	1.208
Bridging H - B bond in B_2H_6	1.344	1.592	1.361	1.348	1.347
B-B distance in B_2H_6	1.815	2.603	1.870	1.829	1.824
Be - H bond in BeH_2	1.351	1.315	1.359	1.361	1.361
Li - H bond in LiH	1.657	1.695	1.674	1.663	1.670

Table 8: Binding energies of several systems with B-null functional in eV

Auxiliary Basis set:	Grid	None	10s5p2d/5s2p	10s5p---2d-- / 9s+3p+-	10s5p---2d----/ 9s+3p+-
O_2 binding	4.42	5.14	4.29	4.25	4.14
F_2 binding	1.34	0.57	0.74	0.65	0.52
B_2H_6 binding	20.66	15.67	21.78	20.85	20.75
BeH_2 binding	5.34	6.00	5.69	5.35	5.53
LiH binding	1.55	4.07	2.15	1.58	1.58

Table 9: F_2 with Slater Functional and cc-pVTZ basis set

Auxiliary Basis	Bond distance (Å)	Binding (eV)
Grid	1.4038	2.82
No auxiliary basis	1.5801	2.93
10s5p2d	1.4231	3.53
10s5p---2d--	1.4037	3.48
10s+5p---2d--	1.4037	3.48
10s-5p---2d--	1.4037	3.48
10s-----+++++5p---2d--	1.4037	3.48
10s5p----2d--	1.4037	3.48
10s5p---+2d--	1.4037	3.48
10s5p------+++2d--	1.4037	3.48
10s5p---2d----++	1.4028	3.48
19s+5p---2d--	1.4037	3.48
10s9p------2d--	1.4037	3.48
Grid (6-31G)	1.4744	2.56
10s5p---2d-- (6-31G)	1.4744	3.10

Table 10: SiH_2 with b-vwn5 functional and Dunning/Hay double zeta basis set (+1d)

Auxiliary Basis	Singlet SiH bond (Ångstroms)	Singlet H-Si-H angle	Triplet SiH bond (Ångstroms)	Triplet H-Si-H angle	Splitting (kcal/mol)
Grid	1.5338	91.2°	1.4932	118.1°	-22.06
None	1.4968	85.5°	1.4651	119.0°	1.12
13s9p2d / 5s2p	1.5419	92.3°	1.5055	120.8°	-26.33
13s+9p---2d-- / 9s+3p+-	1.5480	90.6°	1.5004	120.0°	-24.70
13s+++9p---2d-- / 9s+3p+-	1.5483	90.6°	1.5004	120.0°	-24.73
13s+9p---2d---- / 9s+3p+-	1.5443	90.3°	1.4985	118.6°	-24.06
13s+9p---2d----- / 9s+3p+-	1.5429	90.6°	1.4979	118.9°	-23.90
13s+9p---2d------ / 9s+3p+-	1.5433	90.6°	1.4979	118.9°	-23.90
13s+9p----2d----- / 9s+3p+-	1.5433	90.6°	1.4979	118.9°	-23.90
13s+9p---+2d----- / 9s+3p+-	1.5429	90.6°	1.4981	119.0°	-24.05
13s+9p---++2d----- / 9s+3p+-	1.5429	90.6°	1.4981	118.9°	-23.98

Table 11: Timing comparisons between the grid-free and the grid based approach

Molecule	Grid	10s5p---2d-- / 9s+3p+-	10s5p---2d---- / 9s+3p+-
N	8.6	16.6	16.7
N_2	43	341	322
O	17.1	34.8	35.0
O_2	59	493	465
B_2H_6	2745	6590	7308
BeH_2	12.8	66.6	68.0
LiH	12.8	32.1	31.6

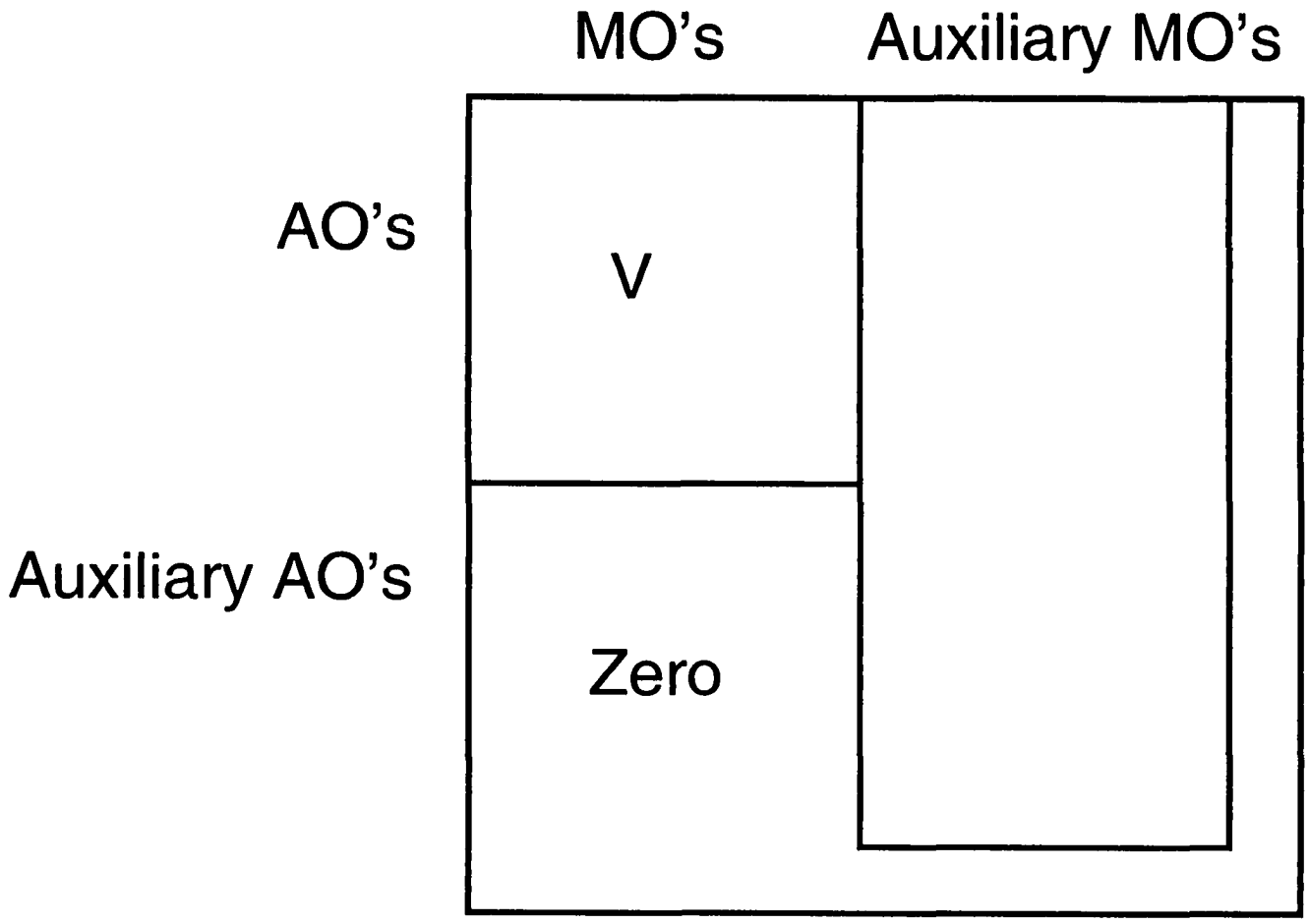

Figure 1: W matrix

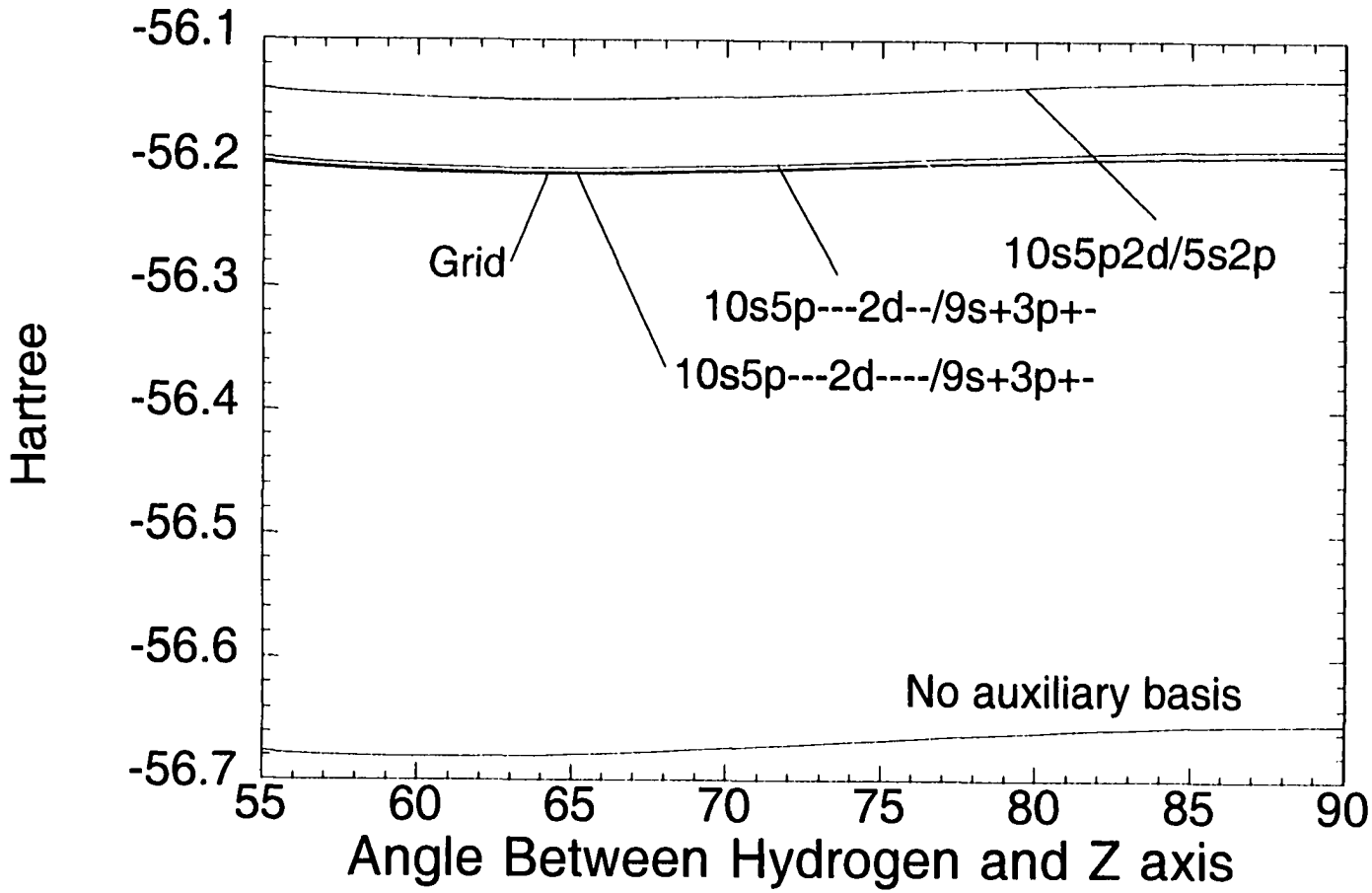

Figure 2: NH_3 bend potential with B-null and cc-pVDZ basis set

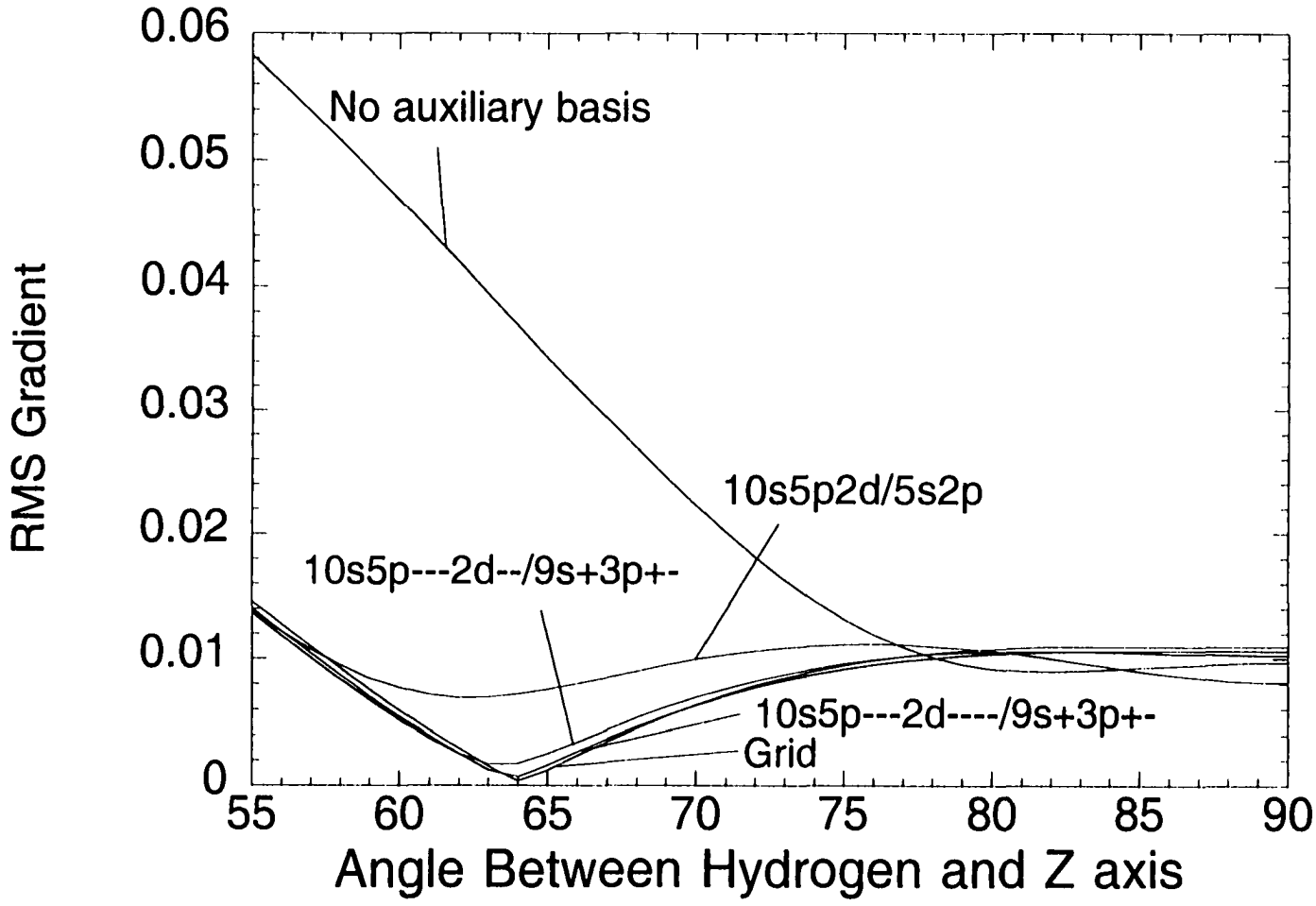

Figure 3: NH_3 RMS gradient with B-null and cc-pVDZ basis set

CHAPTER 5: A STUDY OF $FECO^+$ WITH CORRELATED WAVEFUNCTIONS

A paper submitted to Faraday Transactions

Kurt R. Glaesemann, Mark S. Gordon, and Haruyuki Nakano

Abstract

A study of $FeCO^+$ and Fe^+ using both the second–order multi–configurational quasi–degenerate perturbation theory (MC–QDPT2) method and the coupled cluster method are presented. An all–electron triple–ζ valence plus polarization basis set was used in all calculations. The equilibrium CCSD(T) geometry of $FeCO^+$ is found to be linear ($^4\Sigma^-$) with a Fe^+ to CO distance of 1.905Å and a CO bond distance of 1.133 Å. The dissociation energy D_0 of $^4\Sigma^-$ $FeCO^+$ to ^6D Fe^+ and $^1\Sigma^+$ CO is predicted to be 28.8 kcal/mol, which is within the experimental range. Excited state properties including potential energy surfaces and D_e are predicted for the low lying sextet and quartet states of $FeCO^+$. The first excited state is predicted to be $^4\Delta$ with a D_e of 17.6 kcal/mol. The lowest sextet state is predicted to be $^6\Delta$ with a D_0 of 12.3 kcal/mol. Several examples of pathological behavior at many levels of theory have been discovered and are discussed.

I. Introduction and background.

CO is important in the chemistry of transition metals such as Fe^+, playing a role in many chemical processes and industrial procedures.[1,2,3] Hurlburt *et. al.*[3] pointed out that there are thousands of literature citations that include the phrase "metal carbonyl".[4] In the oxidative addition of H_2 to metals and the reductive elimination of H_2 from metals,[5] CO is important because it effectively stabilizes transition metals, even those that carry negative

charges.[1] The detailed nature of the CO wavefunction has been studied experimentally using electron momentum spectroscopy.[6] Besides Fe^+, CO has been experimentally studied interacting with Ag^+,[3,7] Cu^+,[7] V^+,[8] W^+,[9,10] Fe^-,[11,12] Fe,[12] Ni^-,[11] Cr^+,[10] Mo^+,[10] and Co^+,[13] using diffraction,[3] spectroscopy,[3] collision–induced dissociation (CID) in a guided ion beam tandem mass spectrometer,[7,8,13,14] energy resolved CID,[11] negative ion photoelectron spectroscopy,[12] molecular beam photoionization mass spectrometry,[10] and Fourier transform ion cyclotron resonance mass spectrometry.[9]

$FeCO^+$ has been studied as a catalyst for reactions involving polyhalogenated methane and halogens both in a microwave discharge and without microwaves.[15] This capability makes $FeCO^+$ of particular interest given the role that halogens play in the atmospheric destruction of the ozone layer.[16] Gas phase studies and theoretical calculations have shown that $FeCO^+$ has significantly different reactivity and selectivity than Fe^+ and other complexes such as $Fe(H_2O)_n^+$.[17,18,19] Armentrout and Tjelta found that $FeCO^+$ activates both C–C and C–H bonds in ethane, while $Fe(H_2O)^+$ preferentially activates the C–H bonds.[20] This selectivity can be partially explained by the observation that R groups must interact with the 3dσ orbital in $Fe(H_2O)^+$ instead of the empty 4s orbital in $Fe(CO)^+$.[20] The photodissociation of $Fe(CO)_5$ has been studied with femtosecond lasers. $FeCO^+$ plays an important role in this reaction as the final intermediate, and as the reactant in the slowest step of the mechanism.[21] Careful study of the velocity distribution in the $Fe(CO)_5$ dissociation has also proved useful in analyzing the mechanism.[22] Majima found that using a transversely excited atmospheric (TEA) CO_2 laser to dissociate $Fe(CO)_5$ in the presence of SF_6 resulted in no $FeCO^+$ ion formation, and the loss of the first CO was the rate determining step.[23]

The ground state of $FeCO^+$ is consistently reported to be quartet with $C_{\infty v}$ symmetry,[24,25,26] although Fe^+ is experimentally known to be a sextet[27] and CO is a singlet. None of the experimental or theoretical studies predict $COFe^+$ as the ground state geometry, although neutralization–reionization mass spectrometry (NRMS) had small FeO^+ fragment peaks implying that some $COFe^+$ was present.[28]

A wide variety of experimental studies have been carried out on $FeCO^+$. Selected ion flow tubes (SIFT) and collision–induced dissociation (CID) have proven effective in measuring bond dissociation energies (D_0) of Fe^+ containing compounds such as $Fe(N_2)_n^+$,[29] $Fe(CH_2O)_n^+$,[29] $Fe(CS_2)_n^+$,[30] and $FeCO^+$.[29,31,32] CID gives a $FeCO^+$ D_0 of 36.1±1.8 kcal/mol relative to ^4F Fe^+ and ground state CO. Vibrationally corrected CID gives a D_0 of 30.9±0.9 kcal/mol,[29] relative to ^6D Fe^+. Product kinetic energy release distributions (KERDS) gives a D_0 of 31.8±3 kcal/mol,[33] relative to ^6D Fe^+. Fourier transform mass spectrometry results were analyzed with Cook's kinetic method to give D_0 relative to $Fe(C_2H_4)^+$, yielding $D_0(FeCO^+)$= 31.2±0.2,[19] relative to an unspecified state of Fe^+. Ng *et. al.* have studied $FeCO^+$ using photoelectron–photoion coincidence (PEPICO) and determined the D_0 of $Fe(CO)_n^+$ to be 17.8±0.9, 25.2±1.1, 25.7±1.4, 41.5±1.6, and 39.3±2.0 kcal/mol for n=5,4,3,2,1 respectively,[14] relative to ^6D Fe^+. PEPICO introduces $Fe(CO)_5$ into the photoionization region using a supersonic expansion to reduce rotational and vibrational scattering.[34,35,36,37] In the work of Ng *et. al.*, relative PEPICO intensities for $Fe(CO)^+_n$ had to be estimated for n=2,1,0. The primary focus of that work was on getting good relative intensities. In addition to PEPICO, Ng *et. al.* used CID to study $FeCO^+$. $FeCO^+$ ions were selected with quadrapole mass spectroscopy (QMS) and then collided with Ar to induce dissociation. The ratio of $FeCO^+$ reactant ions and Fe^+ product

ions was analyzed with QMS, to give a D_0 of 33±4 kcal/mol for $FeCO^+$,[14] relative to ^6D Fe^+. Since the PEPICO value is just an estimate, the experimental range for D_0 to ground state ^6D Fe^+ and CO is 30.9–33.0 kcal/mol with experimental error bars out to 28.8–37.0 kcal/mol. D_0 for dissociation to ^4F Fe^+ should be 5.35 kcal/mol larger than this range; that is, the experimental range for dissociation to ^4F Fe^+ is 34.15-42.35 kcal/mol.

The ground state of $FeCO^+$ has been investigated using many different theoretical methods, giving a wide range of dissociation energies. It is important to note that experiments measure D_0, while many calculations predict D_e values. D_e values are always slightly larger than D_0 values; in section III, this difference is predicted to be 0.95 kcal/mol for $^4\Sigma^-$ $FeCO^+$.

The density functional theory (DFT) hybrid functional B3LYP[38] predicts a $FeCO^+$ binding energy of D_e=37.0 kcal/mol relative to ^4F Fe^+ that is within the experimental error bars, unlike BLYP (D_e=47.8 kcal/mol) and LSDA (D_e=50 kcal/mol).[24] The modified coupled pair functional (MCPF) predicts a binding energy (28.9 kcal/mol) that is too small.[24] Single–reference MP2 predicts 30.8 kcal/mol[25] which is also too low. Others have calculated the D_e for dissociation relative to ^6D Fe^+. This D_e is predicted by B3LYP to be 32.7 kcal/mol,[39] which is within the experimental range. The previous calculations predict little significant charge transfer from Fe^+ to CO, and they demonstrate that an explicit treatment of correlation is essential to get proper energetics and geometries for $FeCO^+$,[40] as well as for $FeCO^-$ [41] and FeCO.[26,42,43]

Studying multiple electronic states often requires a multi–configurational wavefunction. The investigation of multiple potential energy surfaces (PES) frequently requires the use of state–averaged (SA) wavefunctions to obtain a consistent treatment of the

various electronic, and especially degenerate, states. A proper description of such species often requires more than a single, simple Lewis structure.[44] This requirement reduces the utility of DFT methods, except for those that implement one of the fractional occupation number (FON) formalisms[45,46,47,48] or the DFT CI singles formalism.[49] In this work the low lying quartet and sextet states of $FeCO^+$ are studied using multi–configurational self–consistent field (MCSCF)[50] wavefunctions, second–order multi–configurational quasi–degenerate perturbation theory (MC–QDPT2),[51,52,53] and single-configuration coupled cluster theory with single and double replacements, augmented by perturbative triples [CCSD(T)].[54] In Section II the theoretical approaches used to study Fe^+ and $FeCO^+$ are explained in detail. In Section III Fe^+ is examined with several different methods and basis sets. In Section IV $FeCO^+$ PES are studied and frequencies of the lowest sextet and quartet equilibrium geometries are presented. In Section V the possible origins of poor behavior in multi-reference perturbation theory are discussed in detail.

II. Theoretical Methods

$FeCO^+$, CO, and Fe^+ were studied using an all–electron triple–ζ valence plus polarization (TZVP) basis set. For Fe, a [10s6p] contraction of Wachters' (14s9p) primitive basis[55] was supplemented with the [3d] contraction of (6d) primitives proposed by Rappé *et. al.*.[56] This basis set was augmented with two sets of p functions (ζ=0.231 and ζ=0.0899) to give an adequate representation of the 4p subshell. This is the Fe triple–ζ valence (TZV)[57] basis set of (14s9p5d)/[10s8p3d]. A set of f functions was added to provide polarization (ζ=1.663)[58]. For C and O the Dunning [5s,3p][59] contraction of the (10s,6p)[60] primitives was used as the triple–ζ valence (TZV)[57] basis set. One set of d

functions was added to provide polarization to the C (ζ=0.72)[61] and O (ζ=1.28).[61] The quantum chemistry code GAMESS[62] was used, unless otherwise noted. The CO bond distance was fixed at 1.1283Å for most PES, since previous work has shown that the positively charged Fe^+ ion causes little relaxation of the CO bond.[24] The geometries of the lowest lying quartet and sextet states were fully optimized including relaxation of the CO bond.

Most calculations presented in this work are based on fully–optimized reaction space (FORS)[63,64] MCSCF wavefunctions, also known as complete active space self–consistent field (CASSCF)[65,66,67,68] wavefunctions. The basic $FeCO^+$ wavefunction has 13 MCSCF core orbitals that are doubly occupied in all configurations and 11 orbitals with 13 electrons in the multi–configurational active space (13/11). The MCSCF active space includes the six valence 3d and 4s orbitals on Fe^+, σ donor lone pair orbital on CO, and the CO π bonding and π^* anti–bonding orbitals. This active space allows for a proper treatment of the Fe^+ ion, carbon σ donation of the CO lone pair, and π backbonding into the CO π system. Reduced active spaces were appropriate in some instances and will be described below. The calculations on Fe^+ have a corresponding active space that includes the Fe^+ valence 3d and 4s orbitals. By carefully choosing orbitals, the MCSCF wavefunction was selectively converged to different spatial and spin symmetries. Dynamical correlation is usually necessary to obtain accurate energetics, therefore multi–configurational quasi–degenerate perturbation theory to second–order (MC–QDPT2)[51,52,53] was applied to the converged MCSCF wavefunction. The $FeCO^+$ MC–QDPT2 calculations correlated all molecular orbitals, except the 11 chemical core orbitals. In other words, the O lone pair and the CO sigma bond orbitals were doubly occupied in the MCSCF wavefunction, but were

correlated at the MC–QDPT2 level. The Fe^+ active space is the same in the MC–QDPT2 and MCSCF wavefunctions, with 9 chemical core orbitals.

The MC–QDPT2 method is not simply a multi–configurational extension of single–configuration Møller–Plesset (MP2)[69] perturbation theory, although MC–QDPT2 does include MP2 as a subset.[53] MC–QDPT is a multi–state and multi–configurational perturbation method based on Van Vleck perturbation theory, while MP2 is based in Rayleigh–Schrödinger perturbation theory. The MC–QDPT2 approach facilitates an accurate treatment of both the ground state and excited states, with various space and spin symmetries (including simultaneously treating truly and nearly degenerate states correctly).[51,52] MC–QDPT2 is a perturb then diagonalize approach, in which the Hamiltonian is improved first with perturbation theory and then diagonalized to obtain the second–order energies.[70,71] The degenerate states ($^4\Delta$, $^4\Phi$, $^4\Pi$, $^6\Pi$, $^6\Delta$) are all treated using SA–MCSCF wavefunctions to properly account for their doubly degenerate nature. Since the states that are averaged are energetically equivalent, discontinuities[72] resulting from state–flipping do not appear in the SA–MCSCF PES.

Multi–reference second–order configuration interaction (MR–SOCI)[73,74] was also used to add correlation to selected MCSCF calculations. MR–SOCI involves single and double excitations out of the MCSCF active space, without reoptimizing the orbitals. This provides a variational method for adding second–order correlation effects to the wavefunction. MR–SOCI provides a variational check on the MC–QDPT2 wavefunction.

Some calculations presented are based on single–configuration wavefunctions. Coupled cluster theory including single and double replacements, with triples added perturbatively, has proven to be a powerful method for predicting the energetics of systems

that can be treated with single–configuration wavefunctions. In this work, the CCSD(T)[75,76] method with the TZVP basis set has been used to investigate the $^4\Sigma^-$ $FeCO^+$ ground state. The results of these calculations are compared with those obtained using the multi–reference methods. To avoid spin–contamination, the ROHF based formalism is used for the CCSD(T) calculations. The approach used is based on the Bartlett definition of RCCSD(T)[77] in which the triples are computed with contributions from both singles and doubles. This is the most common definition of open-shell triples although certainly not the only one.[78] The MOLPRO[79] *ab initio* package was used for most CCSD(T) calculations.

III. Fe^+

The Fe^+ ground and first excited states are known experimentally to be ^6D ($3d^64s^1$) and ^4F ($3d^74s^0$), respectively. The experimental splitting has been determined to be 5.35 kcal/mol.[27] SA–MCSCF calculations were performed to obtain the correct wavefunctions for the ^6D (five fold degenerate) and ^4F (seven fold degenerate) electronic states. MCSCF natural orbital occupation numbers (NOON) for both states are presented in Table 1 and the energy splittings at several levels of theory are given in Table 2. State averaging the wavefunction correctly gives all 3d orbitals the same NOON for each spin multiplicity. The poorly predicted splitting of 38.5 kcal/mol at the MCSCF level of theory is not surprising given the difficult nature of predicting the separation with *ab initio* methods.[80,81,82,83]

MR-SOCI and more efficient MC–QDPT2 calculations were carried out, to provide dynamic electron correlation in addition to the near degenerate correlation provided by the use of a multi–configurational wavefunction. The MC–QDPT2 results are closer to experiment than MCSCF, although this method does slightly overcorrect the MCSCF

splitting. The MR–SOCI wavefunction has a larger absolute error than MC–QDPT2. The error for CCSD(T) lies between the MC–QDPT2 and MR-SOCI errors. Previous calculations on transition metal cations[84] suggest that additional polarization functions (e.g. g functions on Fe) may be necessary to obtain accurate atomic splitting. Adding a set of g functions (ζ=1.7) with the six orbital active space provides little improvement. Therefore g functions are not used in the $FeCO^+$ calculations.

IV. $FeCO^+$

IVA. Ground state PES

Initially the ground state PES for $^4\Sigma^-$ (as a function of the Fe – C distance) was calculated using the MCSCF/MC–QDPT2 method presented in Section II. For MCSCF wavefunctions, $^4\Sigma^-$ is found to be higher than the lowest sextet state (the lowest lying sextet state will be discussed in detail in Section IVB). With the addition of MC–QDPT2 dynamic correlation, the ground state for $FeCO^+$ is correctly found to be $^4\Sigma^-$. Just as in the Fe^+ calculations, correlation lowers the quartet states significantly more than the sextet states. Results are presented in Figure 1, with the zero of energy defined by separated ^{6}D Fe^+ and ground state CO at each level of theory. The D_e with respect to ^{4}F Fe^+ is found to be 33.4 kcal/mol (at the low end of the experimental range) with an equilibrium distance of 1.93 Å. A discontinuity that appears at about 0.34 Å inside R_e is discussed in detail in Section V.

Close examination of the MCSCF and MC–QDPT2 potential energy curves reveals that the virtual 4s orbital on Fe^+ shifts onto CO as the complex dissociates. This results in a D_e that is too small (although the equilibrium geometry is valid). FORS-MCSCF is size-consistent, but size-consistency is only applicable if the active spaces in the separated Fe^+

and CO are the same as in the $Fe^+ \cdots CO$ supermolecule. The shifting orbital resulted in a smaller active space on Fe^+ and a larger active space on CO in the supermolecule. Variational methods such as MCSCF can correct for poorly chosen orbitals and lower the energy, but perturbative methods such as MC–QDPT2 require a well–balanced active space to be reliable. Therefore this orbital was removed from the $^4\Sigma^-$ MCSCF active space. The results with the (13/10) active space are presented in Figure 2; the D_e is found to be 36.5 kcal/mol with respect to ^4F Fe^+ (within the experimental range). The equilibrium Fe – CO distance is 1.75 Å. Unfortunately, this (13/10) $^4\Sigma^-$ PES has a discontinuity near the MC–QDPT2 minimum, making the geometry suspect. Similar behavior is found using the multi-reference CI wavefunction. This discontinuity is discussed in detail in Appendix A.

Since the largest natural orbital occupation number in the virtual space of the $^4\Sigma^-$ state is less than 0.1, it is reasonable to use single–reference CCSD(T) for the ground state.[85,86,87] Thus, although this method does have a lower quality zeroth–order wavefunction (ROHF) than MC–QDPT2 (MCSCF), the final results should be accurate. There are no unusual features in the CCSD(T) PES as shown in Figure 2. By fitting the points on the CCSD(T) PES, the D_e with respect to ^4F Fe^+ is found to be 35.0 kcal/mol with an equilibrium Fe – CO distance of 1.91 Å and the C - O distance fixed at 1.1283 Å. This D_e is in good agreement with the experimental results and close to the MC–QDPT2 D_e, despite the problems encountered with that method.

The geometry of the $^4\Sigma^-$ state was optimized at the CCSD(T) level of theory. The molecule was not assumed to be linear, although all attempts at bending the $FeCO^+$ increased the energy at the MCSCF, MC–QDPT2, and CCSD(T) levels of theory. One cannot assume that excited electronic states are linear, particularly since bent excited and

ground states are not uncommon for third row metal carbonyls.[88] The minimum energy CCSD(T) geometry is $C_{\infty v}$ with a Fe^+ – CO distance of 1.905 Å and a CO bond distance of 1.133 Å. The CO bond did not relax significantly during interaction with Fe^+, because there is little charge transfer into the CO bond region. The CCSD(T) D_e for dissociation of $^4\Sigma^-$ $FeCO^+$ to ^4F Fe^+ is 35.1 kcal/mol. Note that only 0.1 kcal/mol is gained by allowing the CO bond length to relax. Based on the experimental quartet–sextet splitting of 5.35 kcal/mol, the CCSD(T) D_e for dissociation of $^4\Sigma^-$ $FeCO^+$ to ^6D Fe^+ should be 29.7 kcal/mol.

A numerical CCSD(T) hessian was calculated for the $^4\Sigma^-$ state. A double differences approach was used to minimize the possibility of numerical error (see Appendix B). The frequencies are not scaled, because CCSD(T) should give high quality results. The frequencies and associated intensities are compared with experiment and previously calculated spectra in Table 3. Intensities are based on the ROHF dipole derivative tensor and the CCSD(T) hessian. The CCSD(T) predicted CO stretch is smaller than the MP2 and B3LYP frequencies. If the experimental values for $FeCO^-$ and FeCO are a valid guide, then the CCSD(T) frequencies are not unreasonable. A vibrational analysis of the normal modes leads to a zero–point energy (ZPE) of 4.13 kcal/mol. The CO molecule has a ZPE of 3.18 kcal/mol, calculated using closed–shell CCSD(T) with ACESII.[89] This results in a net ZPE correction of 0.95 kcal/mol for the $FeCO^+$ complex. Therefore, the D_0 for dissociation to ^4F Fe^+ is 34.2 kcal/mol. The D_0 for dissociation to ^6D Fe^+ is 28.8 kcal/mol, at the low end of the experimental range presented in Section I.

IVB. Excited states.

The $^6\Sigma^+$, $^6\Delta$, $^6\Pi$, and $^4\Delta$ states were each separately optimized. Degenerate states were state averaged (SA-MCSCF) over both components to preserve orbital and hence state degeneracy. MC–QDPT2 was applied as a perturbation to add dynamical correlation to obtain reliable energetics and geometries, with two roots included in the treatment when the state was degenerate. The (13/11) MCSCF active space presented in Section II was used for the $^6\Delta$ and $^6\Pi$ states.

When a (13/11) active space is used for the $^4\Delta$ state, the virtual 4s orbital becomes a CO virtual orbital as the complex dissociates, resulting in improper energetics, similarly to the $^4\Sigma^-$ state in Section IVA. Thus, this CO orbital was removed from the $^4\Delta$ MCSCF active space, yielding a (13/10) active space. This removal does not reduce the effective size of the active space, because neither this orbital nor the 4s is significantly populated in the quartet states. For Fe^+ ion, removing the 4s orbital raises the MCSCF energy 0.8 kcal/mol, and lowers the MC–QDPT2 energy 0.04 kcal/mol.

For the $^6\Sigma^+$ and the $^4\Delta$ states, the 3dσ orbital should be doubly occupied in all configurations due to spatial and spin symmetry. Therefore, the MCSCF active space for the $^6\Sigma^+$ and the $^4\Delta$ states was reduced by one orbital to force the 3dσ orbital to be doubly occupied in all configurations. This yields (11/10) and (11/9) active spaces, respectively, for the two states. This reduction does not reduce the effective size of the active space relative to the other states, because removing an orbital that is doubly occupied in all configurations does not shrink the effective active space. These reduced, but properly dissociating, active spaces are then used to calculate MCSCF and MC–QDPT2 energies for the $^6\Sigma^+$ and the $^4\Delta$ states. The energies of the $^4\Delta$ (11/9), $^6\Sigma^+$ (11/10), $^6\Pi$ (13/11), and $^6\Delta$

(13/11) states are presented as a function of the Fe – C distance in Figures 3 and 4 for MCSCF and MC–QDPT2, respectively. At the higher level of theory, the potential energy minimum of the $^4\Delta$ state is well below that of the others and has a shorter Fe – C equilibrium distance.

Since the $^4\Pi$ and $^4\Phi$ states could not be individually optimized, an additional set of SA–MCSCF calculations were performed in which all sextet states and all quartet states were state–averaged (separately for each multiplicity) to obtain energies for all 12 states with the (13/11) active space. The results of these calculations are shown in Figures 5 and 6, for MCSCF and MC–QDPT2 respectively. These calculations cannot be used directly to obtain D_e values or geometries, because the state averaging gives geometries and energies that depend on all the states. The curves in Fig. 6 do suggest that the $^4\Pi$ and $^4\Phi$ states should lie between the $^4\Delta$ and $^4\Sigma^-$ states. Therefore the ranges that the D_e and equilibrium distances must fall into are known for $^4\Pi$ and $^4\Phi$, even if exact values are not. All states are found to be bound in all of the calculations. Therefore even if the $FeCO^+$ complex is in a low lying excited state when it initially forms from Fe^+ and CO, it will most likely be a bound state.

Dissociation energies for $FeCO^+$ excited states relative to the ^6D ground state were calculated by assuming a fixed CO distance and a linear $FeCO^+$ at the MC–QDPT2 level. The properly dissociating active spaces presented above in Fig. 4 were used. These results along with the corresponding Fe^+ – CO equilibrium distances are presented in Table 4. As the equilibrium distance increases, the calculated D_e decreases, as one would expect.

MCSCF NOON are presented for all states at the MC–QDPT2 equilibrium geometries in Table 5. For states with active spaces smaller than the original (13/11), the

orbitals not in the active space are designated in Table 5 as integer NOON with no trailing zeros. The quartet states are found to have an empty Fe 4s orbital while the sextet states have a singly occupied Fe 4s orbital. This difference allows the quartet $FeCO^+$ states to more readily accept electron density from other molecules. This explains the experimentally observed greater reactivity of $FeCO^+$ versus Fe^+. All of the quartet states are found to be lower in energy than all of the sextet states. Therefore, the lowest excited states are likely to show this enhanced reactivity.

Because $^6\Delta$ is the lowest sextet state, a numerical MC–QDPT2 hessian was calculated using finite differences. The large basis MP2 scaling factor is 0.94–1.02 depending on whether one is fitting ω, ZPE, $\Delta H_{vib}(T)$, $1/\omega$, or $S_{vib}(T)$.[90] MC–QDPT2 should calculate frequencies more accurately than MP2, so a scaling factor of 1.0 was assumed. Intensities presented are based on the MCSCF dipole derivative tensor and the MC–QDPT2 hessian. These frequencies and intensities are presented in Table 3. The $^6\Delta$ $FeCO^+$ ZPE is 3.44 kcal/mol and the CO ZPE is 3.02 kcal/mol. The net $^6\Delta$ $FeCO^+$ ZPE is 0.42 kcal/mol, resulting in a $^6\Delta$ D_0 of 12.3 kcal/mol.

V. Problems with multi-reference perturbation theory

Careful analysis of the (13/10) $^4\Sigma^-$ PES reveals that a discontinuity is present on the MC–QDPT2 surface at 1.560516Å. Failures of single–reference Møller–Plesset have been reported in the literature, even for a single Ne atom.[91] There are reports of similar problems within the multi–reference CASPT2 extension of MP2.[92,93] The PES of the divergent state is illustrated in Figure 7. The energies plotted are total energies with the zero of energy defined as MC–QDPT2 separated Fe^+ and CO. The MC–QDPT2 "correction" to the

MCSCF energy is positive on one side of the discontinuity and negative on the other side. The energy difference between R(Fe – C) = 1.560515Å and 1.560516Å is 376 Hartree for MC–QDPT2 and only 0.0003 kcal/mol for MCSCF. This discontinuity is particularly troubling because such problems are usually expected to occur in excited state calculations. The MC–QDPT2 PES is smooth elsewhere, so the discontinuity is localized. Fortunately, the discontinuity is not near the minimum energy point or dissociation, so predicted properties are not corrupted.

The choice of perturbation theory does effect the energies calculated; Møller–Plesset (MP) and Epstein–Nesbet (EN) partition differently and achieve perturbation expansions that behave differently.[94,95] The MC–QDPT2 calculation is performed on the canonicalized Fock orbitals, because perturbation theory requires orbital energies. Canonicalization is a rotation within the active space, so the MCSCF wavefunction is unchanged. For a perturbation expansion to be valid, the zeroth–order wavefunction Ψ^0 must be a close approximation to the exact wavefunction Ψ. In the single–state case of $^4\Sigma^-$, the weight of the reference function in the first–order wavefunction is defined by Eq. (1):

$$W = \frac{\langle \Psi^0 \mid \Psi^0 \rangle}{\langle \Psi^0 + \Psi^1 \mid \Psi^0 + \Psi^1 \rangle}, \tag{1}$$

where Ψ^1 is the first–order correction to the wavefunction and $\Psi=\Psi^0+\Psi^1+\Psi^2+\Psi^3+....$ Therefore, $\Psi^0+\Psi^1$ is the first–order wavefunction. Ψ^0 and Ψ^1 are orthogonal and Ψ^0 is normalized, so Eq. (1) simplifies with a little mathematical manipulation to Eq. (2).

$$W = \frac{1}{1+\langle \Psi^1 \mid \Psi^1 \rangle} \tag{2}$$

The weight W is nearly 0% at the discontinuity. Thus, this wavefunction is a truly divergent case at second–order. Several values of W are plotted in Figure 7. The weight is

> 89% from 1.7 Å to dissociation and >87% for R(Fe – C)≤1.4 Å. Clearly, even though the perturbation expansion is failing for the $^4\Sigma^-$ PES, the MC-QDPT2 method is surprisingly robust, giving reasonable energies for values of W as small as 25%.

The MCSCF wavefunction was examined in an effort to obtain some theoretical insight. When orbitals cross, the nature of a state can shift suddenly. The number of degenerate molecular orbitals was not different at the discontinuity, so an orbital crossing (including virtuals) was not causing the divergence. MCSCF NOON provide insight into the multi–reference nature of a wavefunction; however the NOON are smoothly varying in the region of the discontinuity. The largest variance anywhere on the PES from single–reference values of 0, 1, and 2 is only 0.1598, and this is at the unbound geometry.

The gap between the highest energy MCSCF active orbital and the lowest non-active virtual orbital is 62 kcal/mol. Thus, this divergence was not caused by a low lying orbital that should have been included in the MCSCF active space. Using a full CI within the MCSCF active space, the next highest state is found to be 27.9 kcal/mol higher. Therefore a low lying excited state is also not the underlying cause. A variational second–order approach was utilized to further examine the validity of the underlying MCSCF wavefunction. An internally contracted multi–reference second–order CI[96,97](SOCI) produces energies that are reasonable and smooth in the region of the divergence. This suggests that the origin of the MC–QDPT2 divergence does not lie in the MCSCF orbitals, but rather within the perturbation expansion itself.

MC–QDPT2 divergences can be artificially avoided. One way to avoid the divergence is to change the reference function. A logical choice is to replace the canonical Fock orbitals with the natural orbitals.[98] These orbitals diagonalize the first–order density

matrix rather than the generalized Fock matrix. The MC–QDPT2 energy is not invariant with respect to orbital rotations within the active space, unlike the FORS–MCSCF energy. Using natural orbitals results in different orbital energies, and the choice of orbital energies affects convergence of the perturbation expansion.[99] The validity of such a substitution is not known, particularly since orbital energies are not as well–defined for natural orbitals. A CSF selection scheme could be utilized, in which the CSFs that contribute little to the MCSCF wavefunction are not used in the perturbation step.[100] However, this is an arbitrary restriction on the MC–QDPT2 calculation, and this restriction might introduce problems of its own. A chemically important CSF might be left out of the MC–QDPT2 calculation, resulting in spurious results. A third approach is to change the active spaces. Several attempts to vary the MCSCF and MC–QDPT2 active spaces were undertaken and although the divergence shifted to other distances, it usually did not disappear. These three modifications have the downside of changing the nature of the perturbation method, and therefore all calculations would have to be done using these modifications with no guarantee of not introducing another divergence or other problem.

The cause of these divergences may be understood by examining mathematics of expansions. The Hamiltonian is expanded in the space of perturbation parameter λ about $\lambda=0$ and evaluated at $\lambda=1$. In the case of MC–QDPT, $\lambda=0$ corresponds to the MCSCF reference wavefunction and $\lambda=1$ corresponds to the MC–QDPT wavefunction. As λ goes from 0 to 1, the correlation is turned on. If the perturbation expansion converges, the MC–QDPT wavefunction is the exact wavefunction. MC–QDPT2 truncates the expansion at the second–order terms. Singularities can appear within the λ space. The singularity nearest to $\lambda=0$ limits the radius of convergence. The expansion is valid for all λ that are

closer to λ=0 than this singularity. For λ's outside the radius of convergence, it is possible for the perturbation series to converge, but often to the wrong number.[101] This problem is not limited to perturbation expansions; divergences limit the usefulness of all expansions, such as Taylor series.[102] Singularities are not limited to real values of λ and therefore predicting or interpreting these problems is difficult.

VI. Conclusions

Fe^+ and its complexes such as $FeCO^+$ are interesting due to their chemical reactivity as catalysts. CO is of particular interest, because it is especially effective in stabilizing transition metals. The addition of CO to Fe^+ changes the reactivity significantly, because the ground state changes from a sextet to a quartet upon formation of the $FeCO^+$ complex. This change in spin results from a change in the 4s orbital occupation from one to zero. The three low lying excited states are also quartets, therefore this enhanced reactivity is probably present these lowest excited states. Results from a careful study reveal that uncorrelated wavefunctions such as MCSCF fail to properly handle this shift from sextet to quartet. MCSCF predicts that the sextet is always lower than the quartet in energy. Dynamical correlation is found to be necessary to achieve proper energetics. In the present work, dynamic correlation is obtained with both MC–QDPT2 and single–reference ROHF based CCSD(T). These two methods predict dissociation energies for the $^4\Sigma^-$ ground state that are comparable to the experimental values (D_0=28.8–37.0 kcal/mol). With the addition of zero–point corrections, the CCSD(T) predicted D_0 is found to be 28.8 kcal/mol. The MC–QDPT2 D_e is found to be 32.3 kcal/mol. The lowest lying sextet state, $^6\Delta$, is predicted by MC–QDPT2 to have a D_0 of 12.3 kcal/mol. Therefore, $FeCO^+$ gains 16.5 kcal/mol in

energy when it changes spin states. The $^6\Delta$ and $^4\Sigma^-$ states can be differentiated experimentally by their IR spectra. The CO stretch frequencies for the $^6\Delta$ and $^4\Sigma^-$ are very similar, but the $^6\Delta$ intensity is very small. The Fe – C stretch frequencies differ by 229 cm^{-1}. In both states the linear bend has the smallest IR intensity. During the analysis of the $FeCO^+$ system, difficulties at several levels of theory were discovered and analyzed.

Appendix A. A MCSCF discontinuity

The $^4\Sigma^-$ (13/10) MCSCF curve has a discontinuity, which is presented in Figure A1. This jump is caused by a sudden change in the CO π^* NOON from 0.09 to 0.06. This change causes a change in the shape in the MCSCF curve and a break in the MC–QDPT2 curve. The NOON change occurs near the MC–QDPT2 minimum, so optimizing the geometry is not possible. This bump was investigated with SOCI based on the MCSCF reference[103,104] using MOLPRO. This variational method gives a similarly discontinuous PES. This means that the underlying MCSCF wavefunction is pathological or incorrect; therefore, this is not a MC–QDPT2 divergence as discussed in Section V. A full CI within the FORS space was done, and no low lying states were found on either side of the split, and none of the lowest states were $^4\Sigma^-$ states. Removal of the π^* orbital from the MCSCF active space solved the problem; this solution removes all virtual orbitals from the MCSCF active space, leaving a predominantly single–reference wavefunction. An effort to incrementally improve the active space by moving core orbitals into the active space failed to remove the discontinuity.

Appendix B. The calculation of a hessian using a fully numerical approach.

Because $FeCO^+$ is a small linear molecule, the hessian is much simpler to calculate in internal coordinates. The two bending terms are degenerate and therefore only one must be calculated. Because $E(\theta)$ is symmetrical about the linear bend θ, $(\partial E/\partial\theta)_{\theta=180^\circ}$ vanishes. Therefore $(\partial^2 E/\partial S\partial\theta)_{\theta=180^\circ}$ must also vanish, where S is a bond stretch. Therefore in linear $FeCO^+$, the bend–stretch cross–terms vanish. The two stretches (FeC and CO) are not independent, so two pure terms and two equal cross–terms must be calculated. S_1, S_2=distances and L, K=offset are used in the derivation. Offsets of 0.02Å, 0.01Å, 0.005Å and 1°, 2°, 3°, 4°, 5°, 6° were averaged to reduce the possibility of numerical error.

The stretch cross–term is:

$$\left.\frac{\partial^2 E(S_1,S_2)}{\partial S_1 \partial S_2}\right|_{S_1=S_2=0} = \frac{[E(L,L)+E(-L,-L)]-[E(L,-L)+E(-L,L)]}{4\cdot L^2}. \qquad \text{(C1)}$$

Stretch terms, for which $S_1=S_2$, are:

$$\left.\frac{\partial^2 E(S_1)}{\partial S_1 \partial S_1}\right|_{S_1=0} = \frac{[E(K)+E(-K)]-[2\cdot E(0)]}{K^2}, \text{ with } K=2L. \qquad \text{(C2)}$$

Bending terms, for which $E(\theta)=E(-\theta)$, are:

$$\left.\frac{\partial^2 E(\theta)}{\partial\theta\partial\theta}\right|_{\theta=0} = \frac{[2\cdot E(K)]-[2\cdot E(0)]}{K^2}. \qquad \text{(C3)}$$

The resulting hessian is presented in Table B1.[105]

Acknowledgements

This work was supported in part by grants from the Air Force Office of Scientific Research (F49–620–97–1–0522) and by the Ames Laboratory, US–DOE. The authors would like to thank Dr. Mike Schmidt and Dr. Cheuk Ng for many enlightening conversations.

References:

1. J.E. Ellis, *Adv. Organomet. Chem.*, 1990, **31**, 1.
2. P.C. Ford, Ed. *Catalytic Activation of Carbon Monoxide*; ACS Symp. Ser., **152**, ACS: Washington D.C. 1981.
3. P.K. Hurlburt, J.J. Rack, J.S. Luck, S.F. Dec, J.D. Webb, O.P. Anderson and S.H. Strauss, *J. Am. Chem. Soc.*, 1994, **116**, 10003, and references therein.
4. Chemical Abstracts Service Online.
5. G. Henrici–Olivé and S. Olivé, *The Chemistry of Catalyzed Hydrogenation of Carbon Monoxide*, Springer–Verlag, Berlin, (1984), and references therein.
6. X.W. Fan, X.J. Chen, S.J. Zhou, Y. Zheng, C.E. Brion, R. Frey and E.R. Davidson, *Chem. Phys. Lett.*, 1997, **276**, 346.
7. F. Meyer, Y–M. Chen and P.B. Armentrout, *J. Am. Chem. Soc.*, 1995, **117**, 4071.
8. M.R. Sievers and P.B. Armentrout, *J. Phys. Chem.*, 1995, **99**, 8135.
9. P. Mourgues and G. Ohanessian, *Rapid Comm. Mass. Spec.*, 1995, **9**, 1201.
10. Y.–J. C.–L. Liao, and C.Y. Ng, *J. Chem. Phys.*, 1997, **107**, 4527.
11. L.S. Sunderlin, D. Wang, and R.R. Squires, *J. Am. Chem. Soc.*, 1992, **114**, 2788.
12. P.W. Villalta and D.G. Leopold, *J. Chem. Phys.*, 1993, **98**, 7730.
13. S. Goebel, C.L. Haynes, F.A. Khan and P.B. Armentrout, *J. Am. Chem. Soc.*, 1995, **117**, 6994.

14. K. Norwood, A. Ali, G.D. Flesch, and C.Y. Ng, *J. Am. Chem. Soc.*, 1990, **112**, 7508.

15. M. Sablier, H. Mestdagh, and C. Rolando, *J. Phys. Chem.*, 1994, **98**, 8320.

16. J.H. Butler, J.W. Elkins, B.D. Hall, S.O. Cummings, and S.A. Montzka, *Nature*, 1992, **359**, 403.

17. P.B. Armentrout and B.L. Tjelta, *Organometallics*, 1997, **16**, 5372.

18. A. Ricca and C.W. Bauschlicher, *J. Phys. Chem.*, 1995, **99**, 9003.

19. D. Schröder and H. Schwarz, *J. Organometallic Chem.*, 1995,**504**, 123.

20. B.L. Tjelta and P.B. Armentrout, *J. Am. Chem. Soc.*, 1996, **118**, 9652.

21. L. Bañares, T. Baumert, M. Bergt, B. Kiefer and G. Gerber, *Chem. Phys. Lett.*, 1997, **267**, 141.

22. B.K. Venkararaman, H. Bandukwalla, Z. Zhang, and M. Vernon, *J. Chem. Phys.*, 1989, **90**, 5510.

23. T. Majima, *Coord. Chem. Rev.*, 1994, **132**, 141.

24. M. Castro, D.R. Salahub, and R. Fournier, *J. Chem. Phys.*, 1994, **100**, 8233.

25. A. Ricca and C.W. Bauschlicher, *J. Phys. Chem.*, 1994, **98**, 12899.

26. M. N. Glukhovtsev, R.D. Bach and C. Nagel, *J. Phys. Chem.* A, 1997, **101**, 316.

27. *Atomic Energy Levels of the Iron–Period Elements: Potassium through Nickel.* J. Sugar and C. Corioliss, *J. Phys. Chem. Ref. Data Suppl. 2*, 1985, **14**, 407–512.

28. D. Schröder, A. Fiedler, and H. Schwarz, *Int. J. Mass. Spec. and Ion Processes*, 1994, **134**, 239.

29. B.L. Tjelta and P.B. Armentrout, *J. Phys. Chem.*, 1997, **101**, 2064.

30. L. Capron, W.Y. Feng, C. Lifshitz, B.L. Tjelta and P.B. Armentrout, *J. Phys. Chem.*, 1996, **100**, 16571.

31. V. Baranov and D.K. Bohme, *Int. J. Mass. Spect. and Ion Proc.*, 1996, **154**, 71.

32. R.H. Schultz, K.C. Crellin, and P.B. Armentrout, *J. Am. Chem. Soc.*, 1991, **113**, 8590.

33. C.J. Carpenter, P.A.M. van Koppen and M.T. Bowers, *J. Am. Chem. Soc.*, 1995, **117**, 10976.

34. K. Norwood, J.–H. Guo, G. Lou, and C.Y. Ng, *J. Chem. Phys.*, 1989, **90**, 6026.

35. K. Norwood, J.–H. Guo, G. Lou, and C.Y. Ng, *Chem. Phys.*, 1989, **129**, 109.

36. K. Norwood, J.–H. Guo, and C.Y. Ng, *J. Chem. Phys.*, 1989, **90**, 2995.

37. K. Norwood, and C.Y. Ng, *Chem. Phys. Lett.*, 1989, **156**, 145.

38. R.H. Hertwig and W. Koch, *Chem. Phys. Lett.*, 1997, **268**, 345.

39. A. Ricca and C.W. Bauschlicher, *Theor. Chim. Acta*, 1995, **92**, 123.

40. P.E.M Siegbahn, in A*dvances in Chemical Physics*, **XCIII**, ed. I. Prigogine and S.A. Rice, John Wiley & Sons, Inc. 1996.

41. A. Ricca and C.W. Bauschlicher, *J. Phys. Chem.*, 1995, **99**, 5922.

42. C. Adamo and F. Lelj, *Chem. Phys. Lett.*, 1995, **246**, 463, and *J. Chem. Phys.*, 1995, **103**, 10605.

43. B.J. Persson, B.O. Roos and K. Pierloot, *J. Chem. Phys.*, 1994, **101**, 6810.

44. M.W. Schmidt and M.S. Gordon, *Ann. Rev. Phys. Chem.*, 1998, **49**, 233.

45. J. Andzelm, N. Russo and D. Salahub, *J. Chem. Phys.*, 1987, **87**, 6562.

46. S.G. Wang and W.H.E. Schwarz, *J. Chem. Phys.*, 1996, **105**, 4641.

47. W. Weinert and J.W. Davenport, *Phys. Rev. B*, 1992, **45**, 13709.

48. R.W. Warren and B.I. Dunlap, *Chem. Phys. Lett.*, 1996, **262**, 384.

49. S. Grimme, *Chem. Phys. Lett.*, 1996, **259**, 128.

50. B.O.Roos, in *Lecture Notes in Quantum Chemistry*, **58**, ed. B.O.Roos, Springer–Verlag, Berlin, 1994, 177–254,.

51. H. Nakano, *J. Chem. Phys.*, 1993, **99**, 7983.

52. H. Nakano, *Chem. Phys. Lett.*, 1993, **207**, 372.

53. H. Nakano, K. Hirao, and M.S. Gordon, *J. Chem. Phys.*, 1998, **108**, 5660.

54. R.D. Bartlett, in *Modern Electronic Stucture Theory. I.*, ed. D.R. Yarkony, World Scientific, Singapore, 1995, p1047.

55. A.J.H. Wachters, *J. Chem. Phys.*, 1970, **52**, 1033.

56. A.K. Rappé, T.A. Smedley, and W.A. Goddard III, *J. Phys. Chem.*, 1981, **85**, 2607.

57. Selected by GBASIS=TZV keyword in GAMESS.

58. K.R. Glaesemann and M.S. Gordon, unpublished.

59. T.H. Dunning, *J. Chem. Phys.*, 1971, **55**, 716.

60. S. Huzignaga, *J. Chem. Phys.*, 1965, **42**, 1293.

61. Selected by POLAR=HONDO7 keyword in GAMESS. This is the default polarization for the TZV basis set in GAMESS.

62. GAMESS (General Atomic and Molecular Electronic Structure System); M.W. Schmidt, K.K. Baldridge, J.A. Boatz, S.T. Elbert, M.S. Gordon, J.H. Jensen, S. Koseki, N. Matsunaga, K.A. Nguyen, S. Su, T.L. Windus, M. Dupuis, and J.A. Montgomery Jr., *J. Comp. Chem.*, 1993, **14**, 1347; http://www.msg.ameslab.gov/GAMESS/GAMESS.html.

63. K. Ruedenberg, and K.R. Sundberg in *Quantum Science*, ed. J.L. Calais, O. Goscinski, J. Linderberg, and Y. Ohrn, Plenum, NY, 1976, p. 505.

64. L.M. Cheung, K.R. Sundberg, and K. Ruedenberg, *Int. J. Quantum Chem.*, 1979, **16**, 1103.

65. B.O.Roos, *Advances in Chemical Physics*, **69**, ed. K.P.Lawley, Wiley Interscience, New York, 1987, p339.

66. P.E. Siegbahn, A. Heiberg, B.O. Roos, and B. Levy,*Phys. Scr.*, 1980, **21**, 323.

67. B.O. Roos, P.R. Taylor, and P.E. Siegbahn, *Chem. Phys.*, 1980, **48**, 157.

68. B.O. Roos, *Int. J. Quantum Chem.*, 1980, **S14**, 175.

69. J. Pople, J.S. Binkley and R. Seeger, *Int. J. Quantum Chem. Symp.*, 1976, **10**, 1.

70. P.M. Kozlowski and E.R. Davidson, *J. Chem. Phys.*, 1994, **100**, 3672.

71. J.J.W. McDouall, K. Peasley, and M.A. Robb, *Chem. Phys. Lett.*, 1988, **148**, 183.

72. A. Zaitsevskii and J–P Malrieu *Chem. Phys. Lett.*, 1994, **228**, 458.

73. B.Brooks and H.F.Schaefer, *J. Chem. Phys.*, 1979, **70**, 5092.

74. T. Helgaker, J. Gauss, P. Jørgensen and J. Olsen, *J. Chem. Phys.*, 1997, **106**, 6430.

75. G.E. Scuseria, C.L. Janssen, and H.F. Schaefer III, *J. Chem. Phys.*, 1988, **89**, 7382.

76. J.F. Stanton, *Chem. Phys. Lett.*, 1997, **281**, 130.

77. J.D. Watts, J. Gauss, and R.J. Bartlett, *J. Chem. Phys.*, 1993, **98**, 8718.

78. M. J. O. Deegan and Peter J. Knowles, *Chem. Phys. Lett.*, 1994, **227**, 321.

79. MOLPRO is a package of *ab initio* programs written by H.–J. Werner and P.J. Knowles, with contributions from J. Almlöf, R.D. Amos, M.J.O. Deegan, S.T. Elbert, C. Hampel, W. Meyer, K. Peterson, R. Pitzer, A.J. Stone, P.R. Taylor, and R. Lindh.

80. J. Moc and M.S. Gordon, *Organometallics*, 1997, **16**, 27.

81. D.G. Musaev and K.J. Morokuma, *J. Chem. Phys.*, 1994, **101**, 10697.

82. L.F. Pacios and P.G. Calzada, *Int. J. Quant. Chem.*, 1988, **34**, 267.

83. T. Ziegler and J. Li, *Can. J. Chem.*, 1994, **72**, 783.

84. T. Taketsuga and M.S. Gordon, *J. Chem. Phys.*, 1997, **106**, 8504.

85. J.M. Bofill and P. Pulay, *J. Chem. Phys.*, 1989, **90**, 3637.

86. R.G.A. Bone and P. Pulay, *Int. J. Quantum Chem.*, 1992, **45**, 133.

87. P. Pulay and T.P. Hamilton, *J. Chem. Phys.*, 1988, **88**, 4946.

88. R. Fournier, *J. Chem. Phys.*, 1993, **99**, 1801.

89. ACESII is program product of the Quantum Theory Project, University of Florida. Authors: J.F. Stanton, J. Gauss, J.D. Watts, M. Nooijen, N. Oliphant, S.A. Perera, P.G. Szalay, W.J. Lauderdale, S.R. Gwaltney, S. Beck, A. Balkova, D.E. Bernholdt, K.–K. Baeck, P. Rozyczko, H. Sekino, C. Huber, R.J Bartlett. Integral packages: VMOL (J. Almlöf, P.R. Taylor), VPROPS (P.R. Taylor), ABACUS (T. Helgaker, H.J.A. Jensen, P. Jorgensen, J. Olsen, P.R. Taylor).

90. A.P. Scott and L. Radom, *J. Phys. Chem.*, 1996, **100**, 16502.

91. J. Olsen, O. Christiansen, H. Koch, and P. Jørgensen, *J. Chem. Phys.*, 1996, **105**, 5082.

92. B.O. Roos and K. Andersson, *Chem. Phys. Lett.*, 1995, **245**, 215.

93. B.O. Roos, K. Andersson, M.P. Fülscher, L. Serrano–Andrés, K. Pierloot, M. Merchán, and V. Molina, *J. Mol. Struct. (Theochem)*, 1996, **388**, 257.

94. R.J. Bartlett, *Annu. Rev. Phys. Chem.*, 1981, **32**, 359.

95. C.W. Murray and E.R. Davidson, *Int. J. Quantum Chem.*, 1992, **43**, 755.

96. H.–J. Werner and P.J. Knowles, *J. Chem. Phys.*, 1988, **89**, 5803.

97. P.J. Knowles and H.–J. Werner, *Chem. Phys. Lett.*, 1998, **145**, 514.

98. IFORB=2 in the GAMESS $MCQDPT2 input group.

99. S. Wilson, K. Jankowski, and J. Paldus, *Int. J. Quantum. Chem.*, 1985, **28**, 525.

100. ISELCT=1 and THRWGT=1.0d–6 in $MCQDPT2 in GAMESS.

101. B. Simon, *Int. J. of Quantum Chem.*, 1982, **XXI**, 3.

102. G.B. Arfken and H.J. Weber, *Mathematical Methods for Physics.* Academic Press New York, 1995, fourth edition. Section 6.5 in particular.

103. H.–J. Werner and P.J. Knowles, *J. Chem. Phys.*, 1985, **82**, 5053.

104. P.J. Knowles and H.–J. Werner, *Chem. Phys. Lett.*, 1985, **115**, 259).

105. Whether the units of radian^2 should be included in the denominator is debatable. For a description of angular units see the informative article: K.R. Brownstein, *Am. J. Phys.*, 1997, **65**, 605.

Table 1. MCSCF NOON for Fe^+ with a TZVP basis set.

	^6D	^4F
Fe 4s	1.000	0.003
Fe 3d	1.200	1.399

Table 2. Fe^+ relative energies with a TZVP basis set.

State Averaged	^4F - ^6D Splitting	Error
Experiment	5.35 kcal/mol	0.00 kcal/mol
MCSCF	38.5 kcal/mol	33.15 kcal/mol
MCQDPT2	3.9 kcal/mol	-1.42 kcal/mol
MR-SOCI	12.6 kcal/mol	7.29 kcal/mol
MCSCF (g function added)	38.6 kcal/mol	33.24 kcal/mol
MCQDPT2 (g function added)	2.1 kcal/mol	-3.24 kcal/mol
MR-SOCI (g function added)	11.6 kcal/mol	6.24 kcal/mol
Single-reference CCSD(T)	10.0 kcal/mol	4.64 kcal/mol

Table 3. IR frequencies (cm^{-1}) and intensities ($D^2/(amu\text{-}Å^2)$) for $FeCO^+$ $^4\Sigma^-$.

	$FeCO^-$ exp.	FeCO exp.	$FeCO^+$ exp.	$FeCO^+$ MP2	$FeCO^+$ B3LYP	$FeCO^+$ CCSD(T)	$FeCO^+$ $^6\Delta$ MC-QDPT2
Fe-C stretch	565±10[b] 740[a]	530±10[b]	...	405[c]	423[c]	435 (2.79)	206 (1.04)
C-O stretch	1980[a]	1950±10[b] 1815[a]	...	2153[c]	2225[c]	1830 (5.06)	1857 (0.066)
linear bend	230±40[b]	330±50[b]	...	321[c]	319[c]	313 (small)	172 (0.156)

[a] P.C. Engelking and W.C. Lineberger, *J. Am. Chem. Soc.* **101**,1979, 5569.

[b] P.W. Villalta and D.G. Leopold, *J. Chem. Phys.* **98**, 1993, 7730.

[c] A. Ricca and C.W. Bauschlicher, *J. Phys. Chem.* **98**, 1994, 12899.

Table 4. MC–QDPT2 equilibrium distances and dissociation energies for $FeCO^+$ relative to ^6D Fe^+ and CO

		Fe - CO distance (Å)	D_e (kcal/mol)
$^4\Sigma^-$	CCSD(T)	1.91	29.7
$^4\Sigma^-$	(13/11)	1.93	22.7
$^4\Sigma^-$	(13/10)	1.75	32.3
$^4\Delta$	(11/9)	2.1	17.5
$^6\Delta$	(13/11)	2.5	12.7
$^6\Pi$	(13/11)	2.5	11.9
$^6\Sigma^+$	(11/10)	2.7	8.1

Table 5. MCSCF NOON for $FeCO^+$ with a TZVP basis set.

	$^4\Sigma^-$	$^4\Delta$	$^6\Delta$	$^6\Pi$	$^6\Sigma^+$
CO π^*	0.083	0.059	0.059	0.059	0.059
Fe 4sσ	0	0	1.000	1.000	1.000
Fe 3dδ	1.028	1.500	1.500	1.000	1.000
Fe 3dπ	1.931	1.000	1.000	1.500	1.000
Fe 3dσ	1.004	2	1.000	1.000	2
CO π	1.963	1.945	1.945	1.956	1.946
CO σ	1.986	1.981	1.991	1.990	1.990

Table B1. Fully numerical $^4\Sigma^-$ hessian in internal coordinates

	FeC stretch	CO stretch	FeCO bend	FeCO bend
FeC stretch	1.239 h/bohr^2	0.0316 h/bohr^2	0.0000	0.0000
CO stretch	0.0316 h/bohr^2	0.0943 h/bohr^2	0.0000	0.0000
FeCO linear bend	0.0000	0.0000	0.0604 h/radian^2	0.0000
FeCO linear bend	0.0000	0.0000	0.0000	0.0604 h/radian^2

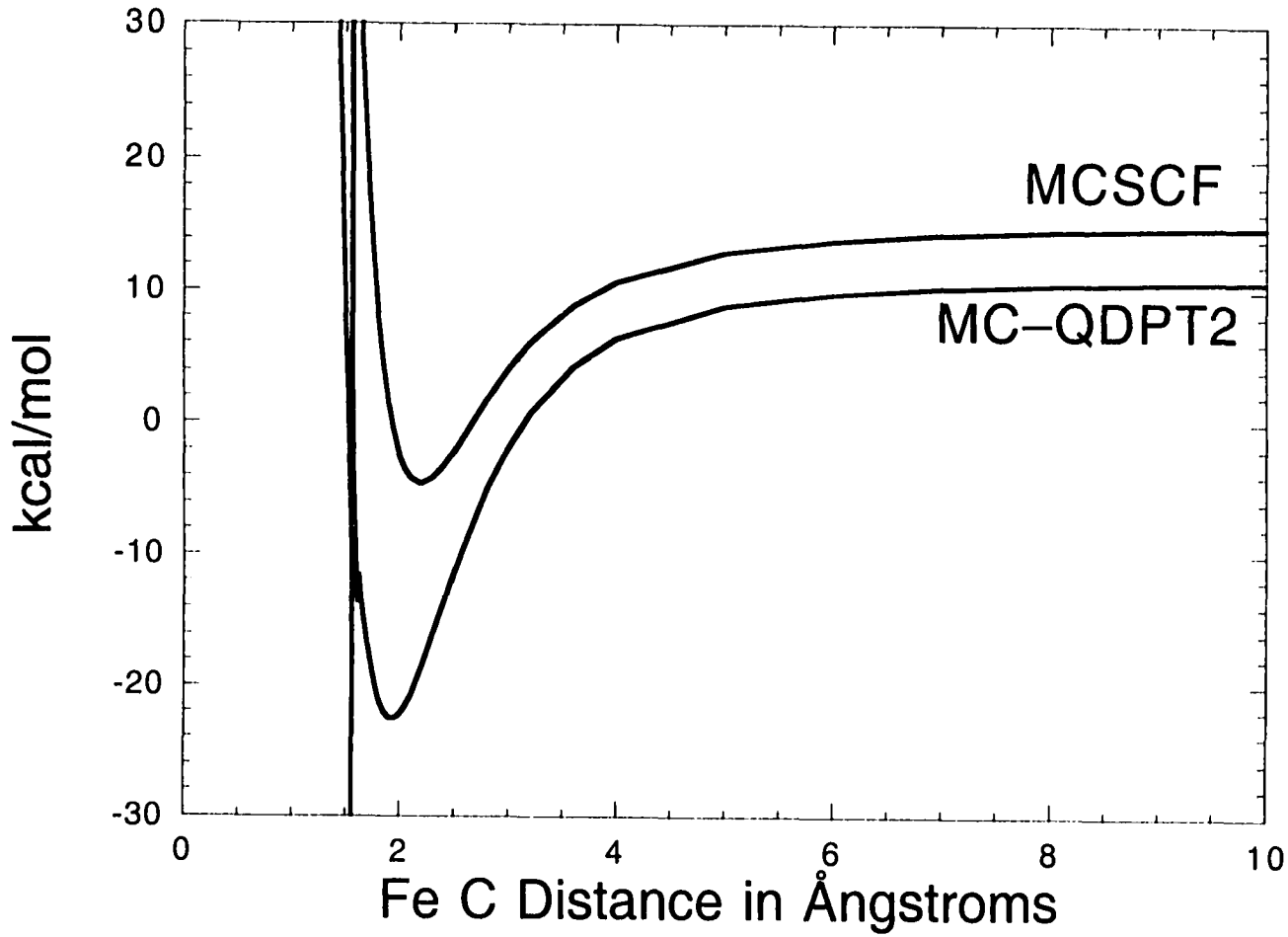

Figure 1: $^4\Sigma^-$ $FeCO^+$ energy with a TZVP basis set and (13/11) active space

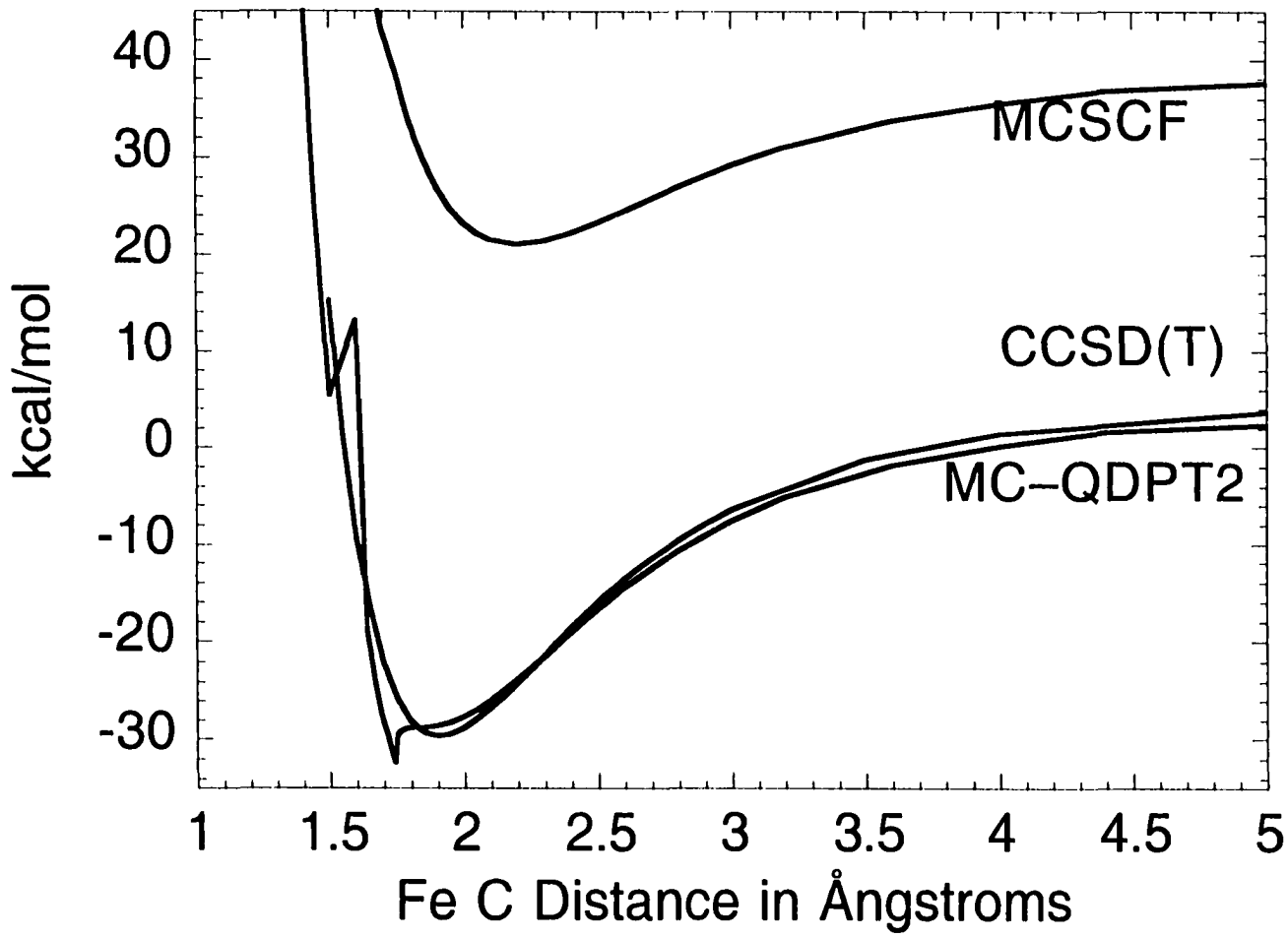

Figure 2. $^4\Sigma^-$ $FeCO^+$ energy with a TZVP basis set with CCSD(T) and MCSCF (13/10)

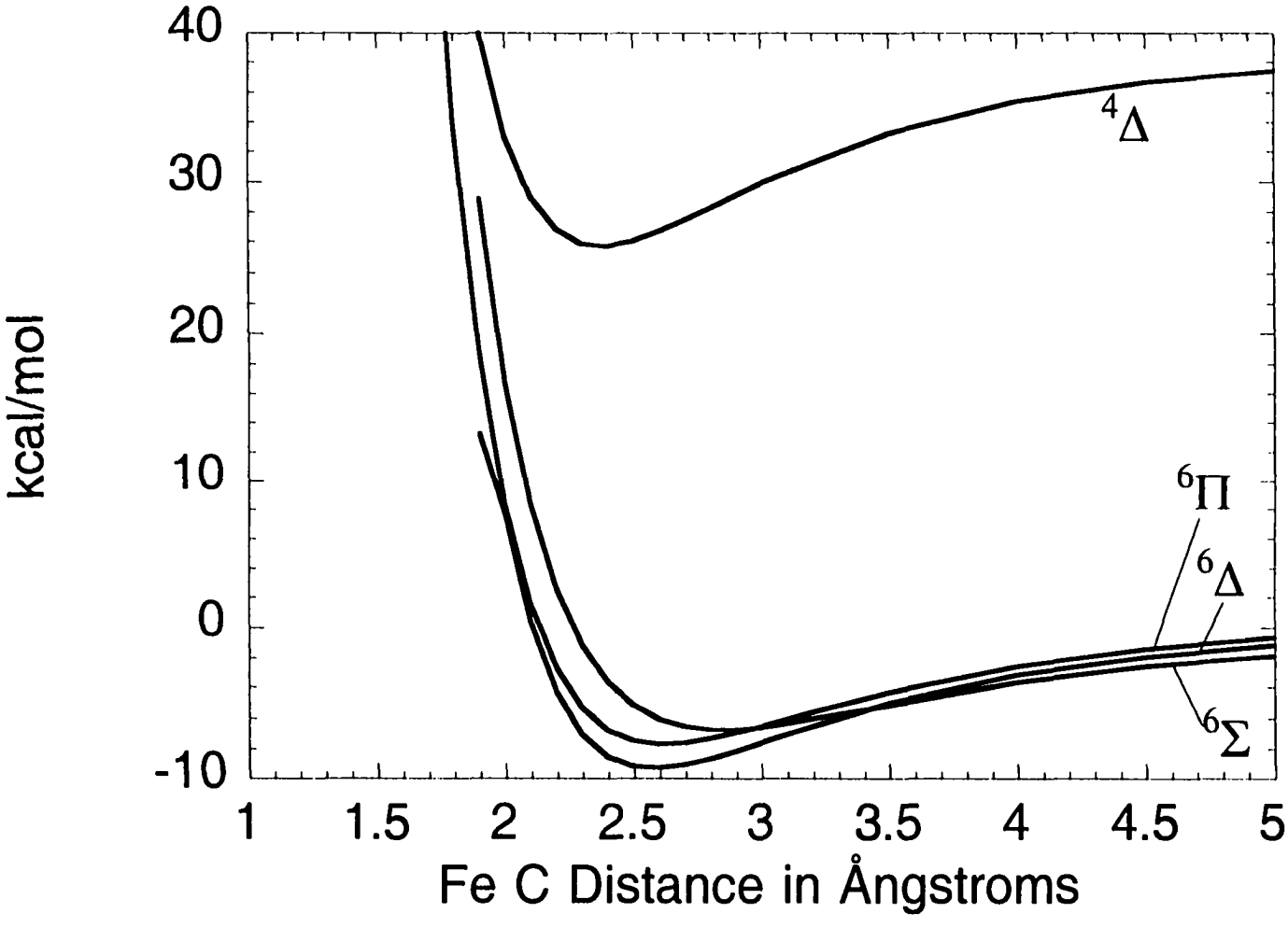

Figure 3. $FeCO^+$ excited state MCSCF energies with a TZVP basis set

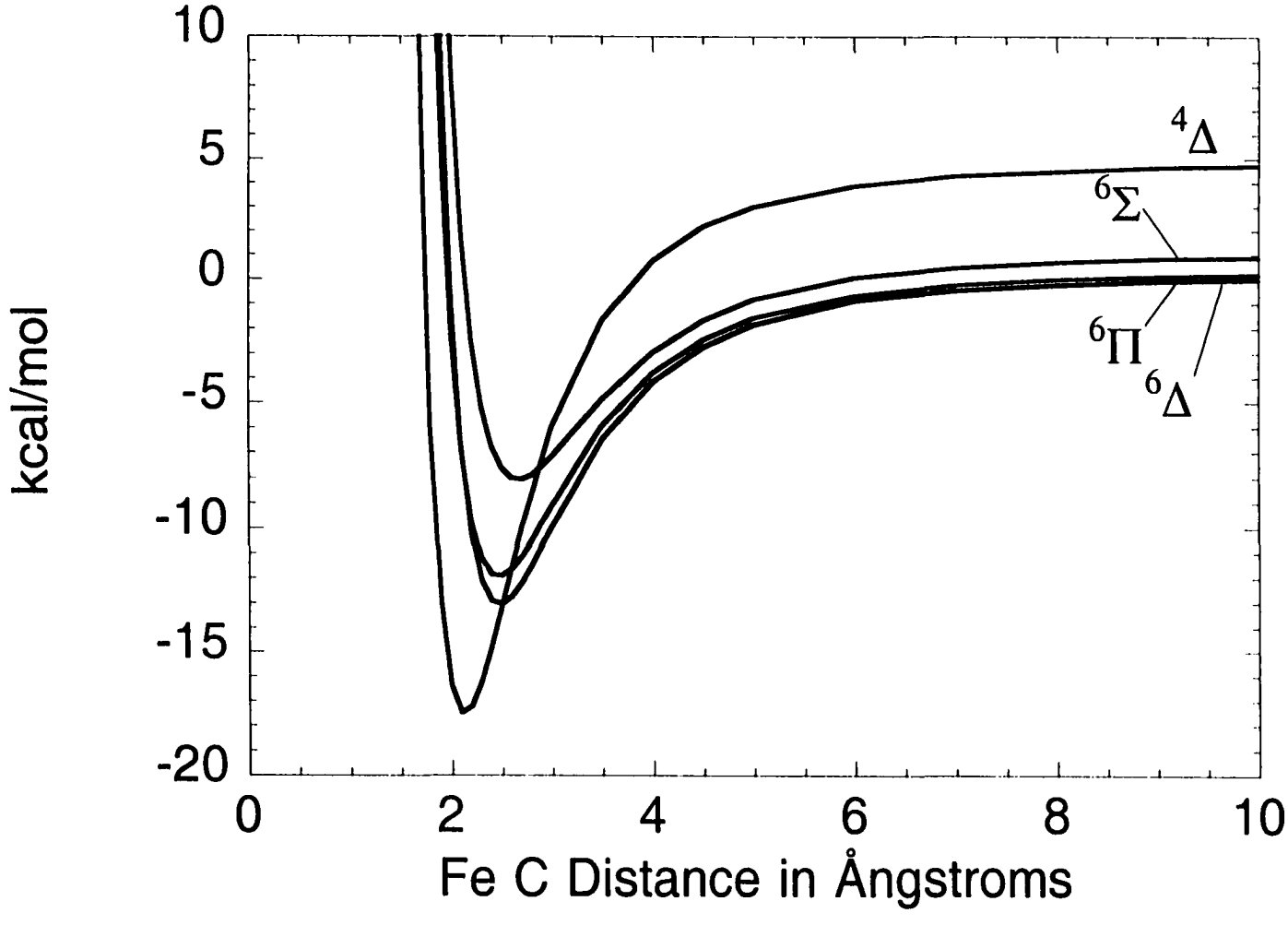

Figure 4. $FeCO^+$ excited state MC–QDPT2 energies with a TZVP basis set

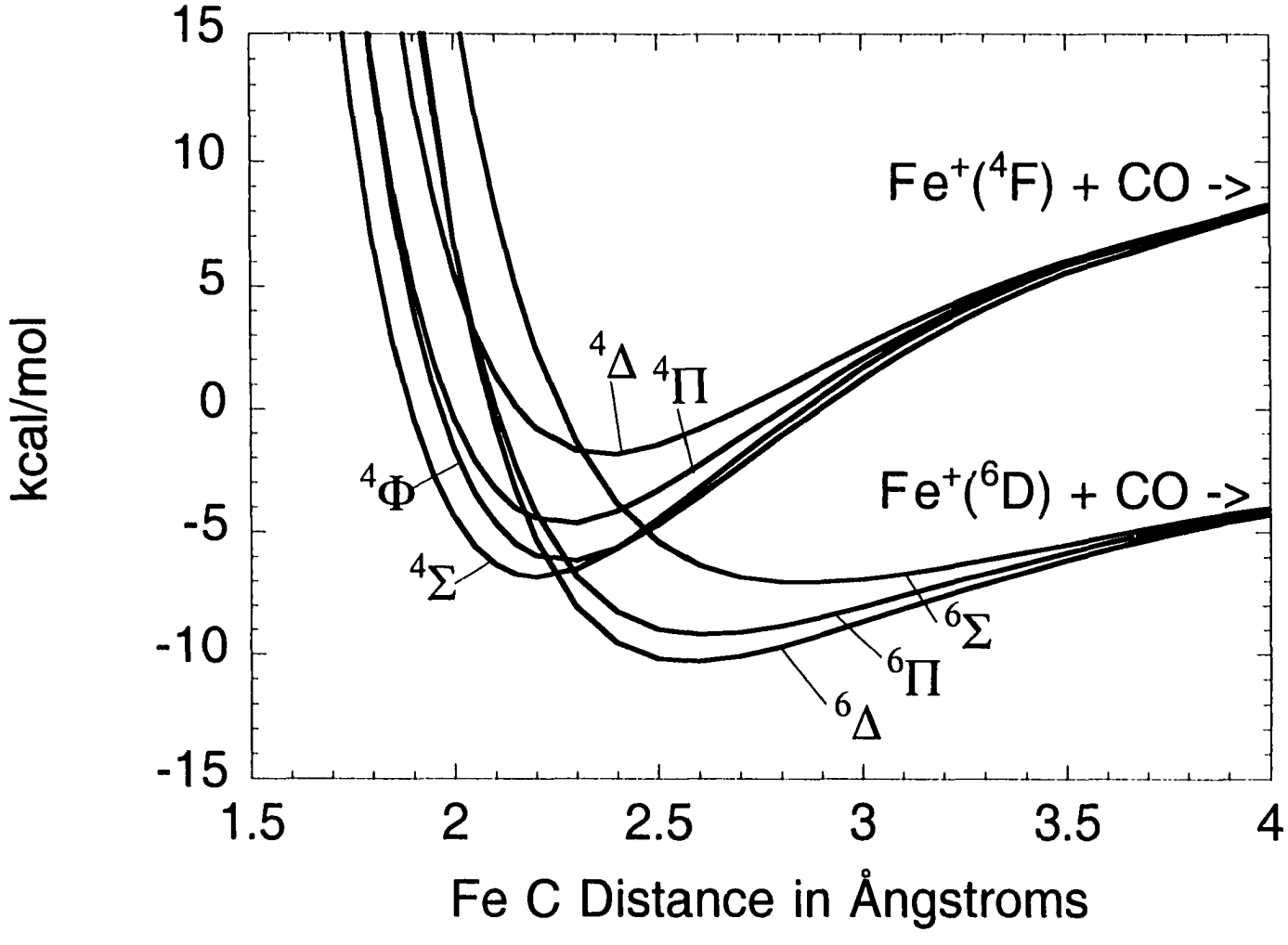

Figure 5. $FeCO^+$ MCSCF energy (all states averaged)

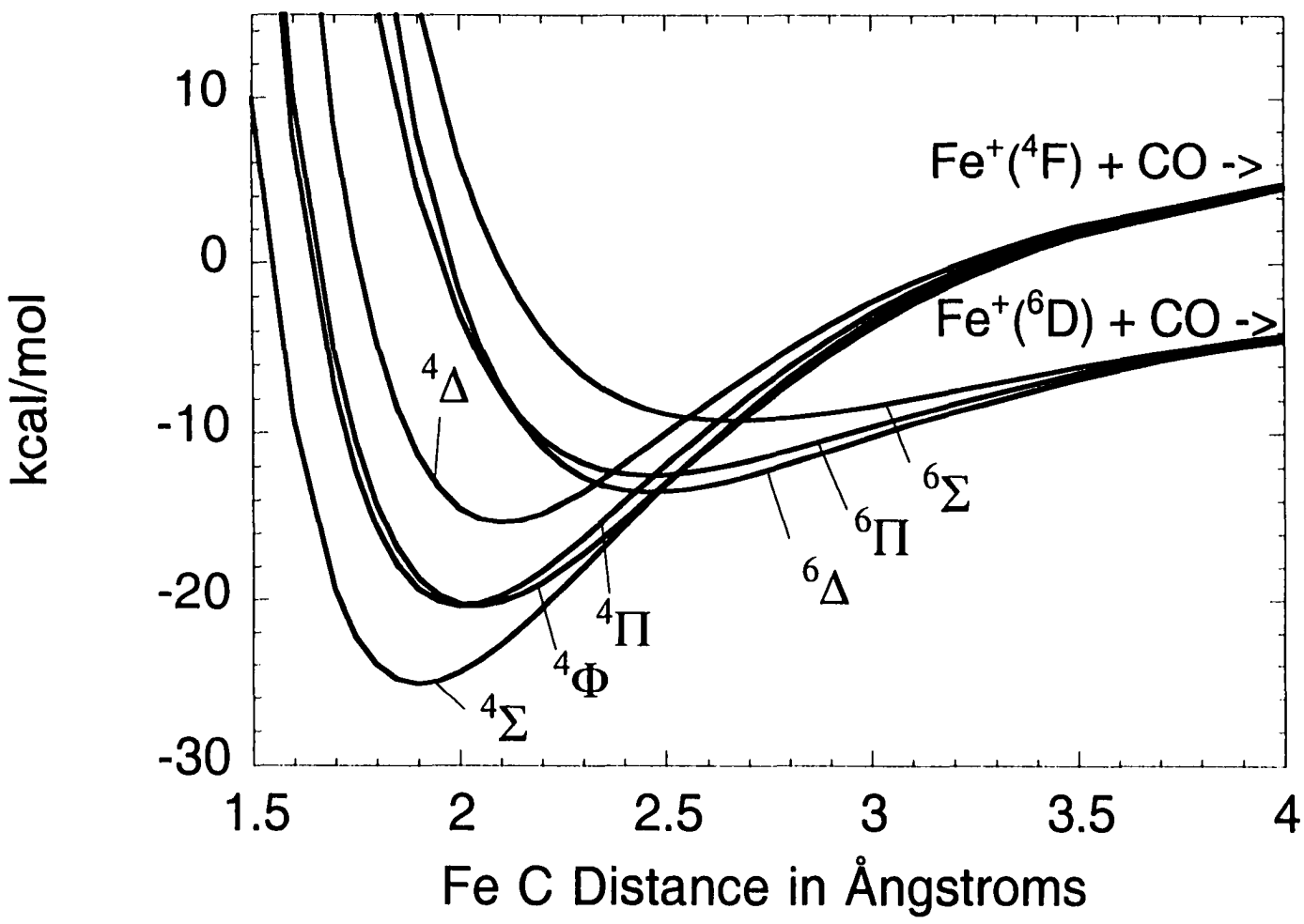

Figure 6. $FeCO^+$ MCQDPT2 energy (all states averaged)

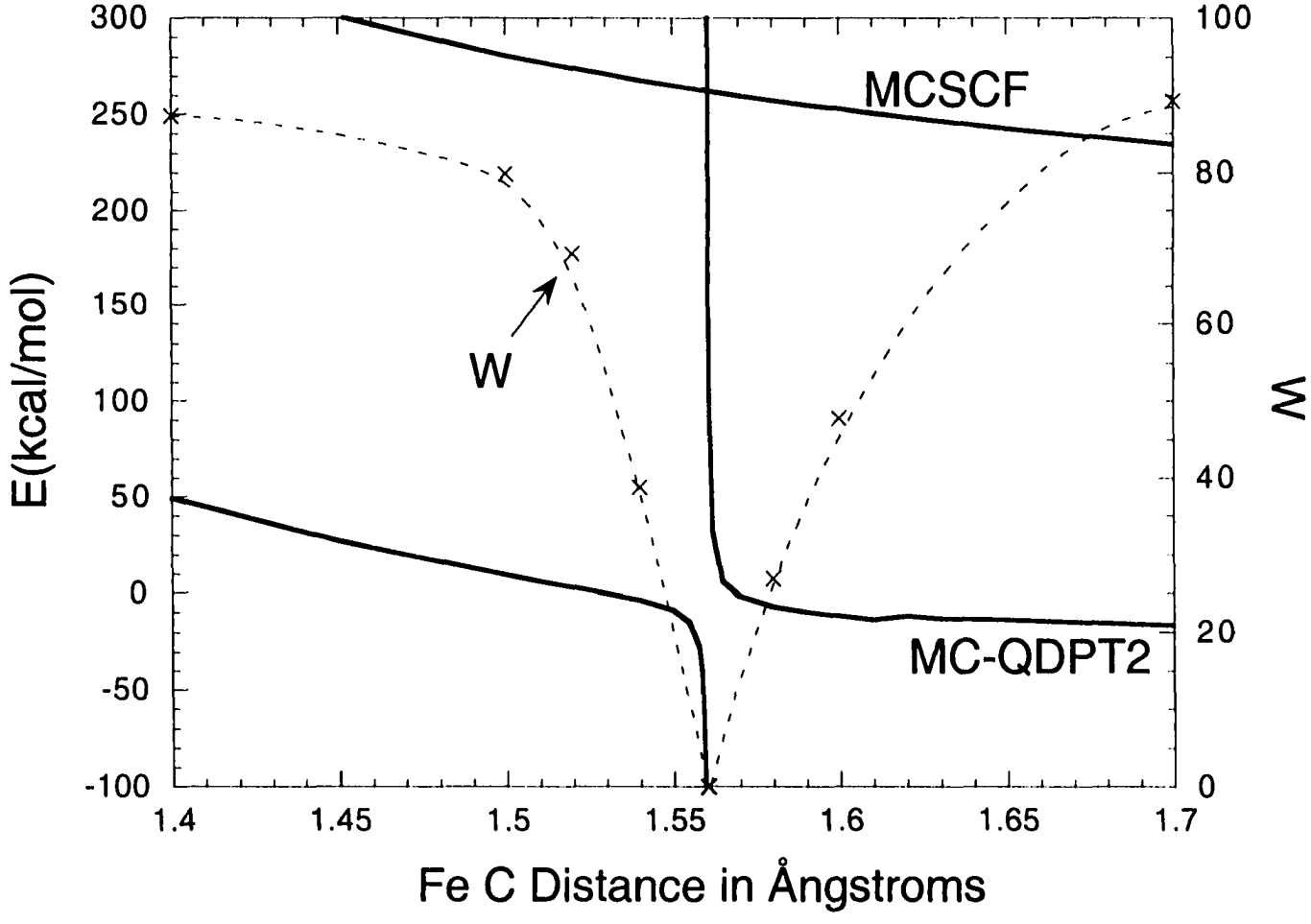

Figure 7. MC-QDPT2 divergence in $^4\Sigma^-$ $FeCO^+$ (13/11) PES.
E=energy, W=weight of reference wavefunction in MC-QDPT2 wavefunction

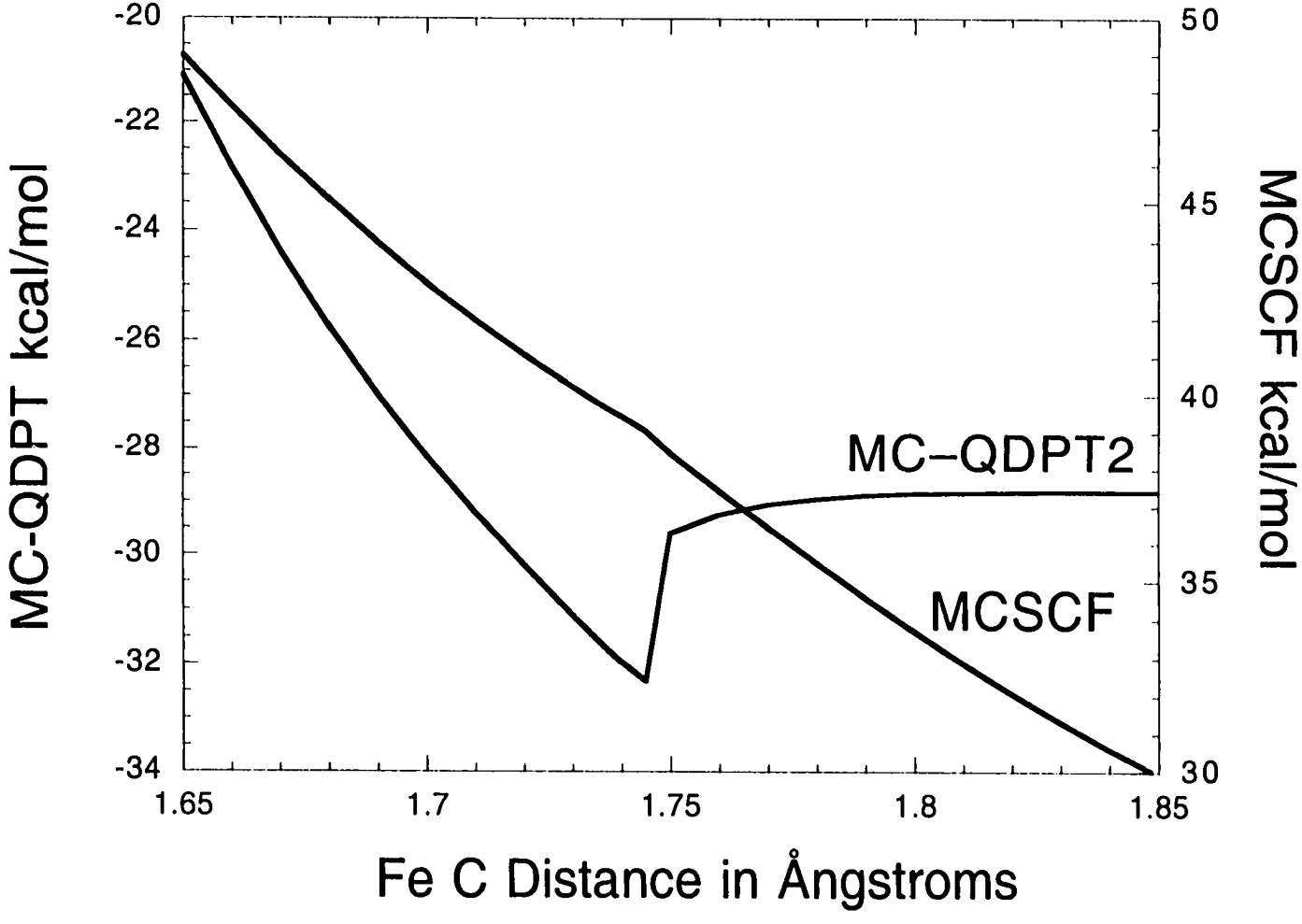

Figure A1. MCSCF discontinuity in $^4\Sigma^-$ $FeCO^+$ (13/10) PES

CHAPTER 6: GENERAL CONCLUSIONS

Because chapters 1 through 5 each have a conclusion of their own, only general conclusions about various methods of calculating electron correlation are included in this chapter.

Chapters 2 through 4 provide insight into the density functional theory (DFT) method of obtaining correlation energy. DFT is computationally less demanding than other methods of obtaining correlation, and therefore gaining popularity. The integrals that arise are shown to be difficult to evaluate. The standard approach has been to use numerical integration. An innovative grid–free approach to evaluation of the integrals that relies on the resolution of the identity is developed in this work. The resolution of the identity (especially for gradient corrected functionals and energy gradient calculations) requires a more accurate basis set than does the wavefunction. The use of such large basis sets results in the calculation of a large number of two-electron integrals that are not otherwise needed. It is found that with a large enough basis set the resolution of the identity does converge to an accurate answer. A more efficient approach that involves augmenting the atomic basis set with auxiliary functions only during the DFT part of the calculation is presented. Unfortunately, the vast knowledge base available for dealing with *wavefunction* basis set completeness was found to be inadequate for addressing this issue, particularly for gradient corrected functionals. Therefore, an even tempered basis set is used to allow for the easy and systematic enlargement of the auxiliary basis set. Because the basis set is even tempered there is no built in bias towards any particular distribution of exponents. By using the Dunning basis sets as a guide for what the range of exponents should be, an effective auxiliary basis set is presented. Results for several systems are presented, and it is found

that by augmenting the basis sets with auxiliary functions in a logical manner, the inadequacies of the atomic basis set are largely overcome.

The derivation of the grid-free method is presented in detail. Several different approaches to calculating the gradient of the density within the grid–free DFT ansatz proposed by AZ are presented. Several approaches suggested by others are shown to be inherently unstable, because the function $n^{-4/3}$ is not well–behaved and therefore the RI cannot be applied reliably. Application of the RI directly to $y^2=(\nabla n/n^{4/3})^2$ provides an inconsistent result. The eigenvalues of y^2 were found to sum to zero, while the y^2 matrix is clearly positive definite. The auxiliary basis sets cannot solve this problem, because it is caused by an inappropriate application of the resolution of the identity. On the other hand, applying the RI to $\pm y=\nabla n/n^{4/3}$ and then squaring the result to get y^2, results in all positive eigenvalues. Therefore this method for evaluating the dimensionless density gradient is used throughout this work. The next step in this area is to extend the approach to more functionals and to extend the auxiliary basis sets to additional atoms. Both of these advances can be done using the straightforward methods presented in this thesis.

Chapter 5 is an investigation of the low lying Fe^+ and $FeCO^+$ states at several levels of theory. Fe^+ and its complexes such $FeCO^+$ are interesting due to their chemical reactivity as catalysts. CO is of particular interest, because it is particularly effective in stabilizing transition metals. The addition of CO to Fe^+ changes the reactivity significantly, because the ground state changes from a sextet to a quartet upon formation of the $FeCO^+$ complex. This change in spin results from a change in the 4s orbital occupation from one to zero. The three low lying excited states are also quartets, therefore this enhanced reactivity probably is also present in the lowest excited states. Results from a careful study reveal that

uncorrelated wavefunctions such as MCSCF fail to properly handle this shift from sextet to quartet. MCSCF predicts the Fe^+ quartet–sextet splitting to be 33 kcal/mol larger than experiment; MC–QDPT2 adds dynamic correlation to predict the splitting within 1.4 kcal/mol of experiment. The $FeCO^+$ complex also requires correlation, with MC–QDPT2 correctly predicting $^4\Sigma^-$ as the ground state, while MCSCF predicts a sextet ground state. The multi-reference wavefunctions allows the calculation of results for excited states.

Because ground state $FeCO^+$ is found to be mostly single-reference, CCSD(T) is used to obtain the D_0 of 28.8 kcal/mol (within the experimental range). The quartet's empty 4s orbital provides an explanation of the increased reactivity of Fe^+, upon interaction with CO. The lowest lying sextet state, $^6\Delta$, is predicted by MC–QDPT2 to have a D_0 of 12.3 kcal/mol. Therefore, $FeCO^+$ gains 16.5 kcal/mol in energy when it changes spin states. The $^6\Delta$ and $^4\Sigma^-$ states can be differentiated experimentally by their IR spectra. The CO stretch frequencies for the $^6\Delta$ and $^4\Sigma^-$ are very similar, but the $^6\Delta$ intensity is very small. The Fe – C stretch frequencies differ by 229 cm^{-1}. In both states the linear bend has the smallest IR intensity. During the analysis of the $FeCO^+$ system, difficulties at several levels of theory were discovered and analyzed. Once MC-QDPT2 natural orbitals become available within GAMESS, further investigation of these difficulties should be undertaken. The knowledge gained from studying $FeCO^+$ could also be extended to other Fe systems.

DFT is compared in several examples to Hartree-Fock and experiment in Chapter 2. DFT in most cases provides better agreement with experiment. In Chapter 5 both ROHF and MCSCF are found to be inadequate to handle the $FeCO^+$ system. By adding electron correlation with CCSD(T) to ROHF and MC–QDPT2 to MCSCF, results that reproduce

experimental results are obtained. Correlation, whether from DFT, perturbation theory, or a cluster expansion, is found to be necessary throughout the work presented in this thesis.

BIOGRAPHICAL SKETCH

Kurt Raymond Glaesemann was born December 29, 1970 in Hibbing Minnesota. He spent most of his pre-college life in Lincoln, Nebraska. He received an American Chemical Society accredited Bachelor of Science in Chemistry from Northeast Missouri State University in 1993. This degree was awarded with both departmental honors in chemistry and general honors as Summa Cum Laude. He was awarded a GAANN fellowship in 1993 and again in 1994. He served both as a teaching assistant and research assistant at Iowa State University.

IMAGE EVALUATION
TEST TARGET (QA-3)

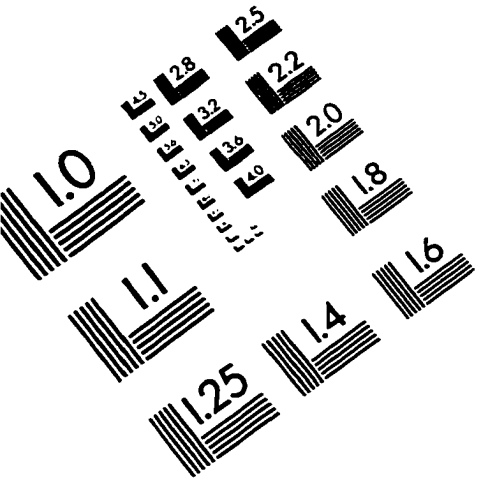

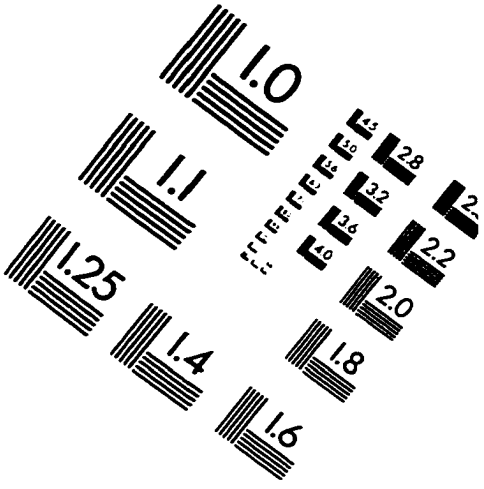

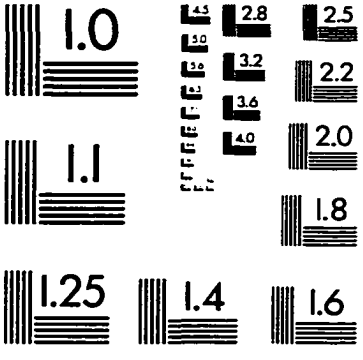

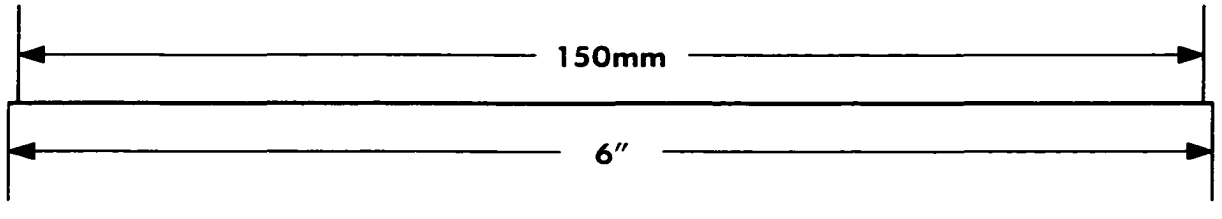

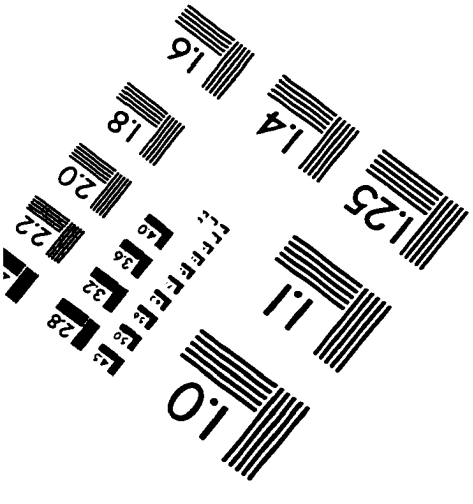

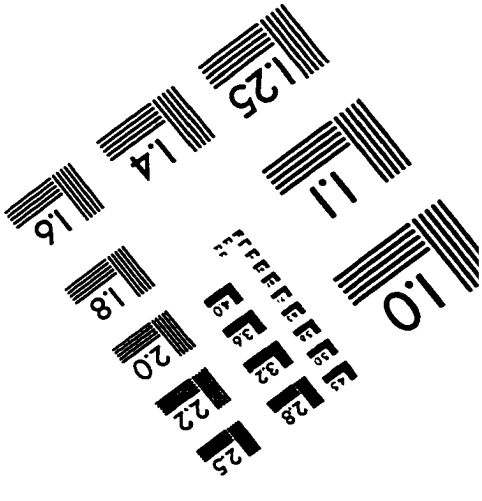

APPLIED IMAGE, Inc
1653 East Main Street
Rochester, NY 14609 USA
Phone: 716/482-0300
Fax: 716/288-5989